EROSION COUNTERMEASURES FOR EASTERN COASTLINE OF KOREA

A Thesis

by

WOONGSUK PAE

Submitted to the Office of Graduate and Professional Studies of
Texas A&M University
in partial fulfillment of the requirements for the degree of

MASTER OF SCIENCE

Chair of Committee,	James M. Kaihatu
Committee Members,	Kuang-An Chang
	Steven F. Dimarco
Head of Department,	Robin Autenrieth

August 2016

Major Subject: Civil Engineering

ABSTRACT

Many coastal areas worldwide have suffered from coastal erosion which has likely been made worse due to rising sea water levels, climate changes, and various man-made reasons. For several years, Wolcheon Beach, in the eastern coastal area of the Republic of Korea has undergone net erosion. Moreover, this problem seems to have been accelerated by a major Samcheok LNG receiving terminal construction project adjacent to Wolcheon Beach.

In order to mitigate this problem, countermeasures to preserve the beach need to be investigated. To facilitate this study, a numerical model using the Delft 3D program developed by Deltares in the Netherlands will be introduced to establish the most nature-like model and incorporated countermeasures including submerged breakwaters, beach nourishments, and groins. For this, various input factors in the FLOW (hydrodynamics) and WAVE model of the Delft 3D, and meteorological information including wind, tidal, and wave data will be presented for setup. Also presented is which established countermeasures is the most effective to alleviate beach erosion through model investigation. Additionally, the economic, environmental, and public analysis of the countermeasures will be shown.

Finally, this study will be useful for not only scholars who study about beach erosion but also stakeholders who have to consider diverse aspects of a policy decision to ultimately improve conclusion outcomes as proper guidance.

DEDICATION

To my wife, two daughters, and son

ACKNOWLEDGEMENTS

First of all, I would like to thank my advisor, Dr. James Kaihatu, I could finish my final goal thanks to his earnest support. I would also like to thank my committee members, Dr. Kuang-An Chang, and Dr. Steven Dimarco, for their sincere guidance and support throughout the course of this research. Thanks also go to Luo, Ping, who is the senior lead IT consultant of the high performance research computing department, sincerely helps to launch the Delft3D suites on the supercomputer ADA system.

I really grateful for my company, Korea Gas Corporation, who honored me with a corporate sponsorship for two years in the United States. I also want to extend my gratitude to colleagues and the department faculty and staff at Texas A&M University for a great experience.

Lastly, thanks to my parents and to my loved one for her dedication and love. Without you, nothing would be possible.

NOMENCLATURE

KOGAS	Korea Gas Corporation
LNG	Liquefied Natural Gas
NE	North-East
NNE	North-North-East
SE	South-East
SSE	South-South-East
SWAN	Simulating Waves Nearshore
GUI	Graphical User Interface
RMSE	Root Mean Square Error
USD	United States Dollar

TABLE OF CONTENTS

Page

LIST OF FIGURES

Page

LIST OF TABLES

Page

1 INTRODUCTION

1.1 Backgrounds

According to Yoshida et al. (2014), rising sea water levels and climate changes have exacerbated coastal erosion, and this has generated severe problems across the globe. In addition, human activities such as coastal development or the placement of hard artificial structures also have contributed to coastal erosion. The equilibrium position of the shoreline is governed by the balance between accretionary and erosional processes; should that balance be upset, the shoreline will evolve accordingly. Both natural and artificial impacts can lead to changes in the shoreline position.

The Ministry of Land, Transport and Maritime Affairs of Korea (2012) announced that there were three primary reasons for coastal erosion (climate change, preponderance of artificial structures, and decreased amounts of sediment from rivers) in the Second Coast Improve Plan. The report showed that beach erosion of the eastern coastline (marked by simple shorelines and a steep slope) is significantly greater compared to the western and southern coastlines. Wolcheon Beach in eastern coastal area of Korea has also suffered from beach erosion by natural climate changes in recent years. Furthermore, a major LNG receiving terminal construction project by KOGAS has aggravated this phenomenon.

1.1.1 Samcheok LNG receiving terminal construction project

In 2005, the Korean government established a natural gas distribution project for people in the eastern region of Korea. According to the established government plan, KOGAS, the state-owned natural gas company, was to construct an LNG receiving terminal at Samcheok city in Gangwon province (2005~2017). Due to this major construction project, the coastline of Wolcheon Beach has receded during the construction period (2010 ~ 2013). Eventually, the beach sand disappeared after completion of construction in June 2014.

Figure 1 presents the locations, and Figure 2 also shows a bird's-eye view. As shown in Figure 1, it can be easily recognized that the location of the Samcheok LNG receiving terminal is located adjacent to Wolcheon Beach (latitude is 37.16 N, and longitude is 129.35 E). Also, Table 1 shows the brief outline of the project.

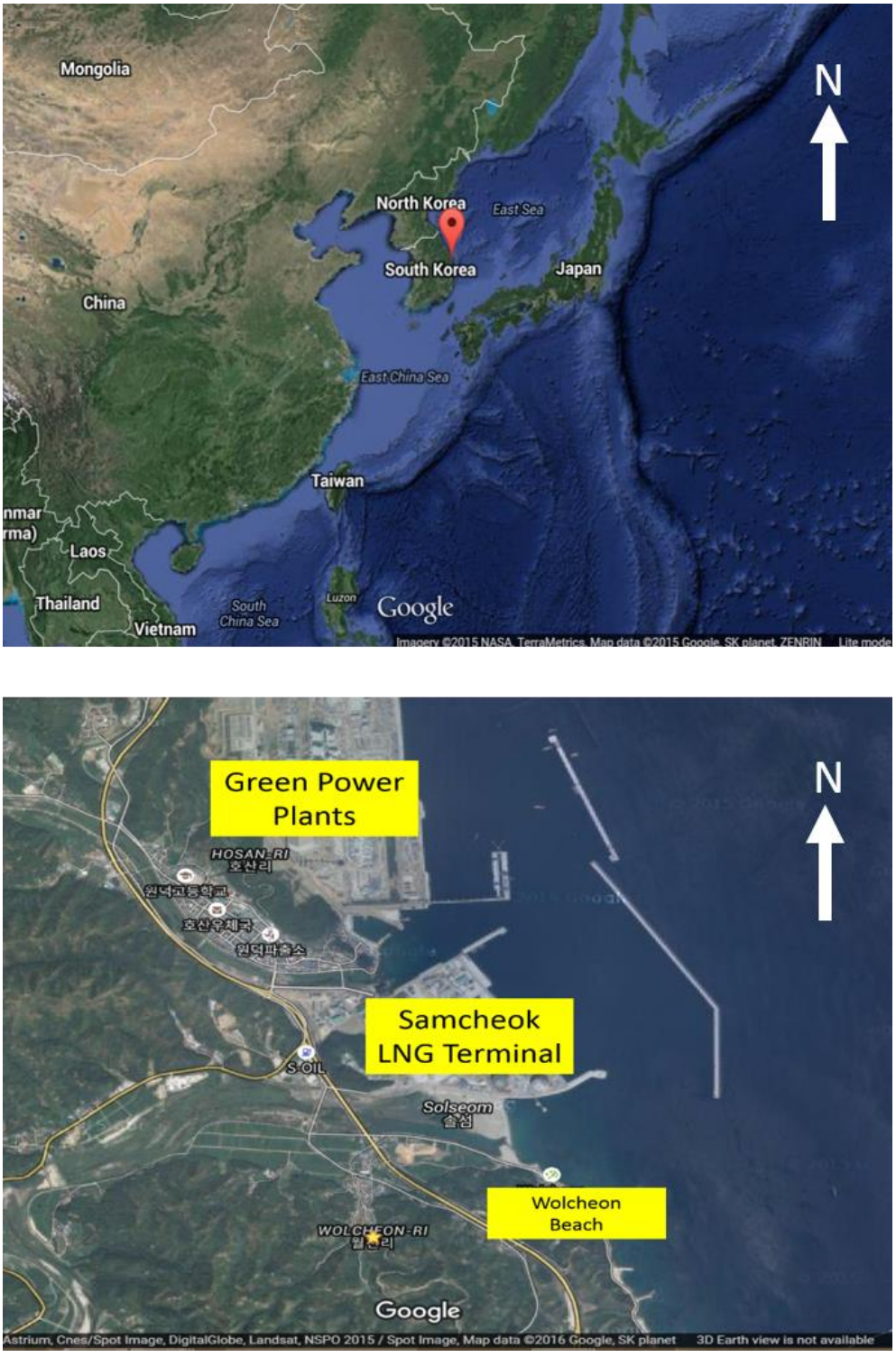

Figure 1. Location of Samcheok LNG receiving terminal and Wolcheon Beach

Figure 2. Aerial view of Samcheok LNG receiving terminal

Table 1. Outline of Samcheok LNG receiving terminal construction project

Project period	2005 ~ 2017		
Total project cost	2.3 billion dollars (USD) (estimated in 2013, calculated by 1,200 won (Korean currency) = 1 USD)		
Main facilities			
	Size	Type	Cost (USD)
Revetment and reclamation	North, east, and south revetment: 3.5km Reclamation area: 590,000m²	Rubble mound and mountain soil reclamation	148,000,000
LNG storage tanks	12 Units: 2,610,000 kl (200,000kl or 270,000kl per each tank)	Full containment	1,578,000,000
Breakwater	1.8km	Concrete caisson	206,000,000
Training dikes	North and south dike: 511m	Rubble mound	21,000,000

1.1.2 Coastal erosion at Wolcheon Beach

Recently beach erosion has become a major problem for local politicians and residents in Wolcheon Beach. This is because beaches are considered important natural features for local governments in coastal cities, and due to the recessions of coastlines, infrastructures such as roads and revetments have been continuously damaged by ocean waves. Revetment and Land Reclamation construction work (October 2010 ~ December 2012) shown in Figure 2, and Breakwater construction work (June 2012~ December 2013) shown in Figure 3, have strongly impacted the recession of the coastline at Wolcheon Beach.

Figure 3. Breakwater construction

Due to these major construction projects, the coastline of Wolcheon Beach receded during the construction period. Eventually, the beach sand disappeared after the completion of construction in June 2014. Figure 4 through Figure 8 depict the shape change of the shoreline of Wolcheon Beach according to the changes in time by an aerial photograph. In Figure 9 (Area B), the south revetment of the LNG terminal plays a key role in the accumulation of sand at the Gagok estuary because it obstructs the natural nearshore currents with sands from the south to the north. Traditionally, waves from NE and NNE direction prevail in winter, and SE and SSE directions prevail in summer on the eastern coast of Korea. Because of this seasonal occurrence, the coastline was in seasonal equilibrium before construction. However, the constructed terminal functioned as an artificial barrier, and has blocked the natural flow of nearshore currents from the north to the south in winter. Impassable nearshore currents by the north revetment of the LNG terminal in winter cannot carry the sand any more to the beach.

Consequently, while the sand continuously accumulated at the Gagok estuary, but has not been able to continue toward Wolcheon Beach. The result was that the sand at Wolcheon Beach was almost completely eroded. Figure 10 briefly describes the associated processes. Currently, hundreds of armor stones and tetrapods made of concrete for the protection of Wolcheon Beach are installed along the revetment. Although all of the sand at the beach has vanished due to the combination of natural impacts and human activities, a new equilibrium of accretion and erosion seems to have been initiated and is currently being sustained after the completion of construction. Figure 11 chronicles the changes of shoreline at Wolcheon Beach.

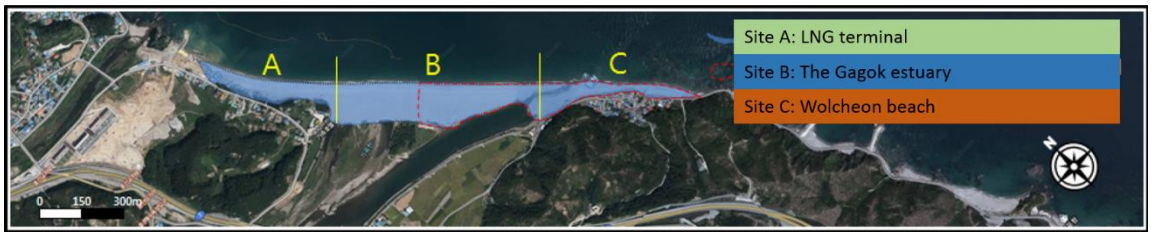

Figure 4. Site position for aerial analysis (Korea Gas Corporation, 2015)

Figure 5. Aerial view (before construction) in 2004 (Korea Gas Corporation, 2015)

Figure 6. Aerial view (before construction) in 2010 (Korea Gas Corporation, 2015)

Figure 7. Aerial view (during construction) in 2011 (Korea Gas Corporation, 2015)

Figure 8. Aerial view (after construction) in 2013 (Korea Gas Corporation, 2015)

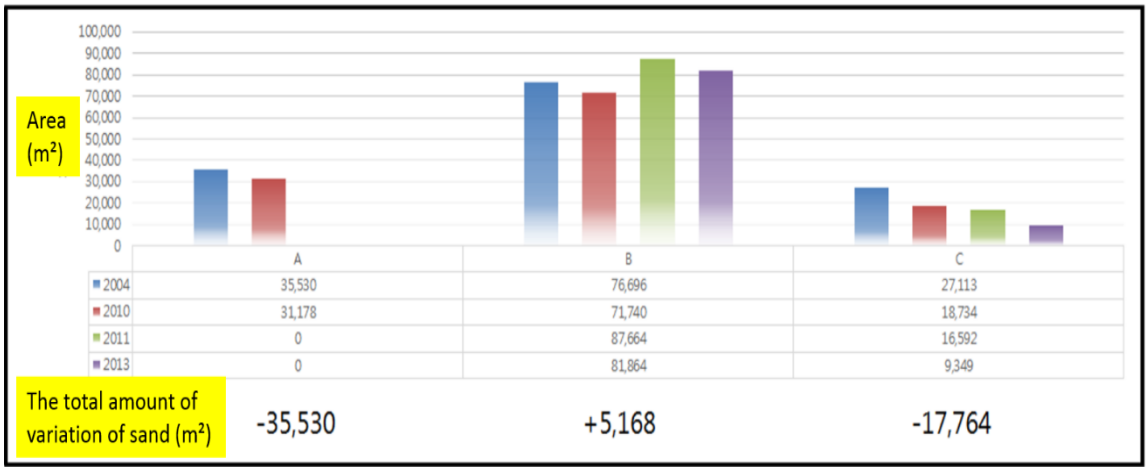

Figure 9. Results analysis of aerial views (Korea Gas Corporation, 2015)

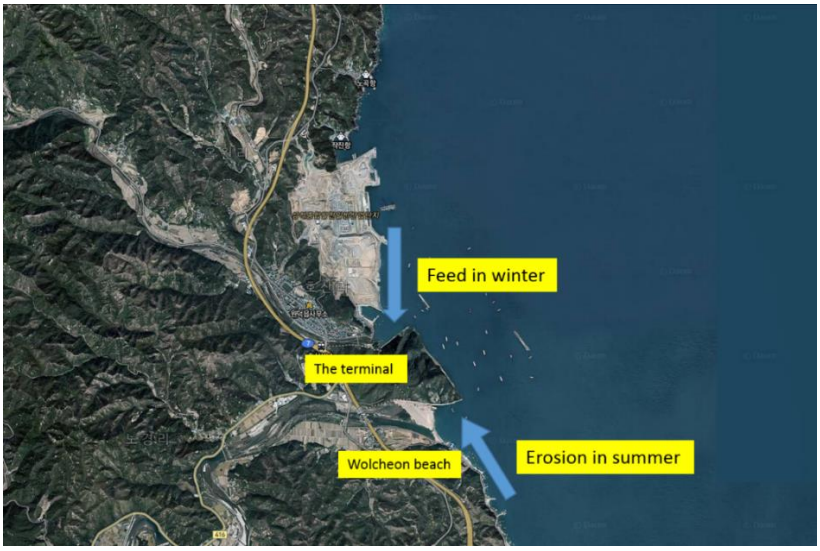

Figure 10. Sediment transport pathways at Wolcheon Beach

Figure 11. Changes of shoreline of Wolcheon Beach

1.2 Objectives

Taxes and profits from tourism or local commercial entities such as hotels and stores at beaches are significant sources of revenue for local governments' budgets, and the destruction of infrastructures has caused risks for local residents. Thus, a primary concern of administrators in the Samcheok city and project managers in KOGAS is how to correct beach erosion effectively, and to determine the best countermeasure.

The aims of this thesis are as follows:

(1) Set up a numerical model using various meteorological data such as winds, waves, tides, and bathymetry in order to simulate the changes in sediment transport characteristics and bathymetry due to these environmental effects;

(2) Develop countermeasures and determine the most effective means to alleviate erosion of Wolcheon Beach, including as possible options: submerged breakwaters, beach nourishment, and groins;

(3) Analyze economic, environmental, and public interest factors associated with each countermeasure;

(4) Determine the best countermeasure considering above all issues.

This thesis is comprised of five sections. Section 1 discusses backgrounds and objectives. Section 2 presents procedures for the establishment of a numerical model. Section 3 investigates the selection of meteorological data and the proposed countermeasures. Section 4 analyzes advantages and disadvantages of the suggested solutions according to viewpoints of effectiveness, conservation by means of SWOT (strength, weakness, opportunity, and threat) method, and relations with communities.

Finally, section 5 determines the conclusions of the above sections and recommendation for future work.

2 SETUP FOR A NUMERICAL MODEL

2.1 Description of the Delft3D suites

Lesser et al. (2004) contended that computer simulations of sediment transport patterns can be useful methods for predicting and understanding morphological changes for use in engineering studies. In this study, the state-of-the-art Delft3D modeling suites are introduced for the establishment of numerical models. The Delft3D package consists of several useful models (Table 2), and these models can either be integrated as an entire modeling system, or activated independently.

Despite this, it is often necessary to couple model components together. In this case, coupling of the FLOW and WAVE modules plays a fundamental role because the FLOW module also determines morphological development and sediment transport. Additionally, in the case of the WAVE module, waves act as main driving forces for coastal processes on the eastern Korean coast.

Table 2. Delft3D package description

Module	Main function	Description
RGFGRID	Grid	Generation and manipulation of curvilinear grids for Delft3D FLOW and Delft3D WAVE
QUICKIN	Bathymetry	Generation and manipulation of bathymetry, initial conditions, and roughness
FLOW	Hydrodynamics (including morphology)	Simulation of multi-dimensional hydrodynamic flows and transport phenomena, including sediments
WAVE	Waves (standalone)	Simulation of short-crested waves with SWAN
PART	Particle tracking	Simulation of mid-field water quality and oil spills, using particle tracking
WAQ	Far-field water quality (all modules)	Versatile water quality modelling in 1D, 2D or 3D systems including physical, (bio) chemical and bio-logical processes

2.1.1 FLOW module

The FLOW module, the heart of the Delft3D package, is an efficient multi-dimensional hydrodynamic model which estimates non-steady flow and transport phenomena which result from forcing by diverse environmental inputs, with waves, tides, and winds chief among them. Outputs from the FLOW module include water level and depth, depth-averaged and depth varying (if 3D) velocity, quantities which can be calculated from the model variables. Moreover, the FLOW module can also (in associated submodules) calculate sediment transport and morphological change.

The FLOW module solves the unsteady, non-linear shallow water equations for an incompressible fluid. According to Lesser et al. (2004), its governing equations are the horizontal momentum equations, the continuity equation, the transport equation, and

a turbulence closure model. The vertical momentum equation is slightly considered because its horizontal scale is significantly larger than the vertical scale. Due to this fact, the FLOW module is well suited to predict the model results in shallow water regions such as shallow seas, coastal areas, lakes, and rivers.

The primary governing equations as follows: The horizontal momentum equations are:

$$\frac{\partial U}{\partial t} + U\frac{\partial U}{\partial x} + v\frac{\partial U}{\partial y} + \frac{\omega}{h}\frac{\partial U}{\partial \sigma} - fV = -\frac{1}{\rho_0}P_x + F_x + M_x + \frac{1}{h^2}\frac{\partial}{\partial \sigma}\left(\nu_V \frac{\partial u}{\partial \sigma}\right)$$

$$\frac{\partial V}{\partial t} + U\frac{\partial V}{\partial x} + V\frac{\partial V}{\partial y} + \frac{\omega}{h}\frac{\partial V}{\partial \sigma} - fU = -\frac{1}{\rho_0}P_y + F_y + M_y + \frac{1}{h^2}\frac{\partial}{\partial \sigma}\left(\nu_V \frac{\partial v}{\partial \sigma}\right)$$

where,

U, V (m/s): generalized Lagrangian mean velocity components,

t (s): time,

u, v (m/s): Eulerian velocity components,

σ: scaled vertical co-ordinate, $= \frac{z-\zeta}{h}$, scaled as ($-1 \leq \sigma \leq 0$),

z (m): the vertical co-ordinate in physical space,

ζ (m): the free surface elevation above the reference level (at z=0),

h (m): depth below datum level (d) + water level above datum level (ζ),

ω (m/s): vertical velocity in the adapting σ co-ordinate system,

ρ_0 (kg/m^3): reference density of water,

f ($1/s$): Coriolis parameter (inertial frequency),

F_x, F_y (m/s^2): radiation Reynold's stress gradient in the x, y directions,

M_x, M_y (m/s^2): source or sink of momentum in the *x*, *y* directions.

The depth-averaged continuity equation is:

$$\frac{\partial \zeta}{\partial t} + \frac{\partial [h\overline{U}]}{\partial x} + \frac{\partial [h\overline{V}]}{\partial y} = S$$

where *S* (*m/s*) is the contributions per unit area due to the discharge or withdrawal of water, evaporation, and precipitation, and $\overline{U}$, $\overline{V}$ are the depth-averaged velocity, respectively.

The transport equation is given by

$$\frac{\partial [hc]}{\partial t} + \frac{\partial [hUc]}{\partial x} + \frac{\partial [hVc]}{\partial y} + \frac{\partial [\omega c]}{\partial \sigma}$$

$$= h\left[\frac{\partial}{\partial x}\left(D_H \frac{\partial c}{\partial x}\right) + \frac{\partial}{\partial y}\left(D_H \frac{\partial c}{\partial y}\right)\right] + \frac{1}{h}\frac{\partial}{\partial \sigma}\left[D_V \frac{\partial c}{\partial \sigma}\right] + hS$$

where *c* (kg/m^3) is mass concentration, D_H, D_V (m^2/s) are eddy diffusivity in the horizontal and vertical direction.

Finally, the turbulence closure model that is represented by combination of horizontal and vertical eddy viscosity is implemented. The horizontal eddy viscosity is:

$$\nu_H = \nu_{SGS} + \nu_{3D} + \nu_H^{back}$$

where ν_{SGS} (m^2/s) is the sub grid scale (SGS) horizontal eddy viscosity, ν_{3D} (m^2/s) is the part of eddy viscosity due to 3D turbulence , and ν_H^{back} (m^2/s) is the background horizontal eddy viscosity specified by user at input. Additionally, the vertical eddy viscosity is:

$$\nu_V = \nu_{mol} + \max(\nu_{3D}, \nu_V^{back})$$

Where ν_{mol} (m^2/s) is the kinematic viscosity of water, and ν_V^{back} (m^2/s) is the background vertical eddy viscosity specified by user at input.

2.1.2 WAVE module

The WAVE module using the third-generation Simulating Waves Nearshore (SWAN) model (Booij et al., 1999) simulates wave propagation, wave generation by wind, dissipation by white capping, bottom friction, and depth-induced breaking, nonlinear wave-wave interactions (both quadruplets and triads), and wave-current interaction. The spectral action balance equation in Cartesian coordinate is used to the evolution of the wave spectrum (Hasselmann et al., 1973). This equation is:

$$\frac{\partial}{\partial t}N + \frac{\partial}{\partial x}c_x N + \frac{\partial}{\partial y}c_y N + \frac{\partial}{\partial \sigma}c_\sigma N + \frac{\partial}{\partial \theta}c_\theta N = \frac{S}{\sigma}$$

where N (σ, θ) is action density spectrum, σ is the relative frequency, θ is wave direction, c_x, c_y are velocity propagation in x and y space, respectively, and S is the source/sink term with respect to energy density.

The WAVE module can choose a stationary mode and a non-stationary mode. When the stationary mode is chosen, outputs (hydrodynamic results) from the FLOW module will be used such as bathymetry, water level, current, wind, and time step. On the contrary, if the non-stationary mode is chosen, this will simulate with the SWAN model as quasi-stationary with repeated model runs, so time step should be given.

2.1.3 Morphology module

The Morphology module performs as a part of the FLOW module. It predicts bed-load and suspended load transport for cohesive (muddy) and non-cohesive (sandy) sediments using the transport equation above mentioned in 2.1.1. A primary reason why this module is a part of the FLOW application is that the morphological input factors and calculated results continuously influence the FLOW module during the simulation, and vice versa. Through these coupled mechanisms, the bottom level changes and water depth changes will be determined. Furthermore, this process plays an integral role regarding comparisons of the models and measured bathymetry data in this study.

Lesser et al. (2004) developed the suspended sediment change of the computational cell at location (m, n) as follows:

$$\Delta S_{sus}^{(m,n)} = f_{mor}\,(Sink - Source)\Delta t$$

where f_{mor} is the morphological acceleration factor given by the user, Sink and Source are the suspended-sediment sink and source terms, and Δt means computational time step. Additionally, they also argued the bottom sediment change as follows:

$$\Delta S_{bed}^{(m,n)} = f_{mor}\,(S_{b,uu}^{(m-1,n)}\,\Delta y^{(m-1,n)} - S_{b,vv}^{(m,n)}\,\Delta y^{(m,n)} + S_{b,vv}^{(m,n-1)}\,\Delta x^{(m,n-1)} - y^{(m,n)}\,\Delta x^{(m,n)})\,\frac{\triangle t}{A^{(m,n)}}$$

where,

$A^{(m,n)}$ (m^2): the area of computational cell at location (m, n),

$S_{b,uu}{}^{(m,n)}$, $S_{b,vv}{}^{(m,n)}$: the bed-load sediment transport vector components at the *u* and *v* velocity points, respectively,

$\Delta x^{(m,n)}$, $\Delta y^{(m,n)}$ (*m*): the width of cell (*m*, *n*) in the *x* and *y* directions, respectively.

2.2 General description of the models

In this study, a baseline model is established for further investigation, and its entire simulation period is a year (01/01/2014 ~ 12/31/2014). Based on this baseline model configuration, three models using three different meteorological data (data for the year 2014, average-annual data during 2001 to 2014, and maximum-annual data during 2001 to 2014) from the National Climate Data Service System of Korea are developed to determine which the most confident model is.

The Delft3D numerical model, needs physical parameters as input components, which must be specified for all grid domains. For this, the grid domain must be first established for each module. In particular, the FLOW application requires more diverse characteristics (Appendix A) than the WAVE module (Appendix B), including but not limited to, sediment, gravity, and roughness. This is because, as mentioned above, the FLOW and the WAVE applications are implemented in a coupled mode in the models.

In most model configurations using the Delft3D, the WAVE module is run first, with results then applied as the input factors for the FLOW module. Although the two applications have different (though consistent) grid and bathymetry setups, the calculations at every time step for the model are wholly consistent. A significant penalty of this connection is that it requires significant computational time; this mainly depends

on the time step, the simulation duration time, and the grid size (connected to the time step via the Courant number). In order to alleviate this problem, the Texas A&M University Supercomputing Center was engaged, and the Delft3D model compiled and installed in the center. This fact will be discussed in the 2.3.1.3 Time frame section.

2.2.1 Basic model

The smaller and finer FLOW grid is comprised of 18,900 cells with one vertical layer, and covers approximately 34km^2. The larger and coarser WAVE grid is comprised of 35,952 cells with one vertical layer, and covers approximately 274km^2. Figure 12 describes the relationship between location and both model grids. The small blue grid is for the FLOW module, and the large grey grid is for the WAVE module on the right side of the Figure 12. Finer spacing yields higher resolution, but it also requires significantly greater computational resource and model complexity. Thus, through the combination of two grids, bathymetric changes that we need to calculate in the finer FLOW grid can be acquired, and it can also simultaneously reduce the entire simulation time due to the coarser WAVE grid.

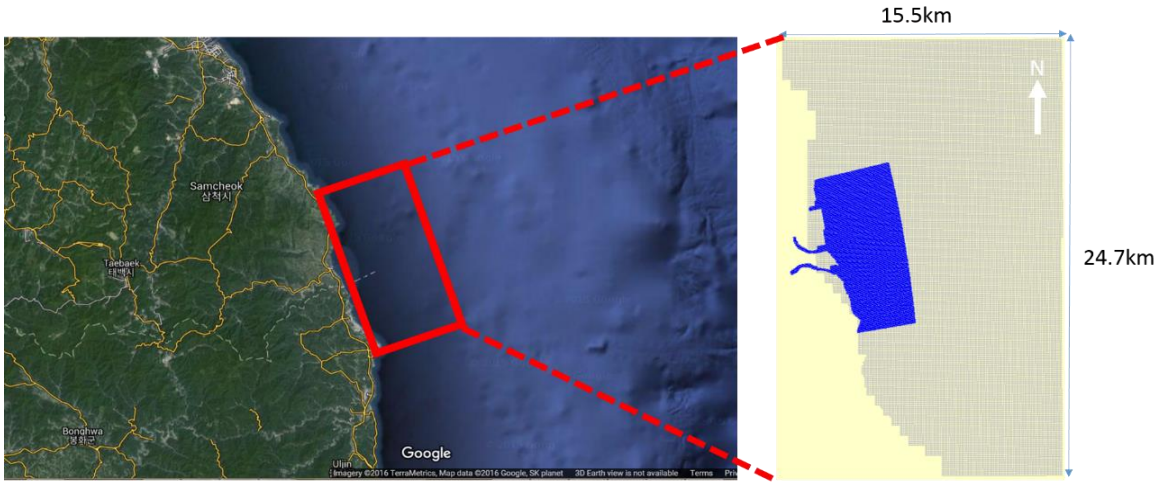

Figure 12. Relationship between location and two grids

Jiang (2010) suggested that the most appropriate extension ratio A/B between the FLOW grid and the WAVE grid is 0.5. A is the length of the extension of the WAVE grid, and B is the total length of the FLOW grid (Figure 13). The relationship of the two grid sizes in this research is referred from Jiang (2010). Overall investigation for the FLOW and the WAVE modules will be shown in the next 2.3 section.

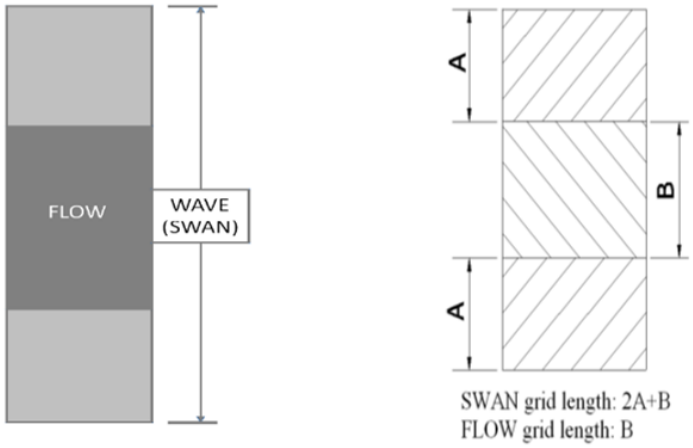

Figure 13. Definition of the extension ratio A/B (Jiang, 2010)

2.2.2 Developed models using diverse meteorological data sets

In general, it is not straightforward to establish a model to properly reflect any given field scenario. Various test conditions must be simulated in order to determine the optimal configuration for further modeling. An efficient model setup greatly facilitates these simulations. There are also diverse parameters such as bathymetric data, river discharge, wind, waves, and so on that must be judged for their suitability for the Delft3D model. In this study, most input characteristics are fixed in the baseline model except for wind, tides, and waves. In order to validate the models using climate data, (1) data for the year 2014, (2) average-annual data, (3) maximum-annual data, and bathymetric data from the nearest locations of Wolcheon Beach from KOGAS are compared to the models' results.

In the case of wind data, hourly wind speed (m/s) and direction (degree) are used from May 18, 2001 to December 31, 2014, and this observation is served by the National Climate Data Service System of Korea. All measured data are from the Donghae buoy (latitude: 37° 32´ N, longitude: 130° 00´ E). It can record air temperature, wind speed, atmospheric pressure, moisture, maximum wave height, significant wave height, wind direction, sea water temperature, peak period, wave direction, and averaged wave height. Wind data are required by both FLOW and WAVE modules.

Input wave conditions for the model also come from the same buoy and during the same time period as the wind data. With respect to the model, significant wave height, peak period, wave direction, direction speed, wind velocity, and wind direction are the "forcing" conditions for the WAVE model.

The baseline model also incorporates tidal information. The discrepancy is significantly minor between the neap tide water level and the spring tide water level in this region (Figure 14). The Mukho tidal observatory (latitude: 37° 33´ 01¨ N, longitude: 129° 06´ 59¨ E) provides tidal water level fluctuations from January 1, 2001 to December 31, 2014. The tides are employed as the flow condition of the east water level boundary for the FLOW grid.

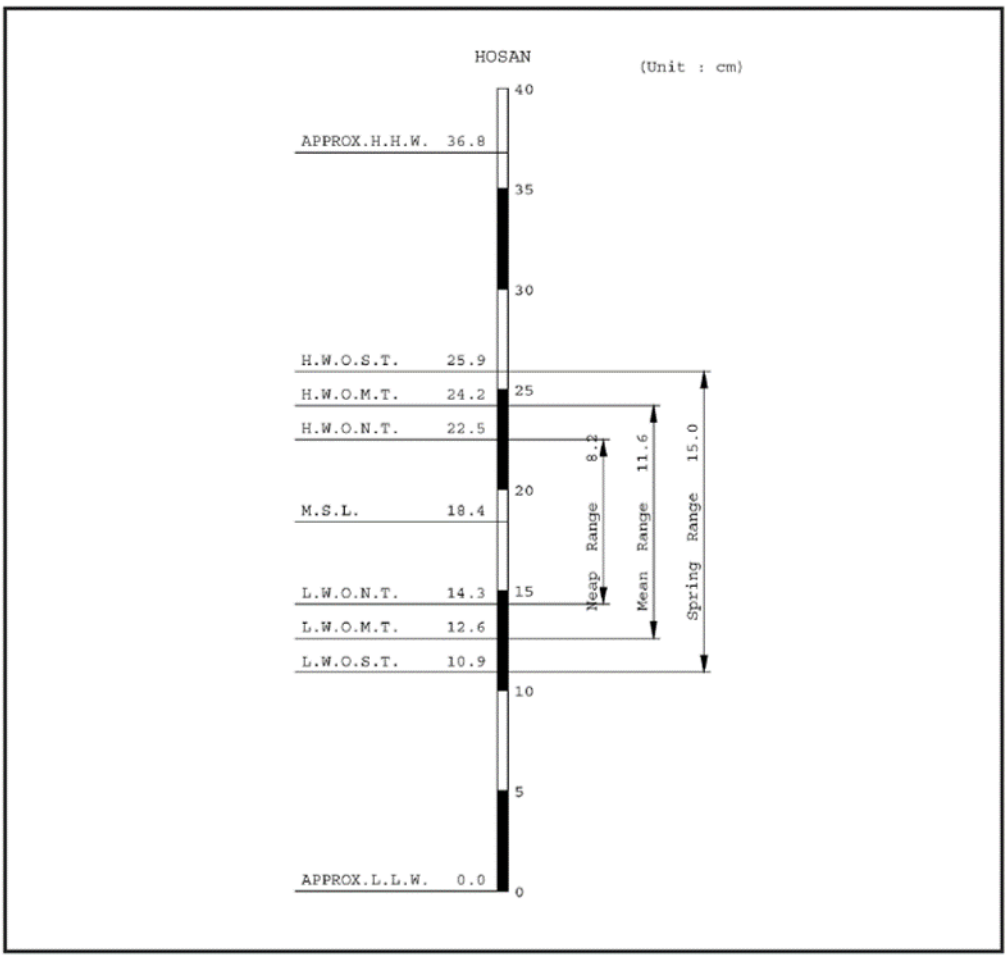

Figure 14. Tide mark at Wolcheon Beach (Korea Gas Corporation, 2009)

2.2.3 Proposed countermeasures

KOGAS (2014) has planned to protect Wolcheon Beach and endeavored to alleviate the anxiety of local residents for several years, but as with numerous civil engineering projects, this project is regulated by a limited construction period and expenses. Considering these two issues, three main countermeasures have emerged as potential solutions. These are: a submerged breakwater, beach nourishment, and groins. Nine possible combinations of three solutions are as follows:

Table 3. Nine countermeasures for Wolcheon Beach

	Countermeasure type
Case A	Do Nothing
Case B	2 Submerged breakwaters + nourishment
Case C	2 Submerged breakwaters + nourishment + 1 north groin (124m)
Case D	2 Submerged breakwaters + nourishment + 1 south groin (124m)
Case E	2 Submerged breakwaters + nourishment + 2 middle groins (62m x 2 units)
Case F	2 Submerged breakwaters + nourishment + 3 middle groins (62m x 3 units)
Case G	Nourishment
Case H	Nourishment + 3 middle groins (62m x 3 units)
Case I	3 middle groins (62m x 3 units)

In this study, Delft3D model configurations are established to match the above solutions. The submerged breakwater is modeled by manipulation of the bottom level at specific grid points, beach nourishment is represented by the function “Dredging and Dumping,”, and the groin is incorporated into the models by the use of thin dams along the grid lines. All of these countermeasures are produced in the FLOW module.

2.3 Input descriptions for the initial model

2.3.1 FLOW

The primary functions of the FLOW module are enumerated in this section. All information of the FLOW model in this section are recorded in the MDF (Master Definition Flow) file (Appendix A) except for sediment and morphology information. Moreover, user-defined attribute files also contribute to the model simulation.

2.3.1.1 Grid and bathymetry

Figure 15 describes the FLOW grid and bathymetry. Nearshore depths for the all grid points come from the Korea Hydrographic and Oceanographic Agency (KHOA) and measured data from KOGAS. To combine and interpolate the grid points and bathymetry data, the RGFGRID and QUICKIN module are employed.

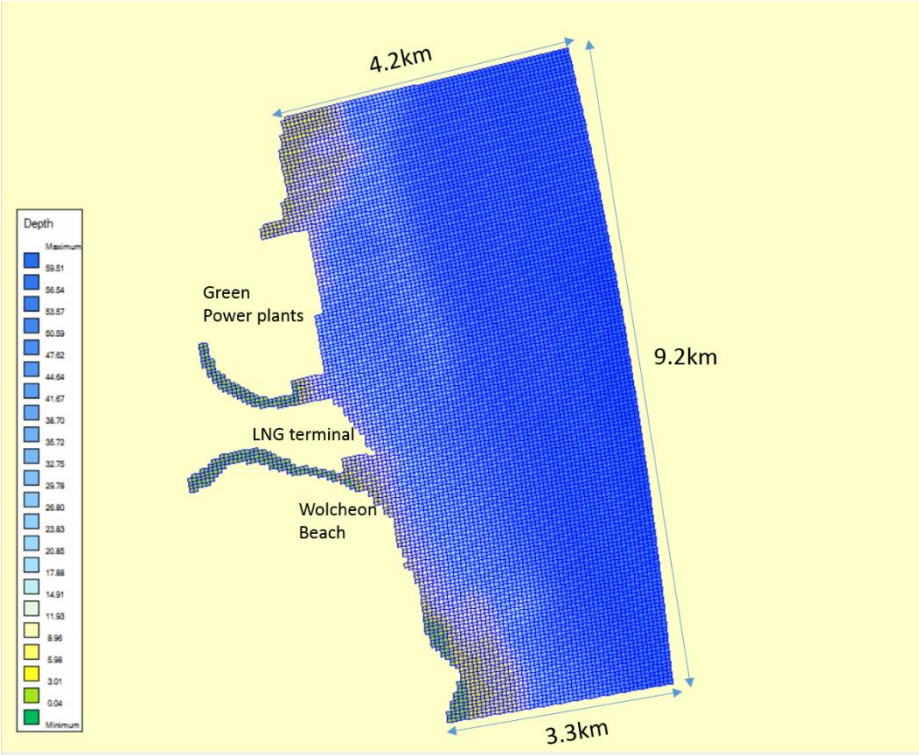

Figure 15. FLOW grid and bathymetry

The smaller grid size can depict geographical features of the sea bed in detail, but it inevitably increases computation time. Due to this restriction, the entire FLOW domain is comprised of 18,900 cells, and the size of a cell is 62m x 50m. In general, the depths of the western area in Figure 15 are relatively shallower than those of the eastern region. Closer to the eastern edge, the depths are continuously deepened to 59.51m.

2.3.1.2 Thin dams

There are four artificial structures that can be described as “Thin dams” in the FLOW grid. The breakwater (1.8km) for the Samcheok LNG terminal and another breakwater (0.9km) for the Green Power plants are large concrete structures, and the

north (300m) and south (211m) training dikes for the LNG terminal are made of rubble mound. Thin dams are represented along the grid lines, and their role is to block flow exchange between two adjacent grid cells. Four yellow lines in Figure 16 display “Thin dams”.

Figure 16. Overview of the "Thin dams"

2.3.1.3 Time frame

The time frame capability defines the simulation of start time, stop time, and the time step. The time step is a critical parameter for evaluating computational speed and efficiency. This is because accuracy and stability of the model are determined by this characteristic. That means, variations of the time step are the main reason for the

fluctuated computation time. The increase of only 0.1 minute can cause more than 24 hours of simulation time in a single processor PC in this study. The time step 0.4 minute concluded by numerous attempts and failures is employed for this study. A criterion for determining the time step based on the spatial resolution is the CFL criterion, and this parameter should not exceed a value of ten.

$$CFL = \frac{\Delta t \sqrt{gH}}{\{\Delta x, \Delta y\}}$$

where,

CFL: Courant (Friedrichs-Levy) number,

Δt: time step (in seconds),

g: acceleration gravity,

H: (total) water depth,

$\{\Delta x, \Delta y\}$: minimal value of the grid spacing in the *x*, *y* directions.

The simulation start time is set on 01 01 2014 00 00 00 (dd mm yyyy hh mm ss), and simulation stop time is on 31 12 2014 23 00 00. The estimated simulation time mainly depends on performance of a single processor PC. Brief test results for the entire simulation period (one year) using average-annual climate data are represented in Table 4 and Figure 17.

Table 4. Simulation time records according to the changes of the time step (single processor PC)

Time step	Computational time	Simulation period
0.05 minute	19 days 11 hours	1 year
0.1 minute	13 days 7 hours	
0.4 minute	8 days 19 hours	
0.5 minute	8 days 14 hours	
1 minute	7 days 23 hours	
5 minute	7 days 12 hours	
10 minute	7 days 7 hours	
Computer performance: Windows 8.1 64 bit, Intel core(TM) i7-4710HQ CPU @ 2.50GHz (8 CPUs), ~ 2.5GHz, 12288MB memory RAM		

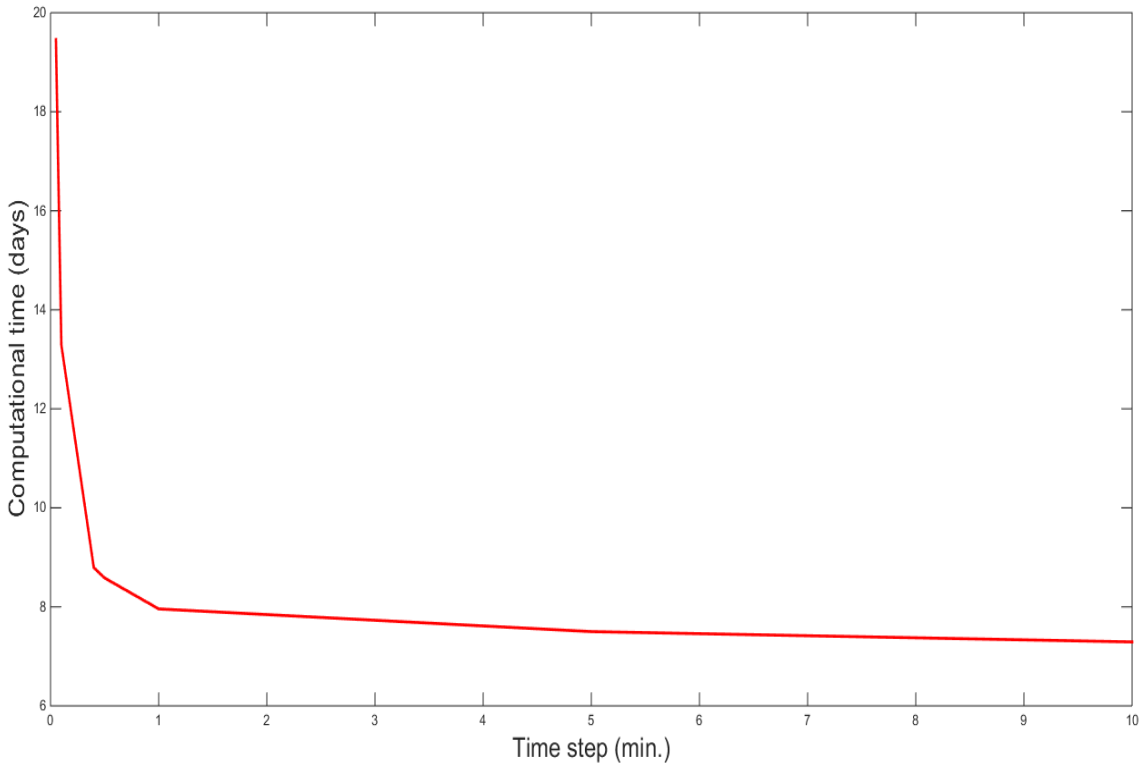

Figure 17. Graph for relationship between computational time and the time step (single processor PC)

An increased time step, while leading to decreased computation time, can lead to errors in the model. These usually manifest themselves as an unacceptably high change in water level or velocity. Technically speaking, water level and velocity in each cell are estimated for the specific time step. After calculating the previous time step, the FLOW module reproduces results for the present time step. When the gap between two time steps exceeds the standard limit, the model is automatically exited. Normally, the limitation for water level change is 25m, and the limitation for velocity change is 5m/s. For these reasons, the baseline model should have stability and reduced computation time, simultaneously. In order to accomplish this, a significant number of models should be tried and failed to determine the most appropriate time step, and this process should be take numerous computational time.

In order to alleviate this problem, we made use of the supercomputing facility in Texas A&M University. We made use of a 17,500 core IBM cluster known as “Ada”. The system is Linux operated, and the nodes are based mostly on Intel’s 64-bit, 10-core IvyBridge processors. The advantage of using ADA involves the parallel processing capability, in which the computational load can be spread over several processors rather than just one. In particular, this helps when running the WAVE module in “stationary” mode, which is relevant for the domain size but also time-consuming, as the model must be iterated until the wave conditions at a certain percentage of points match (within a given tolerance) between two successive iterations, or until the maximum number of iterations is reached. Another main advantage of the supercomputer is that a large number of models can run simultaneously and independently. These two factors, which

help decrease simulation time and running of the model, concurrently contribute to building this research.

Table 5 and Figure 18 show the computation time by the supercomputer ADA, and these models use the same conditions with Table 4 and Figure 17.

Table 5. Simulation time records according to the changes of the time step (normal mode of ADA system)

Time step	Computational time	Simulation period
0.05 minute	39 days 22 hours	1 year
0.1 minute	20 days 22 hours	
0.4 minute	6 days 2 hours	
0.5 minute	5 days 5 hours	
1 minute	3 days 4 hours	
5 minute	1 day 7 hours	
10 minute	22 hours	
Computer performance: Linux, 845/20-core @ 2.5GHz IvyBridge, 811 nodes with 64GB/node; 34 nodes with 256GB memory RAM, normal mode		

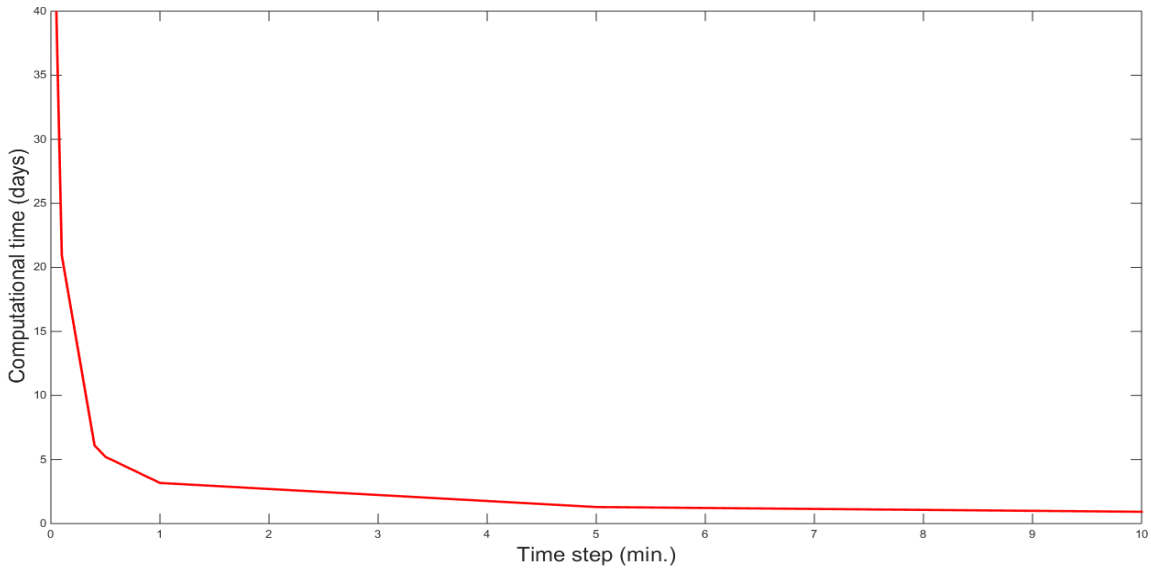

Figure 18. Graph for relationship between computational time and the time step (normal mode of ADA system)

Moreover, the MPI (Message Passing Interface) based a parallel mode of the ADA system is used to divide the FLOW domain according to the number of processors of the ADA system. The computations over a sub-domain are then assigned to several separated processors, and finally the results from each processor amalgamated. Due to this feature of the MPI parallel mode, several functions of the FLOW module become inoperable, but this mode can significantly reduce the entire simulation time. One of these functions is “domain decomposition”, which allows for the overall domain to be split into different subdomains and the overall solution iterated among them. While useful for this work, this functionality is not implemented in the MPI parallel mode. For that reason, the MPI parallel mode is only used to discover the optimum time step. Also, Table 6 and Figure 19 describe computational time from the MPI parallel mode of the ADA system.

Table 6. Simulation time records according to the changes of the time step (MPI parallel mode of ADA system)

Time step	Computational time	Simulation period
0.05 minute	5 days 11 hours	1 year
0.1 minute	3 days 12 hours	
0.4 minute	1 day 21 hours	
0.5 minute	1 day 19 hours	
1 minute	Crashed	
5 minute	Crashed	
10 minute	Crashed	
Computer performance: Linux, 845/20-core @ 2.5GHz IvyBridge, 811 nodes with 64GB/node; 34 nodes with 256GB memory RAM, 20 processors for MPI parallel mode		

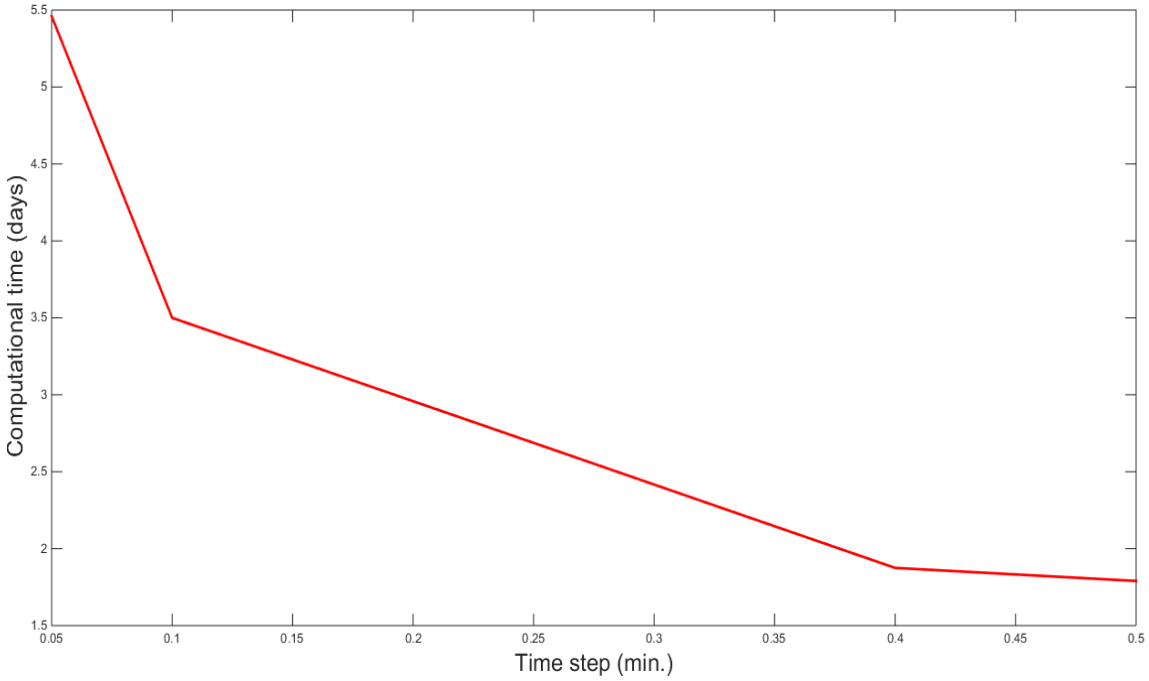

Figure 19. Graph for relationship between computational time and the time step (MPI parallel mode of ADA system)

Also, a morphological time scale factor that can accelerate the morphological changes are conveniently found by the parallel mode. However, this mode is more unstable than the single processor PC and the normal mode of the supercomputer.

The three models (time step: 1, 5, and 10 minutes) which are listed as “crashed” in Table 6 were subjected to the error “water level change too high” occurring at the incipient simulation time. This fault will be introduced in the 2.3.1.6 Morphology section. Although the MPI mode has a handicap, the parallel computation is used so much in this study for the establishment of the incipient model due to its great merits. After finishing this procedure, a normal mode of the ADA system is continuously used to acquire reliable modeling results.

To perform the simulations, approximately 140,000 Sus of the ADA system were utilized. One Su is defined as one (wall-clock) hour's use of one CPU/core. Thus, a 100 CPU job that runs for one hour will consume 100 Sus.

2.3.1.4 Boundaries

To solve the governing equations outlined in section 2.1, initial and boundary conditions must be specified. Thus, location, type, forcing type, flow conditions, and transport conditions of the boundaries are stored in the MDF file, the control file for FLOW. Figure 20 displays the overview of the boundary conditions. The Neumann boundary condition developed by Roelvink and Walstra (2004) for the north and south boundary is introduced to avoid artificial circulation near the edges of the FLOW domain. The water level boundary condition is also developed for the east boundary.

In the case of the Neumann boundary condition, the water level gradient of the grid is applied, using the hourly time series over the entire simulation period. Likewise, water level from tidal data is utilized at the water level boundary. Although the water level boundary condition is the easiest to specify and the most widely used, in general, water levels can change spatially and are hard to track. This deviation could generate spurious flows, especially in the corners where the open boundaries meet. Therefore, the combination of the Neumann boundary condition and the water level boundary condition is used herein.

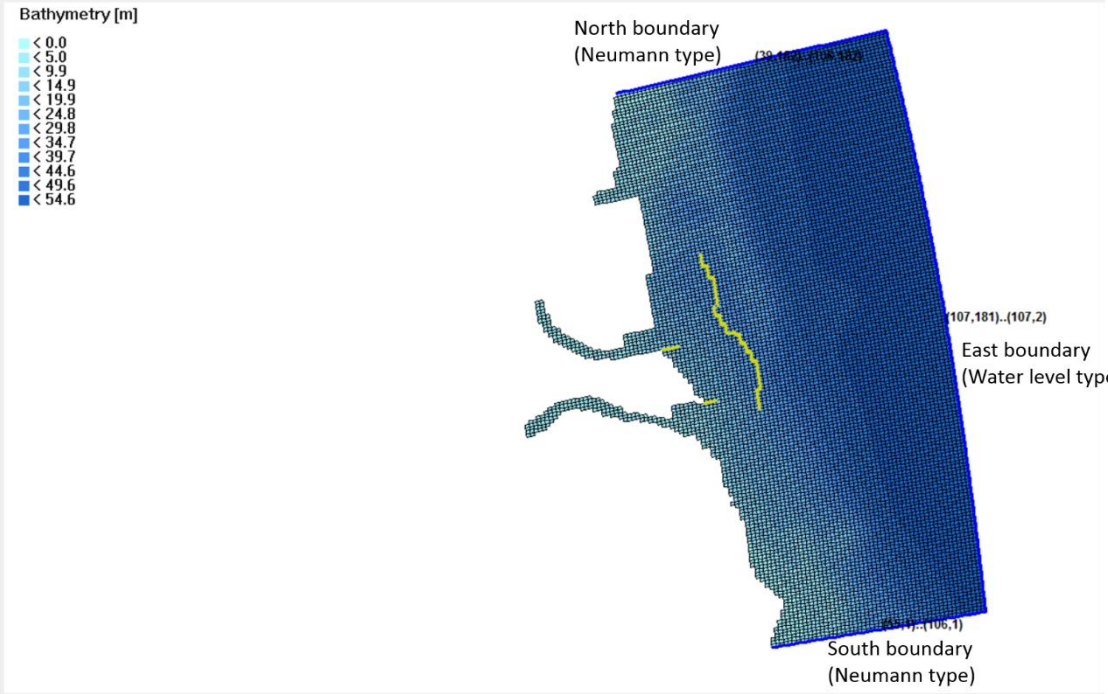

Figure 20. Overview of the "Boundary Conditions"

2.3.1.5 Physical parameters

Physical parameters related to physical conditions in the model's area can be described in this data group for model input. This group is divided into "Constants", "Roughness", "Viscosity", "Sediment", "Morphology", and "Wind". Important factors (bottom roughness in "Roughness", horizontal eddy viscosity/diffusivity in "Viscosity", sediment diameter and initial sediment layer thickness at bed in "Sediment") are represented in Table 7. While all information in physical parameters are recorded in the MDF file (Appendix A), the wind data is included in a "wnd" file. Most input values in physical parameters are from the Investigation Reports regarding Environmental Impacts by KOGAS (2015), or defaulted data by the Delft3D program itself.

Table 7. Values for "Physical Parameters" (FLOW)

Data group	Parameter	Value	Unit
Constants	Gravity	9.81	m/s^2
	Water density	1,025	kg/m^3
	Air density	1.275	kg/m^3
Roughness (Chezy formula)	U	5	$m^{0.5}/s$
	V	5	$m^{0.5}/s$
Viscosity	Horizontal eddy viscosity	300	m^2/s
	Horizontal eddy diffusivity	30	m^2/s
Sediment	Reference density for hindered settling	1,600	kg/m^3
	Specific density	2,636	kg/m^3
	Dry bed density	1,691	kg/m^3
	Median sediment diameter (D50)	374.705	μm
	Initial sediment layer thickness at bed	32	m

2.3.1.6 Morphology

The online combination between the FLOW module and the WAVE module produces the hydrodynamic flow in the FLOW domain, this flow then interacts with previously specified initial conditions such as sediment parameters, bathymetry, and the initial water level. This procedure finally generates the morphological developments by the morphology tool of the Delft3D. Morphological changes incorporate the above mentioned sediment conditions to calculate bed load transport, suspended transport, and fractions for both cohesive sediments and non-cohesive sediments. For this study a non-cohesive sediment (sand) model is assumed. The results from the morphology module continuously updates bathymetry during the FLOW simulation.

One of the important features of the morphology module is the use of a morphological scale factor, which reduces the gap between the time scale of flow variation, sediment transport variation, and bed level and shoreline changes. Normally, changes in flow occur over a time period of several hours, but significant bed level or shoreline changes can require weeks or months to occur. The morphological factor serves to elongate the forcing by that factor, thus accelerating the rate of morphological change. Roelvink (2006) represented a role of the morphological factor in Figure 21.

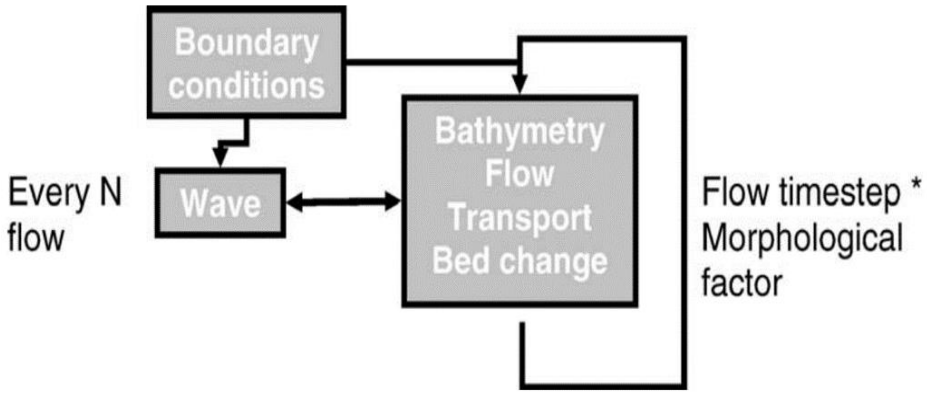

Figure 21. Flow diagram of "online" morphodynamic model setup (Roelvink, 2006)

One possible side effect of the morphological factor is the appearance of errors in the FLOW module such as "water level change too high" and "velocity change too high". The morphological scale factor ultimately causes more differences between the water level and the sea bottom level than would result by hydrodynamic and transport calculations. The rationale behind this is that the scale factor can accelerate the sea bed variations. However, our interest is to simulate the erosion and accretion over a time

scale sufficiently realistic to properly evaluate the proposed countermeasures, so herein the morphological scale factor used is one. Other information regarding morphology can be seen in the Appendix C.

2.3.1.7 River discharges

There are two rivers in the area of interest. Gagok River is located nearby Wolcheon Beach, and serves as the natural southern border of the Samcheok LNG terminal. Likewise, the Hosan River also acts as the natural northern boundary of the Samcheok LNG terminal. These two discharges are described below in Figure 22. Discharge data, such as time-varying flows and suspended sediments, are developed by the Investigation Reports regarding Environmental Impacts by KOGAS (2015). To implement the river data, all measured values are distributed into four seasons (spring, summer, autumn, and winter). According to the change of seasons, the averaged amount of transported sands by the two rivers are also inputted. All employed data are shown as Table 8.

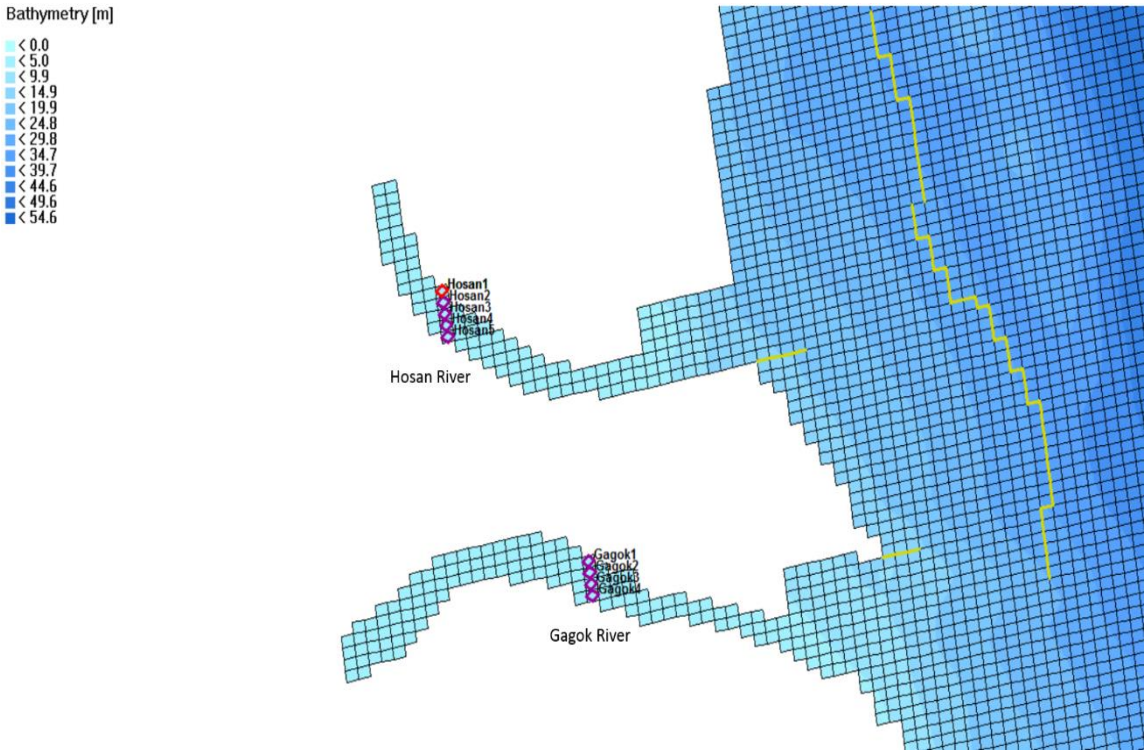

Figure 22. Overview of the "River Discharges"

Table 8. Values for "River Discharges" (Korea Gas Corporation, 2015)

	Time	Flow (m^3/s)	Sediment movement (kg/m^3)
Hosan River	Spring	0.961	0.0008
	Summer	20.244	0.0117
	Autumn	49.333	0.0526
	Winter	12.783	0.0005
Gagok River	Spring	3.922	0.0007
	Summer	116.37	0.0005
	Autumn	122.504	0.0473
	Winter	57.06	0.0007

2.3.2 WAVE

All information of the WAVE model in this section are recorded in the MDW (Master Definition Wave) file (Appendix B).

2.3.2.1 Hydrodynamic result from the FLOW module

The online combination of the FLOW module and the WAVE module that acts as the heart of this study was already explained several times. Bathymetry, water level, current, and wind result from the FLOW application can be used by the selection of the WAVE GUI menu.

2.3.2.2 Grid and bathymetry

Figure 23 describes the WAVE grid and bathymetry. Depths for the all grid points also come from the Korea Hydrographic and Oceanographic Agency (KHOA) and measured data from KOGAS.

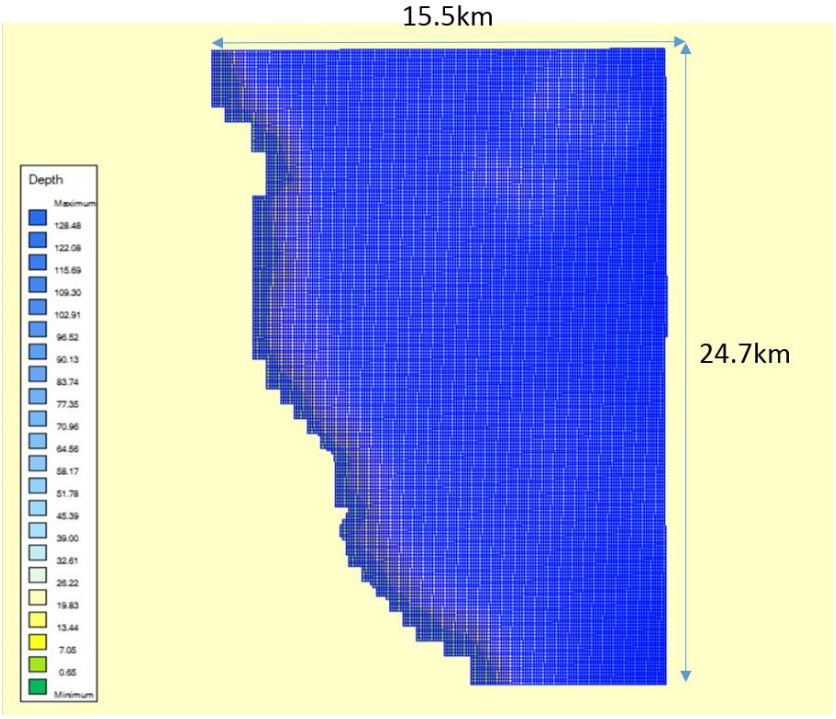

Figure 23. WAVE grid and bathymetry

The entire WAVE domain is comprised of 35,952 cells, and the size of a cell is 93m x 113m. Generally, the depths of the western area in Figure 23 are relatively shallower than those in the eastern region. Closer to the eastern edge, the depths increase to 128.48m. The FLOW grid is overlapped on the WAVE grid in order to simulate the effects of coupled wave-flow characteristics.

2.3.2.3 Spectral resolution

The WAVE module employs directional space and frequency space in the spectral resolution to calculate the model. Table 9 shows the above mentioned factors. In particular, a sector option is applied in order to retain reasonable results regarding

meteorological data while reducing computational time spent calculating wave results in non-relevant directions. Another option of directional space is a circle option which indicates that the spectral directions cover a full circle, but we are mostly interested in waves arriving from offshore. Thus, the sector option is implemented.

Table 9. Values for "Spectral Resolution"

Type	Factor	Value
Directional space (Sector option)	Start direction	340 (deg)
	End direction	160 (deg)
	Number of directions	36
Frequency space	Lowest frequency	0.05 (Hz)
	Highest frequency	1 (Hz)
	Number of frequency bins	24 (Hz)

2.3.2.4 Obstacles

Artificial hard structures, such as the two great breakwaters for the Samcheok LNG terminal, the Green Power plants, and the north/south training dikes can be described as obstacles in the WAVE module. The obstacles interrupt the wave propagation along specified grid lines, similar to thin dams in the FLOW module. The obstacle type, reflection coefficient, transmission coefficient, and segment co-ordinates (location) can be implemented in this section. With respect to the obstacle type, the transmission coefficient of the sheet type is a constant along the obstacle. On the contrary, the coefficient of the dam type changes according to the incident wave conditions. Table 10 displays used values for the model among the above explained factors.

Table 10. Values for "Obstacles"

Structure	Obstacle type	Transmission coefficient	Segment co-ordinates (m)	
Samcheok LNG terminal breakwater	Sheet	0	X start	531,921
			Y start	4,114,773
			X end	532,605
			Y end	4,113,167
Green power plants breakwater	Sheet	0	X start	531,717
			Y start	4,115,587
			X end	531,794
			Y end	4,114,776
North training dike	Sheet	0	X start	531,149
			Y start	4,114,093
			X end	531,392
			Y end	4,114,143
South training dike	Sheet	0	X start	531,775
			Y start	4,113,256
			X end	531,958
			Y end	4,113,293

2.3.2.5 Physical parameters

A number of applied physical parameters for the model display in Table 11.

Table 11. Values for "Physical Parameters" (WAVE)

Physical parameter	Parameter	Value
Constants	Gravity	9.81 (m/s^2)
	Water density	1,025 (kg/m^3)
	North w.r.t. x-axis	90 (deg)
	Minimum depth	0.05 (m)
	Convention	Nautical
	Wave set-up	Non-activated
	Forces	Wave energy dissipation rate

Table 11. Continued

Processes	Generation mode for physics		Third generation
	Depth-induced breaking (B&J model)		Alpha:1, Gamma: 0.73
	Bottom friction		Type: JONSWAP Coefficient: 0.067
Various	Processes activated	Wind growth	Activated
		White capping	Activated
		Quadruplets	Activated
	Wave propagation in spectral space	Refraction	Activated
		Frequency shift	Activated

2.3.2.6 Numerical parameters

Numerical parameters in Table 12 mainly affect the entire computation time of the model.

Table 12. Values for "Numerical Parameters"

Numerical parameter	Parameter	Value	Remarks
Spectral space	Directional space (CDD)	0.5	CDD and CSS determine the numerical scheme: 0= central, 1= upwind
Spectral space Accuracy criteria	Frequency space (CSS)	0.5	CDD and CSS determine the numerical scheme: 0= central, 1= upwind Hs-Tm01
	Relative change; the change in the local significant wave height from one iteration to the next	0.04	
Accuracy criteria	Percentage of wet grid points	90 (%)	
	Maximum number of iterations	8	

Among these factors, the value of the percentages of the wet grid points and the maximum number of iterations in the accuracy criteria play a significant role in the required simulation time for stationary computations in the WAVE model. With respect to this fact, Roelvink (2006) contended that there is an inverse proportion between accuracy and the time required to complete a computational simulation. If increased accuracy criteria were implemented, it could inevitably cause a corresponding increase in simulation time.

Additionally, calculations for the WAVE module require more time than for the FLOW module. This fact can be a major disadvantage while using a single processor PC. Figure 17, Figure 18, and Figure 19 show that, while an increased time step can reduce the computation time, it has limitations because of the simulation time for the WAVE module. In this study, accuracy criteria are slightly diminished compared to the defaulted data due to the long modeling period which is one year.

2.3.3 Meteorological data

Meteorological data including wind, tides, and waves are input in the models in the form of time-varying inputs with one-hour time frames. Regarding the operation of the climate data, three cases are designed in this study which include data for the year 2014, average-annual data during the entire simulation period, and maximum-annual data during the entire simulation period. Average-annual data are data that, for each hour, have been averaged over 14 years (2001 ~ 2014). This was done for significant wave heights and peak periods.

Although the averaged data are normally introduced in most other numerical modeling cases, three meteorological data sets are implemented for the purpose of establishing the most analogous model for the east coast of Korea through comparing the results of the three cases.

2.3.3.1 Wind data

Wind data are used for both the FLOW module and the WAVE module. In the case of the FLOW application, hourly wind speed and direction are introduced. All wind information is included in the form of the "wnd" file. Similarly, for the WAVE application, hourly wind speed and direction are functioned as a part of the "wavecon" file. This "wavecon" file also has input wave information such as significant wave heights and peak periods. Used wind information that was provided by the National Climate Data Service System of Korea is from the Donghae buoy, and its location is shown in Figure 24.

The data for the year 2014 is easily employed for the reason that the National Climate Data Service System of Korea provides the hourly wind information by an Excel file from the Donghae buoy. However, it is not convenient to produce the hourly averaged data and maximum data because they must be properly manufactured by the source data set by some Excel functions, especially regarding calculation of the wind direction.

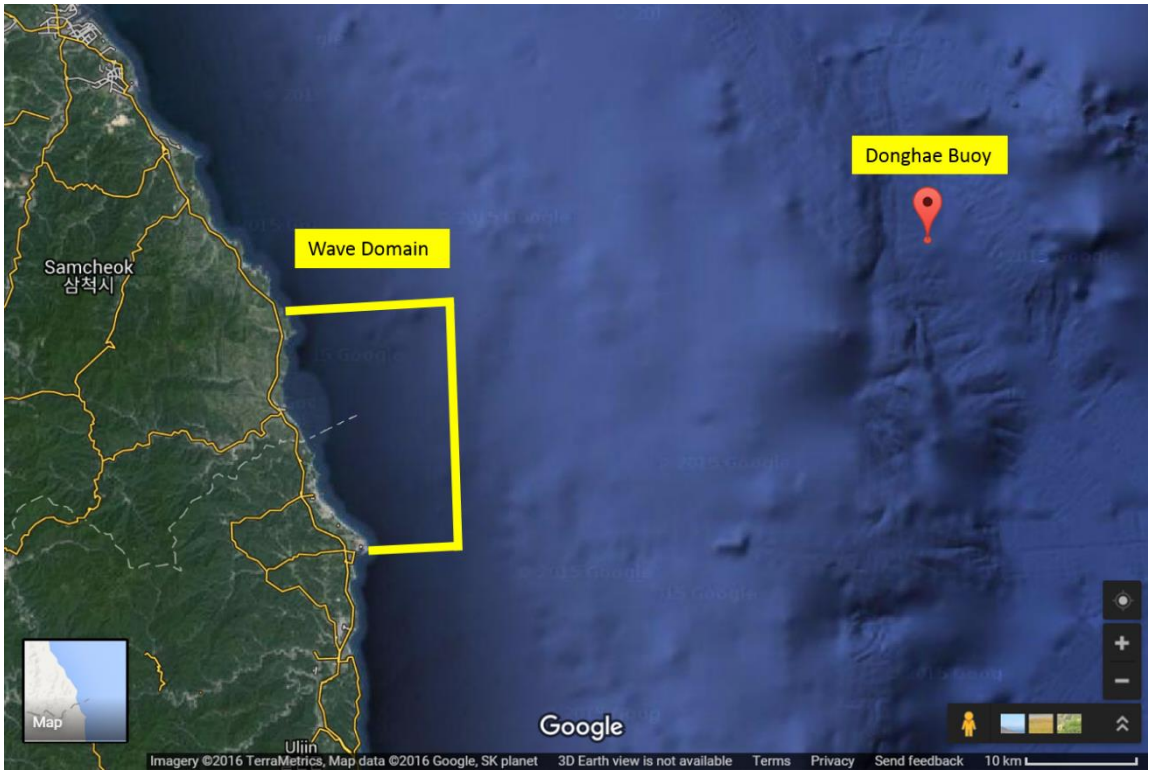

Figure 24. Location of the Donghae buoy

Figure 25 shows a wind rose for the year 2014. Figure 26 also shows the averaged data, and Figure 27 shows the maximum data. It can be seen from Figure 26, that the wind rose from averaged data represents the lower wind speeds compared to Figure 25 and Figure 27. This fact should largely and continuously affect the stability of the Delft3D models during the entire simulation period. Figure 28 is also well described by the more stable wind speed of averaged data.

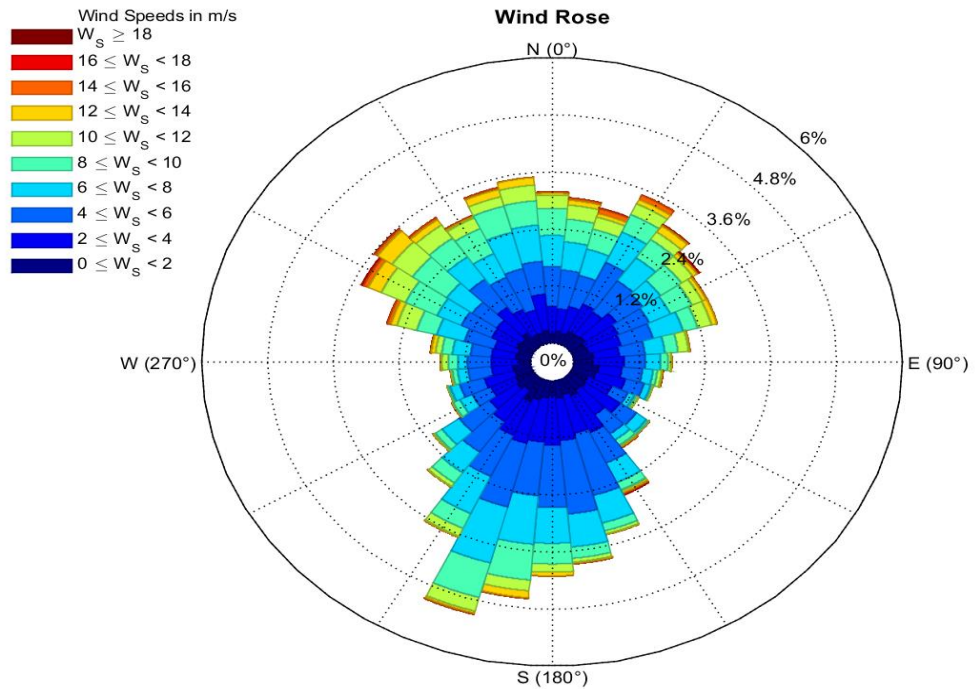

Figure 25. Wind rose for the year 2014

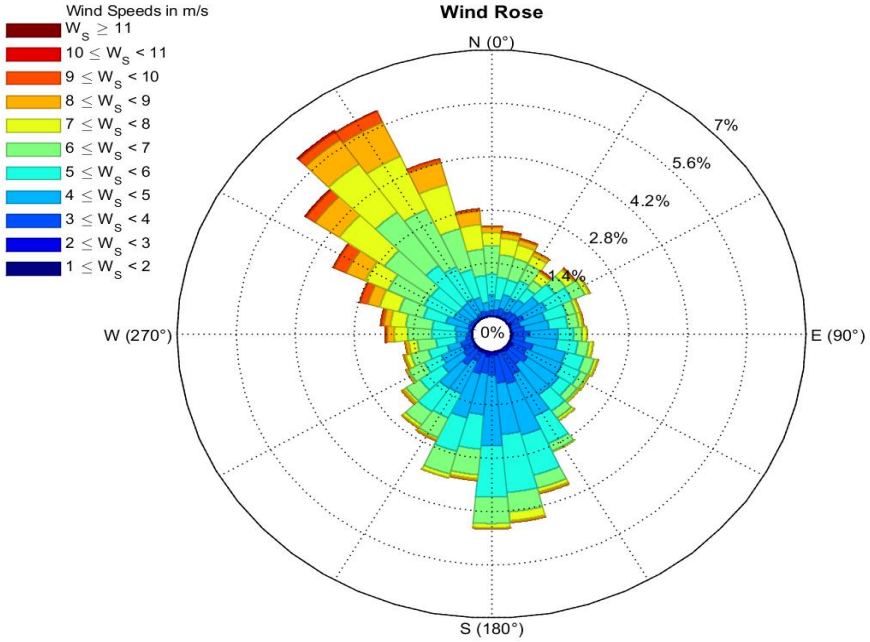

Figure 26. Wind rose for average-annual data during the entire simulation period (2001~2014)

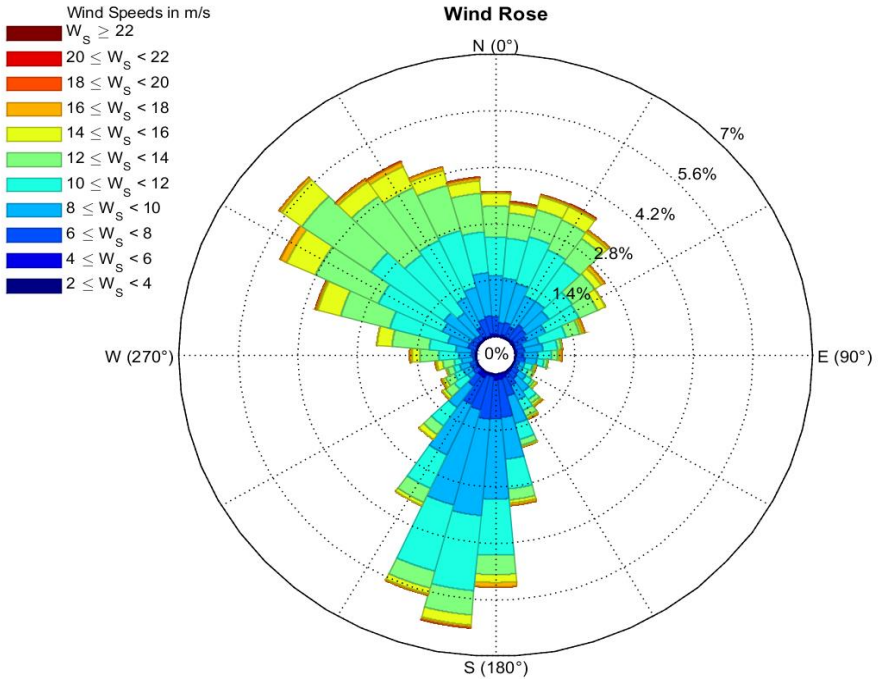

Figure 27. Wind rose for maximum-annual data during the entire simulation period (2001~2014)

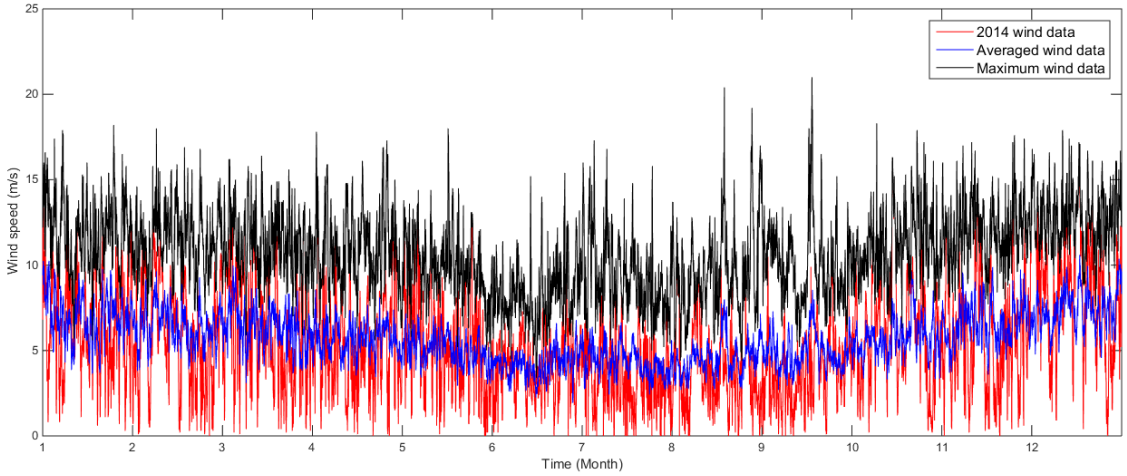

Figure 28. Comparison graph of fluctuation of the wind speed for three cases

2.3.3.2 Tidal data

Tidal data are used for the FLOW and WAVE module; these data are also employed by the above mentioned three cases. Mainly, tidal data contribute to set up the hourly time-varying water level conditions at the east boundary. The Mukho tidal observatory shown in Figure 29 is located at the Mukho port. The fluctuation of tidal data according to the three cases displays in Figure 30.

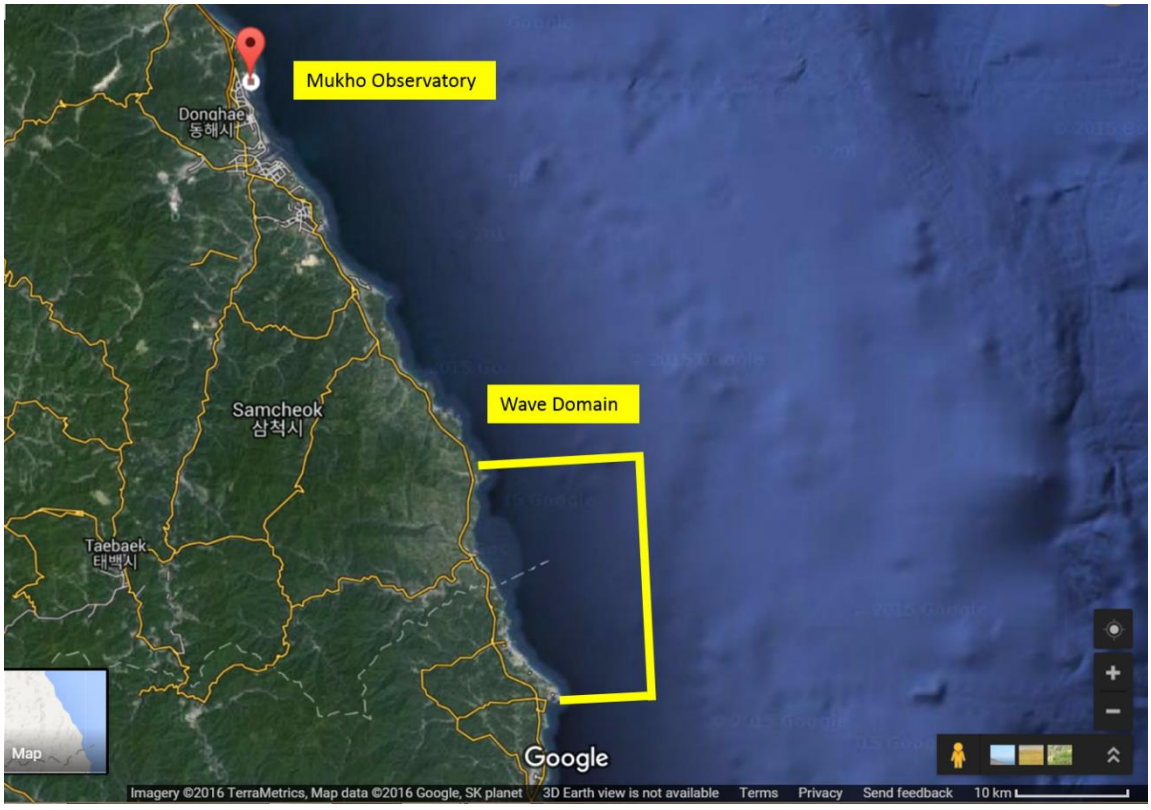

Figure 29. Location of the Mukho observatory

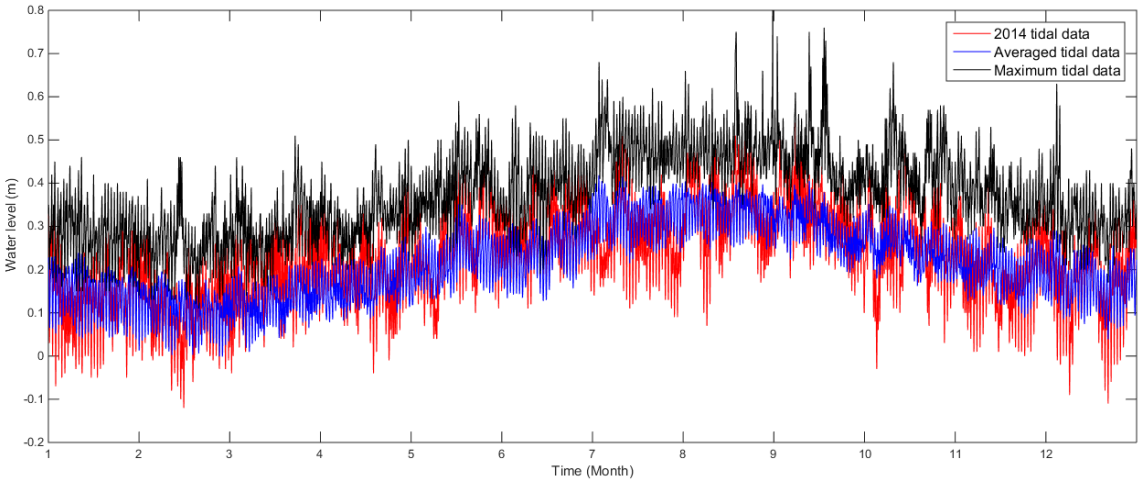

Figure 30. Comparison graph of fluctuation of the tidal level for three cases

In similarity with the wind data, the variation of averaged data is relatively small to the data from the other two cases. The tendency of averaged data shows that the water level is decreased during autumn and winter, and increased during spring and summer.

2.3.3.3 Wave data

Wave data are only input to the WAVE module. Like wind and tidal data, wave data are also introduced as the above mentioned forms of the three cases. These data are comprised of eight data which are hourly time point, significant wave height, peak period of energy spectrum, mean wave direction, width energy distribution, additional water level, wind speed at 10m elevation, and wind direction. Wave information from the Donghae buoy is also used.

From Figure 31 to Figure 39, these pictures sequentially describe wave data information depending on different three meteorological data.

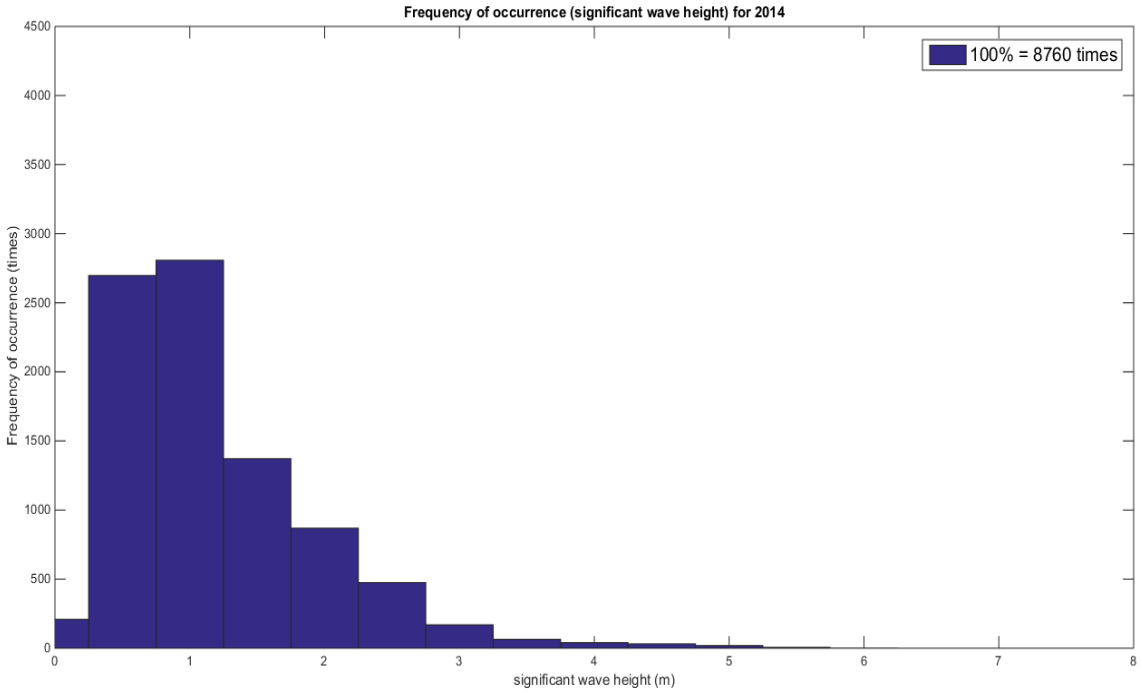

Figure 31. Histogram of significant wave heights for the year 2014

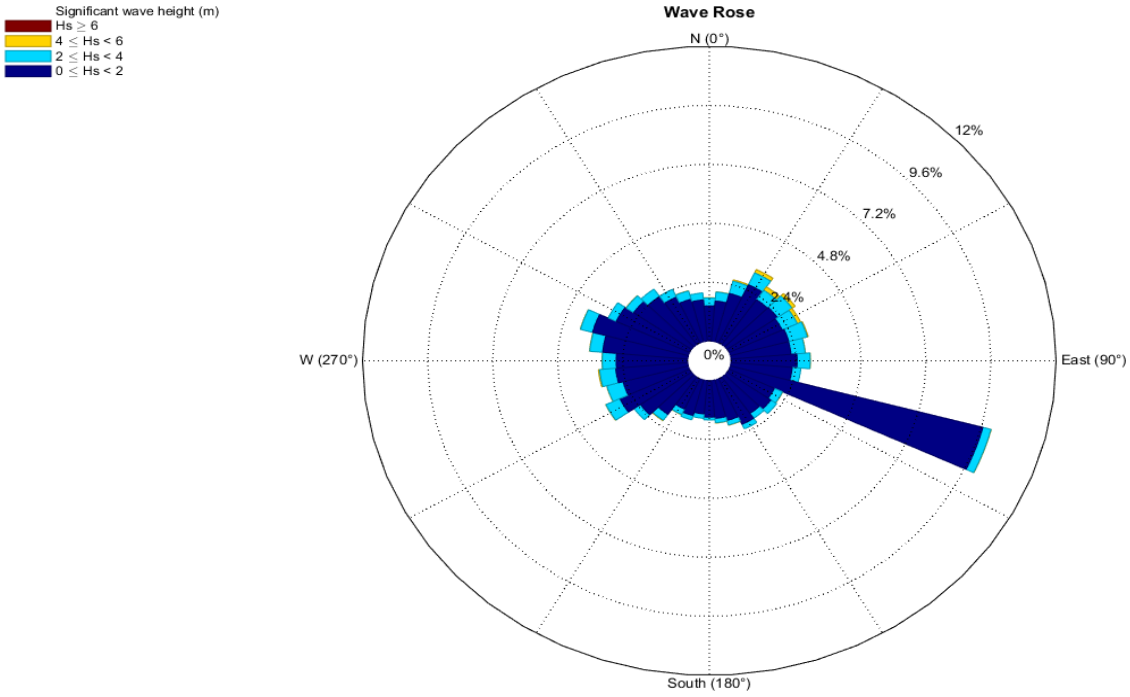

Figure 32. Wave rose of significant wave heights for the year 2014

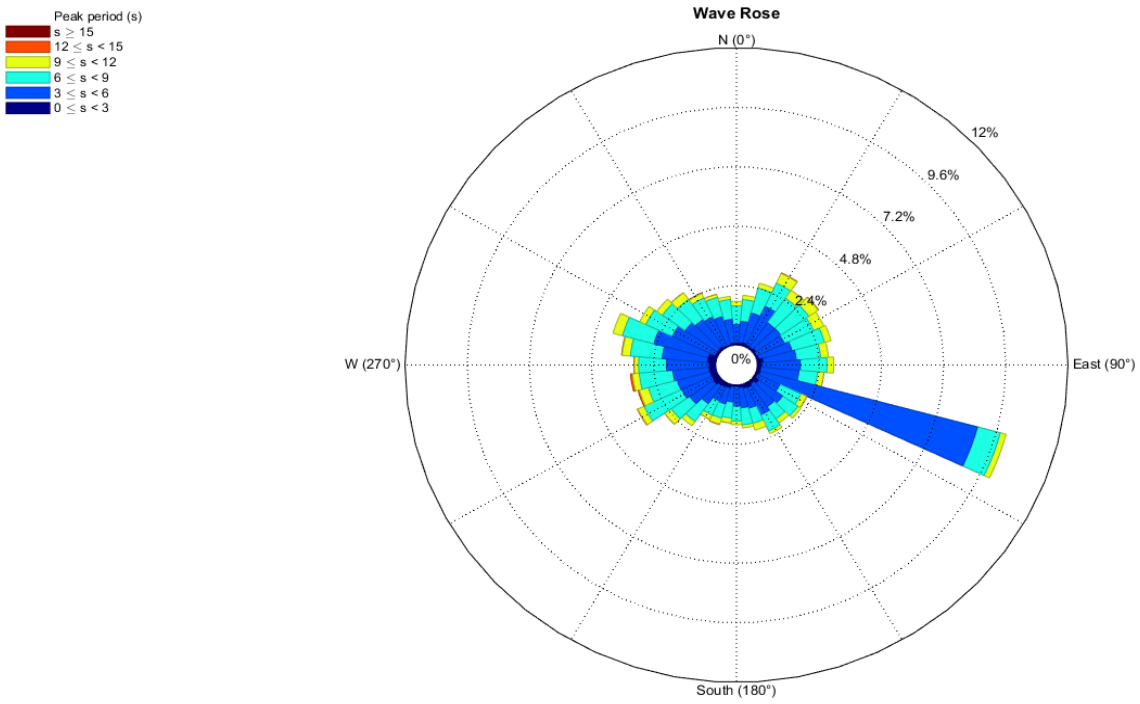

Figure 33. Wave rose of peak periods for the year 2014

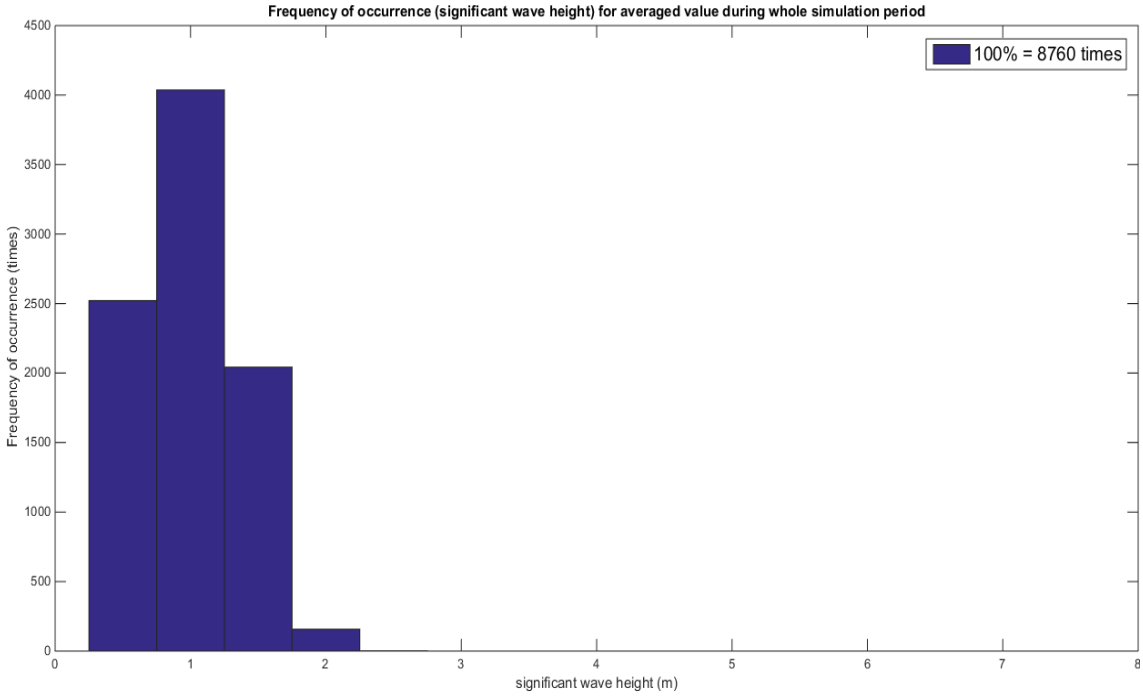

Figure 34. Histogram of significant wave heights for averaged values

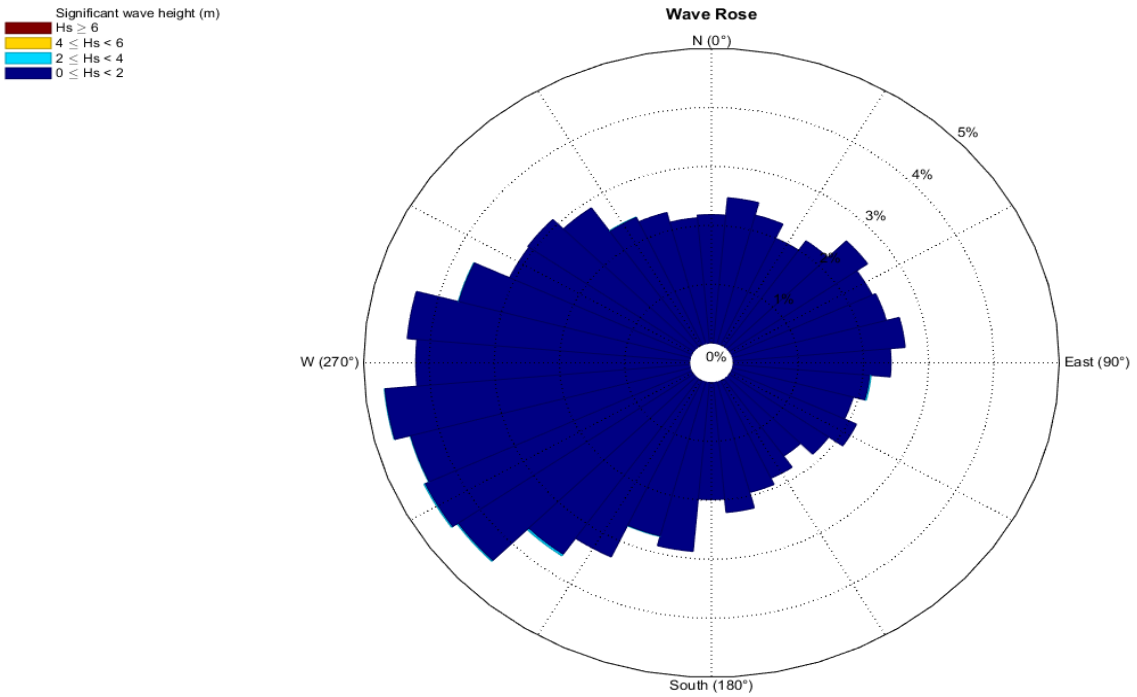

Figure 35. Wave rose of significant wave heights for averaged values

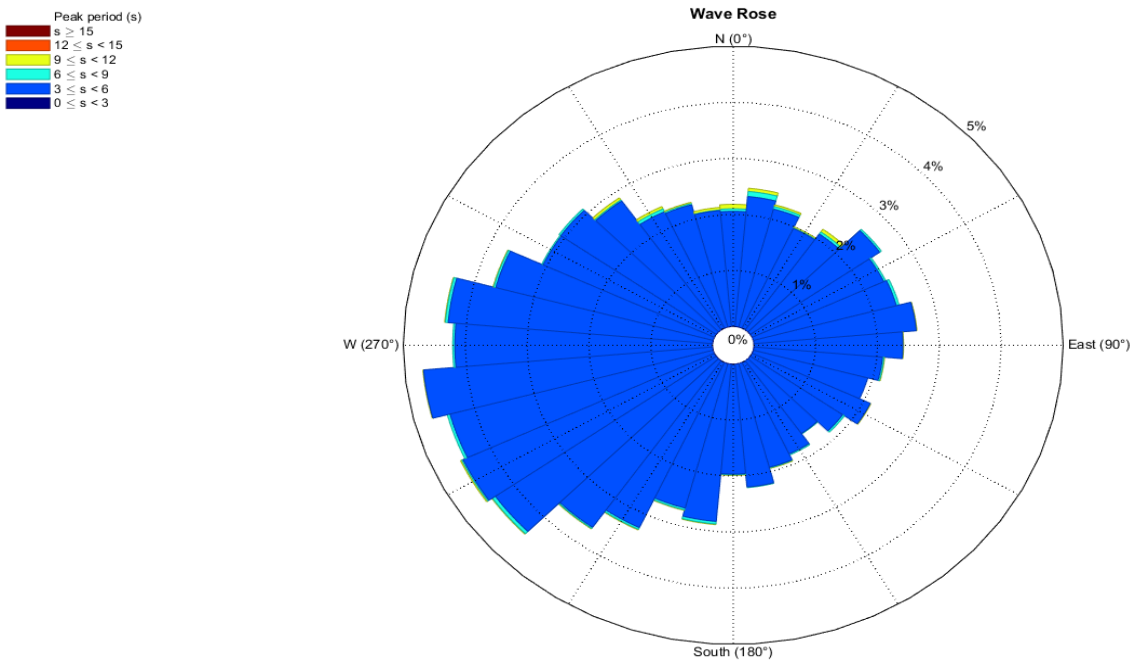

Figure 36. Wave rose of peak periods for averaged values

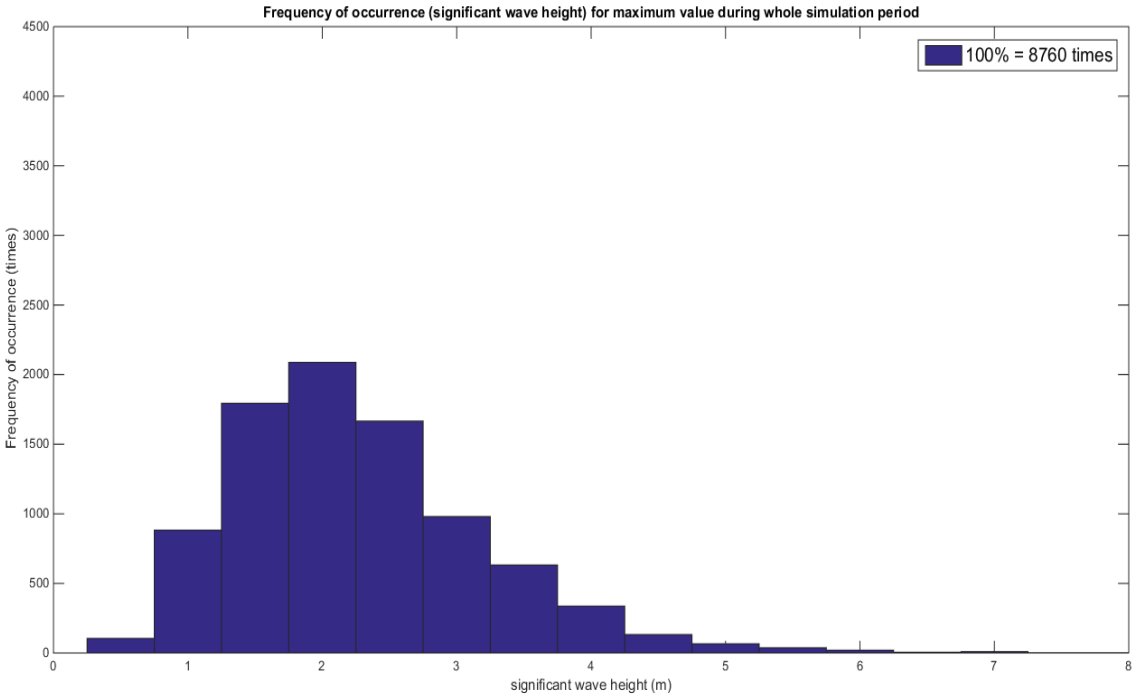

Figure 37. Histogram of significant wave heights for maximum values

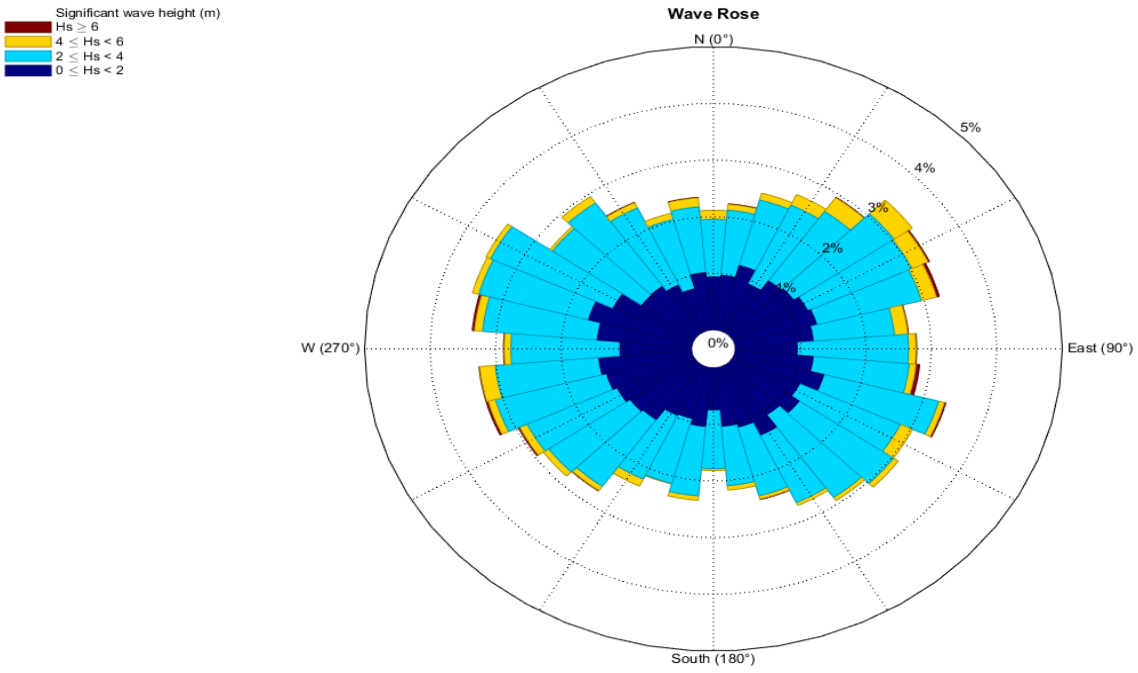

Figure 38. Wave rose of significant wave heights for maximum values

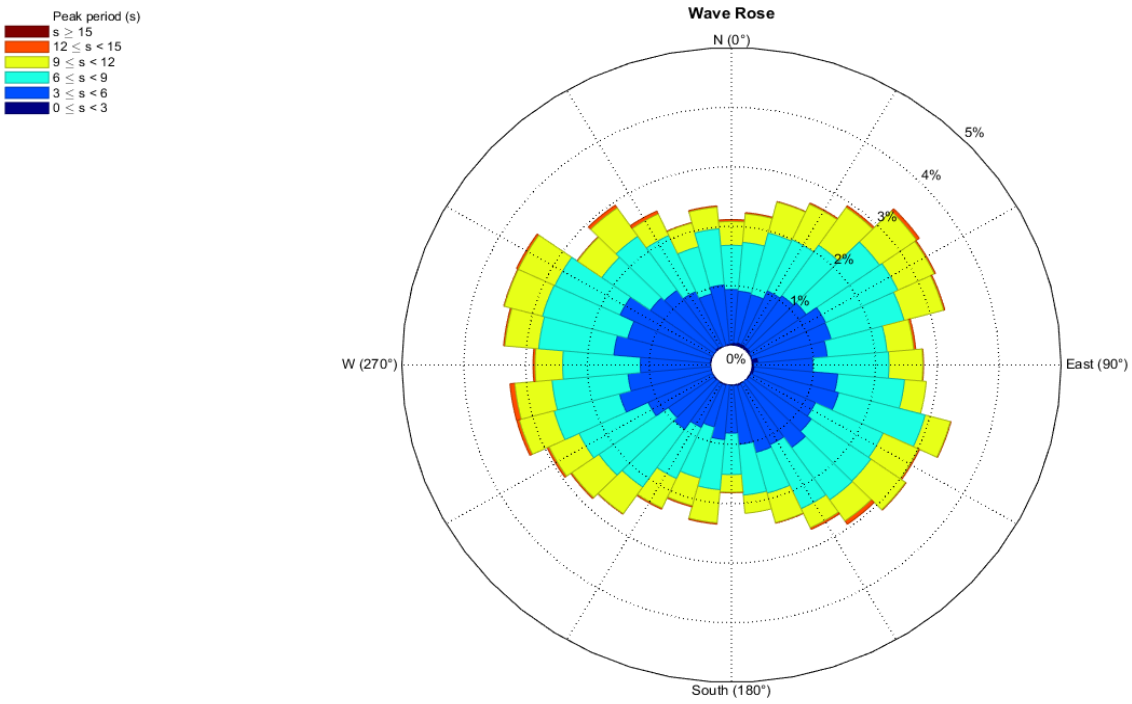

Figure 39. Wave rose of peak periods for maximum values

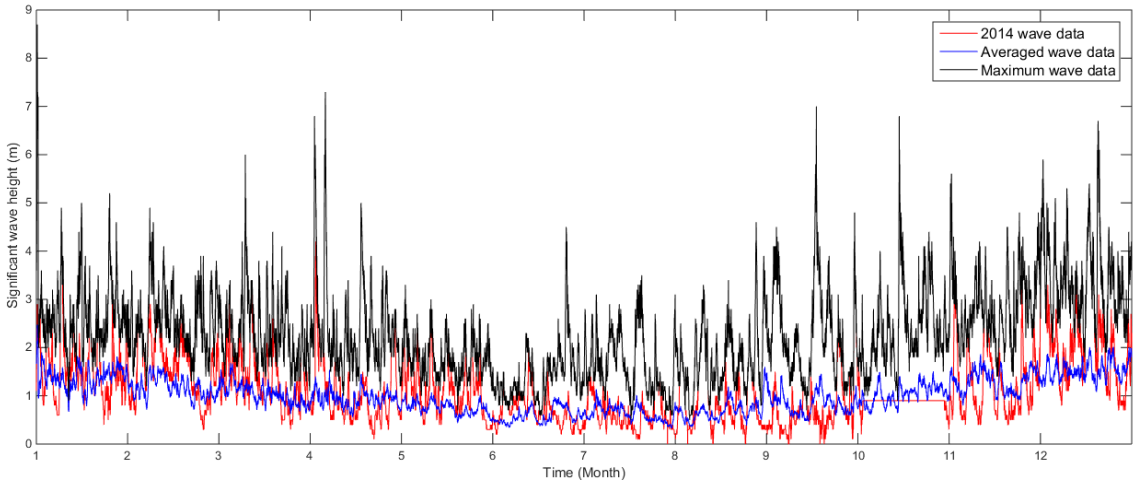

Figure 40. Comparison graph of fluctuation of the significant wave heights for three cases

3 MODEL INVESTIGATION

Firstly, in this section, an amalgamation between the established basic model and three meteorological data, which are (1) data for the year 2014, (2) average-annual data, and (3) maximum-annual data, will be explained. Secondly, it will be discovered which climate data should be used for the most similar model with bathymetric measurement data. Lastly, this section determines which countermeasure is the most effective solution against beach erosion among proposed solutions using concluded climate data.

For comparing the designed models to measured bathymetry from KOGAS, the QUICKPLOT module of the Delft3D is employed so that this module can easily describe the results from the FLOW and the WAVE modules. Moreover, it can simply extract the values in the form of the mat file to use for the Matlab program. Therefore, all graphs in this section are plotted using Matlab.

The point-to-point comparison of the bathymetry method is applied in this study because our work is focused on the variation of specific points. Thus, spatial changes in the entire domain are not considered. The rationale behind this is that an ultimate goal of this study is to solve beach erosion problems at Wolcheon Beach caused by human activities for the local residents and environment. For these reasons, all eight points of comparison are the nearest locations to the Wolcheon Beach in the FLOW domain. Figure 40 shows the relationship of the grid points in the FLOW grid with the topographical map.

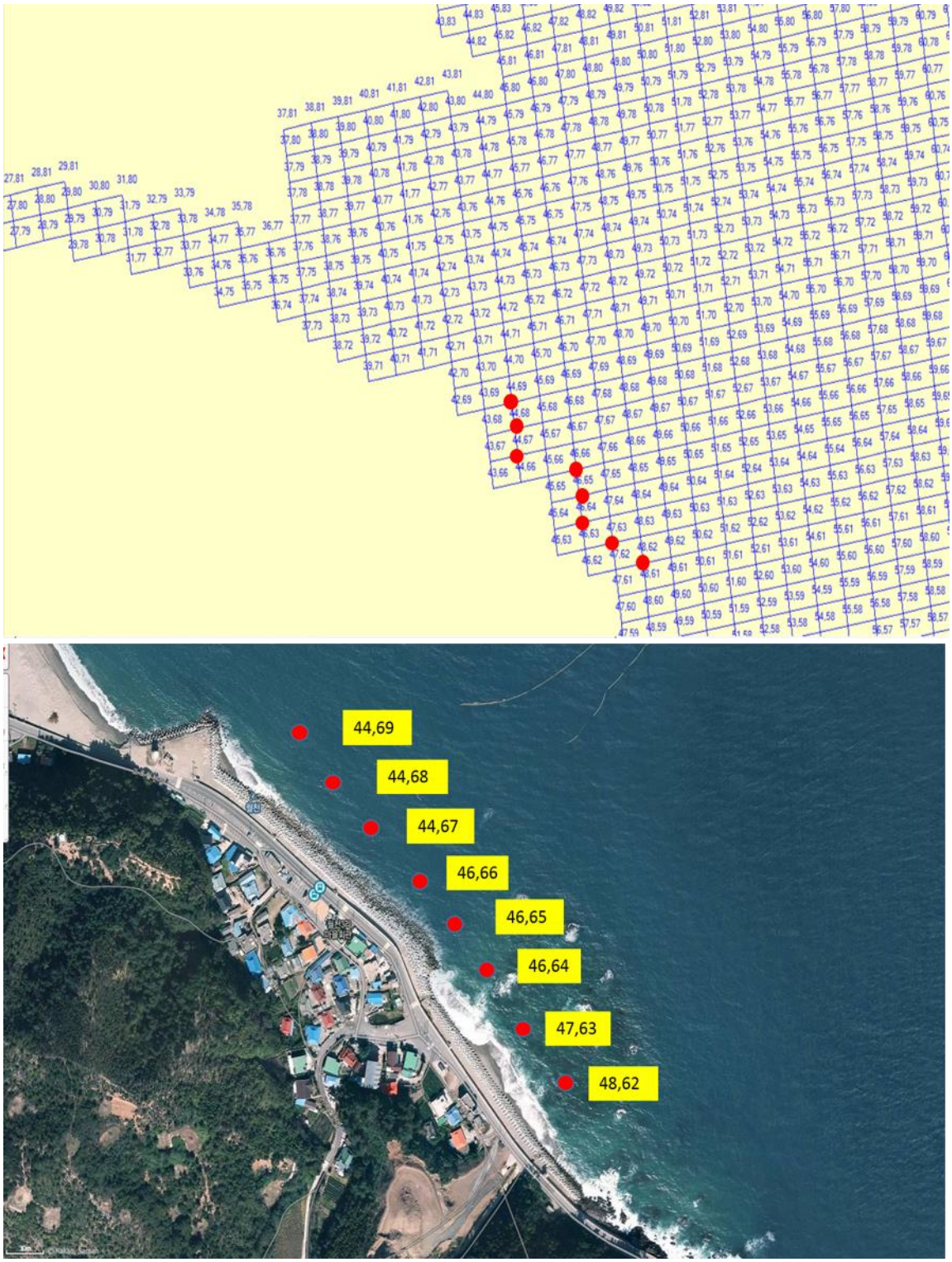

Figure 41. Locations of comparison points

3.1 Selection of proper meteorological data

Measured bathymetric data from KOGAS are comprised of 5 sets: (1) September, 2009 (before construction), (2) March, 2014, (3) June, 2014, (4) September, 2014, and (5) December, 2014. Among these data, (1) is used for the incipient depth for the FLOW grid, and other measurements are implemented to directly compare the annual models' results. The bathymetry of the models is simulated every two hours during the entire simulation period which is one year.

3.1.1 Results comparison according to different meteorological cases

Figure 42 to Figure 49, display the measured water depth versus the results from the above mentioned three different meteorological models.

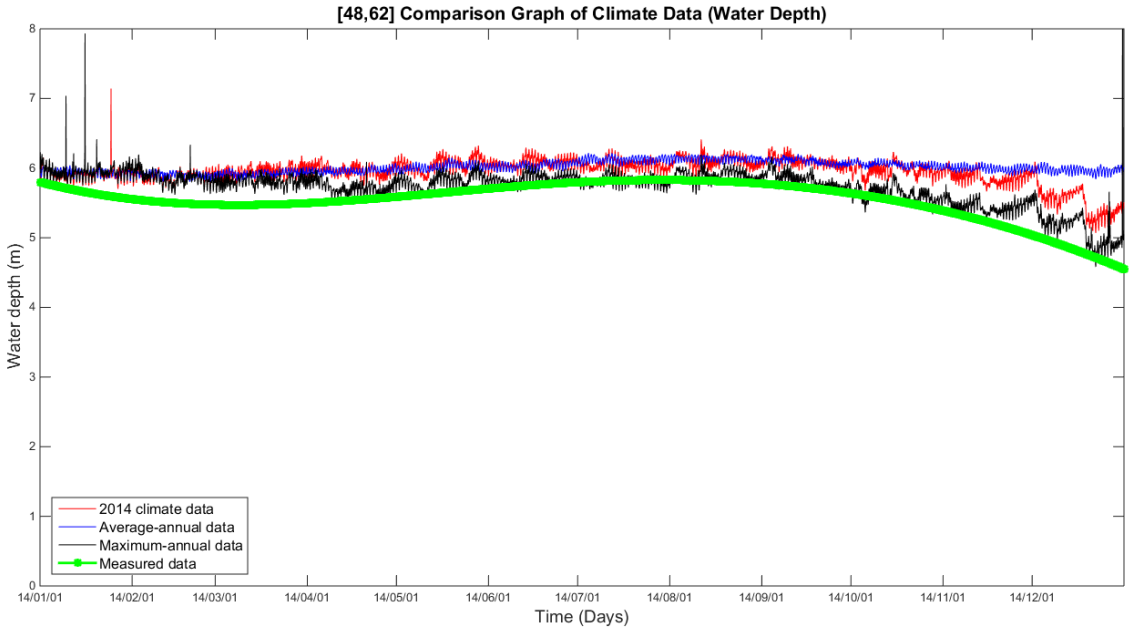

Figure 42. Comparison graph of meteorological data for [48, 62]

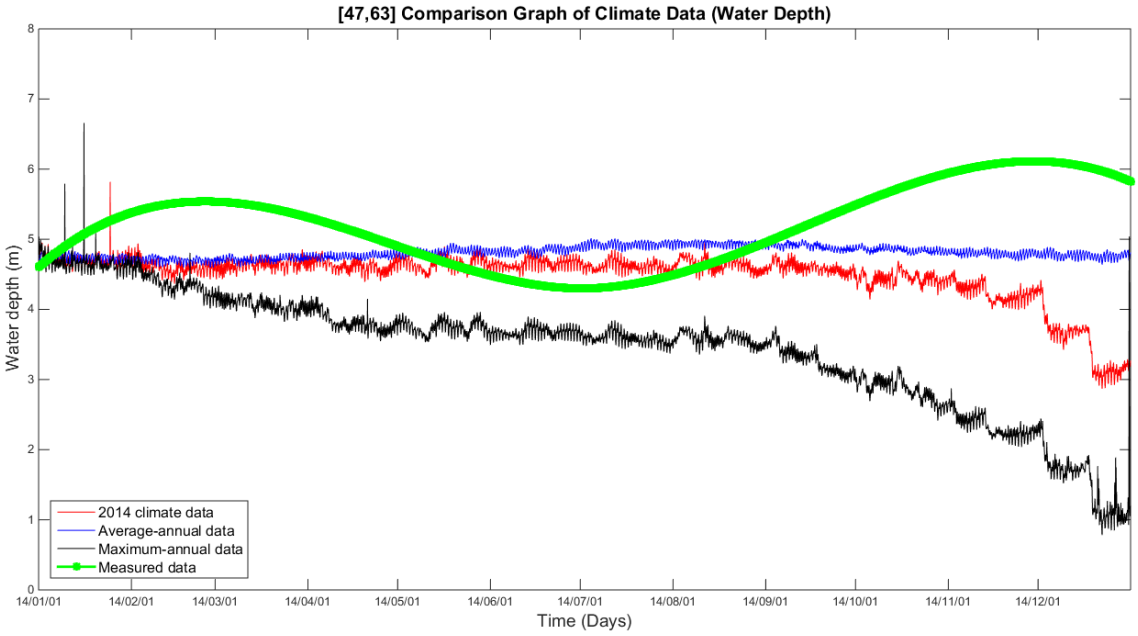

Figure 43. Comparison graph of meteorological data for [47, 63]

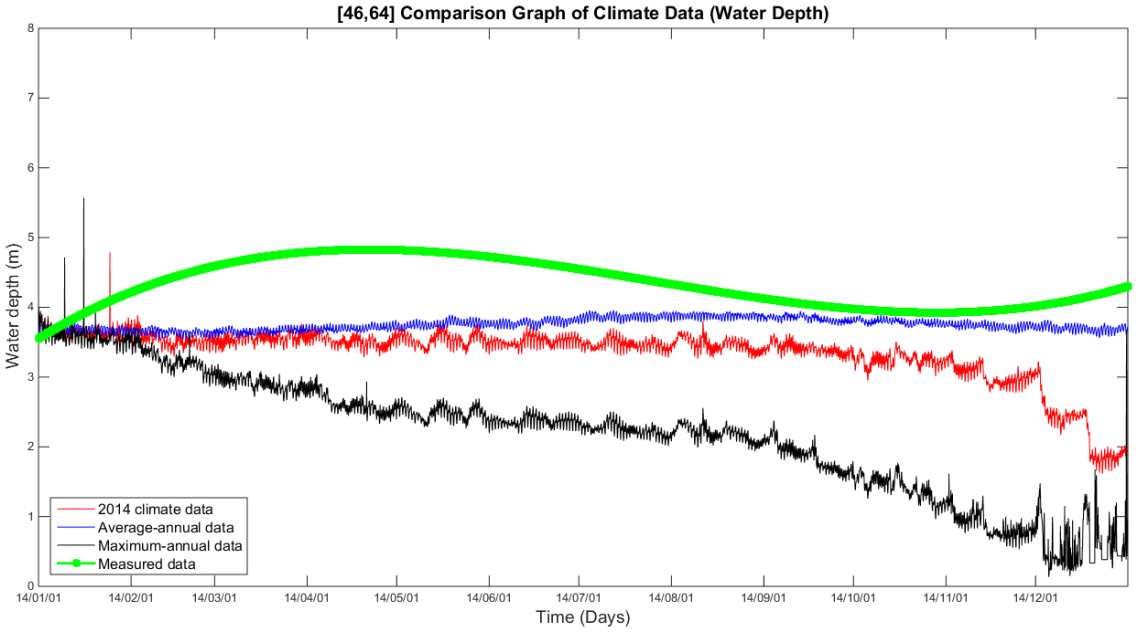

Figure 44. Comparison graph of meteorological data for [46, 64]

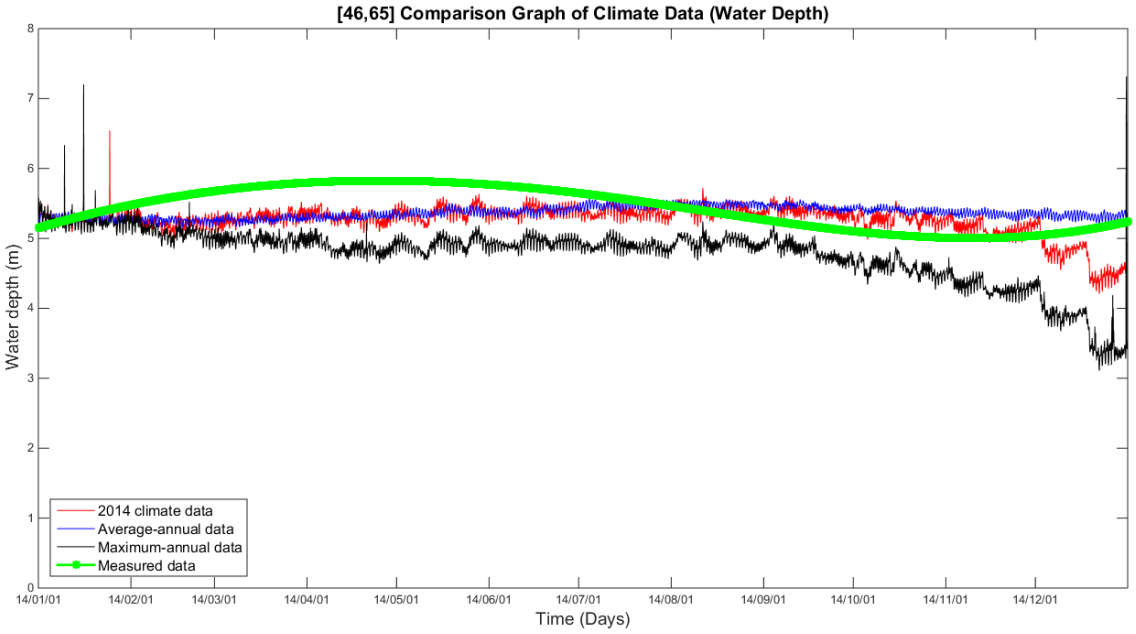

Figure 45. Comparison graph of meteorological data for [46, 65]

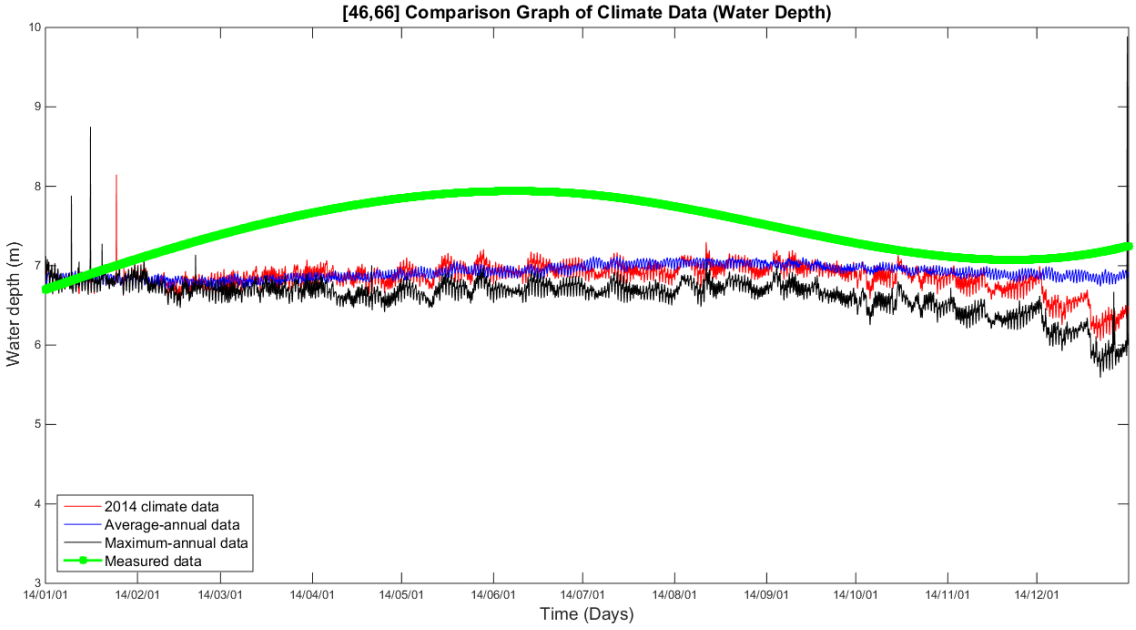

Figure 46. Comparison graph of meteorological data for [46, 66]

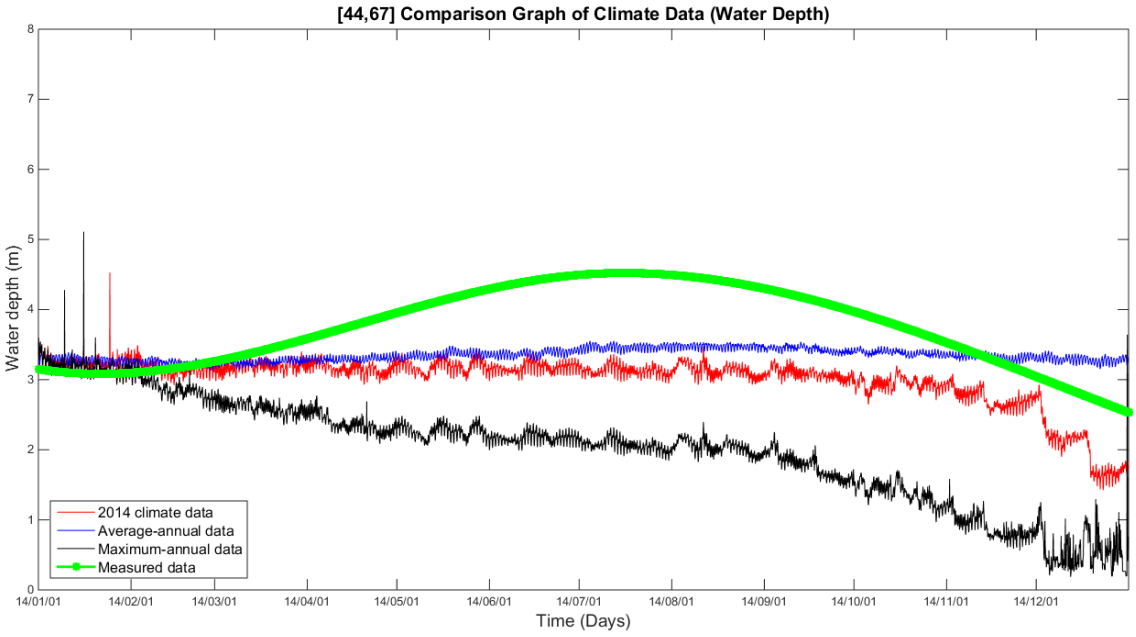

Figure 47. Comparison graph of meteorological data for [44, 67]

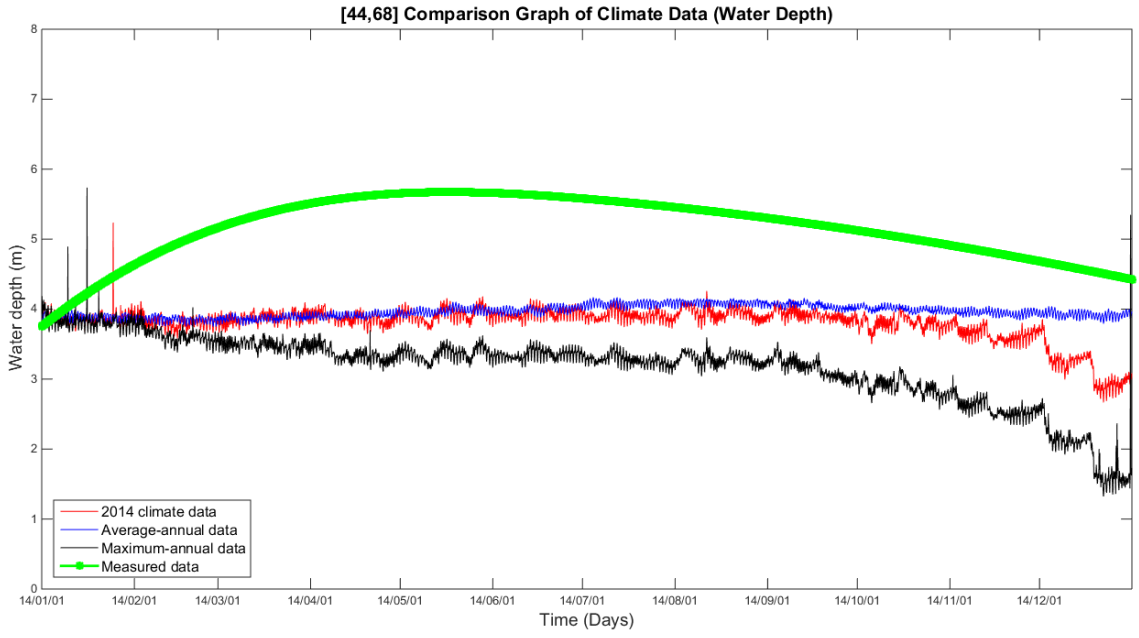

Figure 48. Comparison graph of meteorological data for [44, 68]

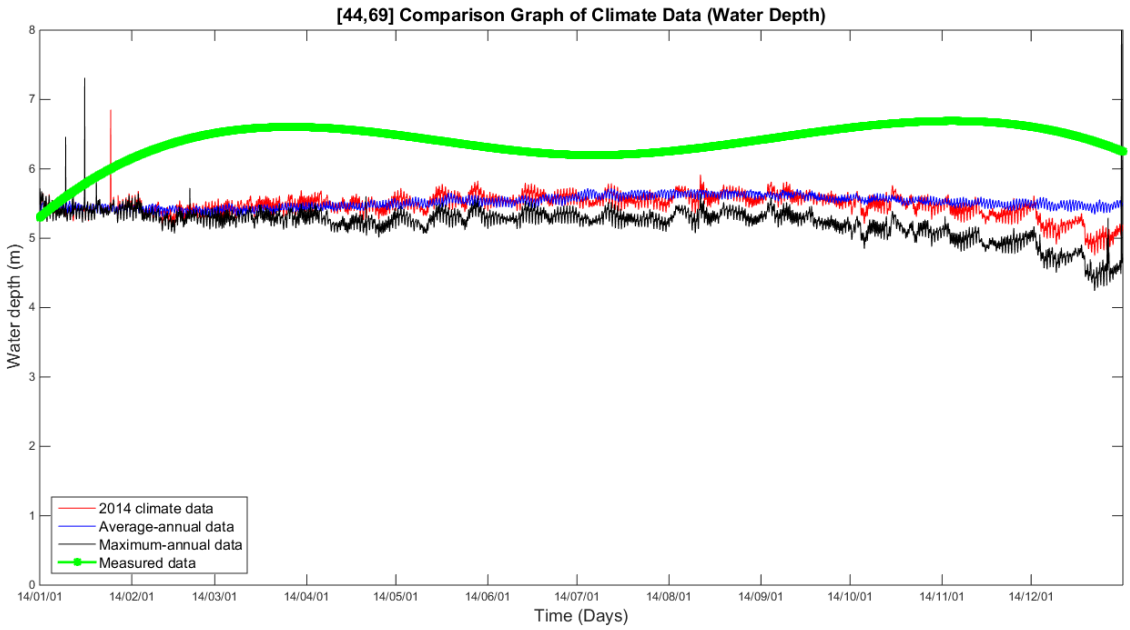

Figure 49. Comparison graph of meteorological data for [44, 69]

The average-annual data shows a more stable tendency of the water depths than data for the year 2014 and maximum-annual data. It can be anticipated from the wind, wave and tidal sources of the amplitude from averaged data that minor differences of the amplitude conclude more constant wave energy forcing to the nearshore area. Therefore, the maximum variation of the water depths from average-annual data is approximately 40cm, but in the case of maximum-annual data, its difference between the lowest water depth and the highest water depth is approximately 4m. Additionally, the year 2014's climate data indicates that its maximum deviation is approximately 2m.

At a first glance of the all comparison graphs, the model using average-annual data is the most suitable to the measured data, but there are discrepancies between the model and the real field data. There are several possible reasons for this:

(1) A few measurement sources of the bathymetric survey (five data points in a year); to evaluate every two hours bathymetric data, spline function in Matlab is used for making direct comparison. This interpolation function might generate mathematical errors;

(2) Inaccuracies in the meteorological data by faults at the measurement facilities;

(3) Single buoy information; this assumes a uniform wave and wind on the boundary;

(4) Different definition of direction; wave direction from the Donghae buoy is the direction of peak wave frequency, but mean wave direction is implemented in the WAVE module. That means, the average direction of the entire spectral domain is used for establishing the models.

3.1.2 Error analysis

A root mean square error method (hereafter RMSE) is used to determine the discrepancies a model exhibits with measured data. In this section, RMSE values at eight observational grid points of the three meteorological data are represented. The scatter plots for both measured water depth versus the modeled water depth are presented in from Figure 50 to Figure 57.

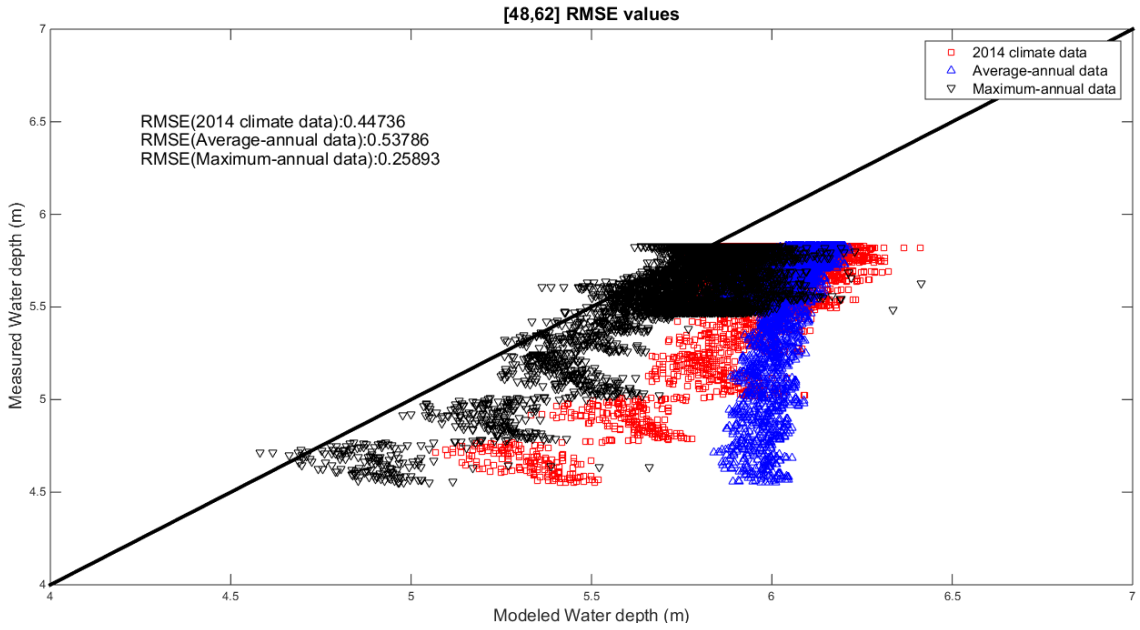

Figure 50. Comparison RMSE graph for [48, 62]

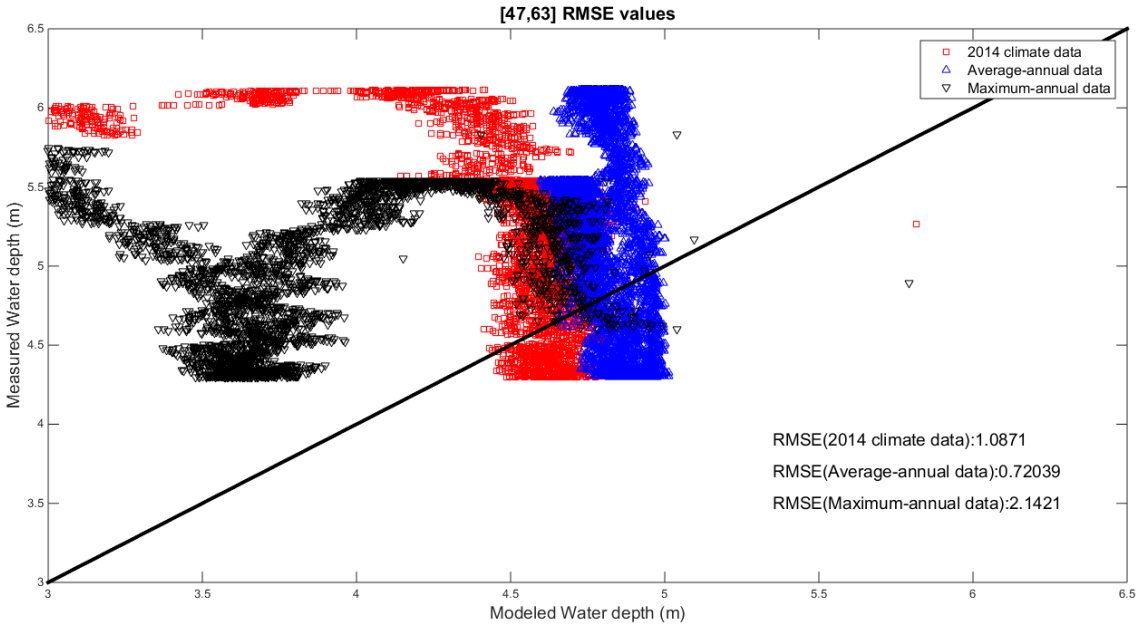

Figure 51. Comparison RMSE graph for [47, 63]

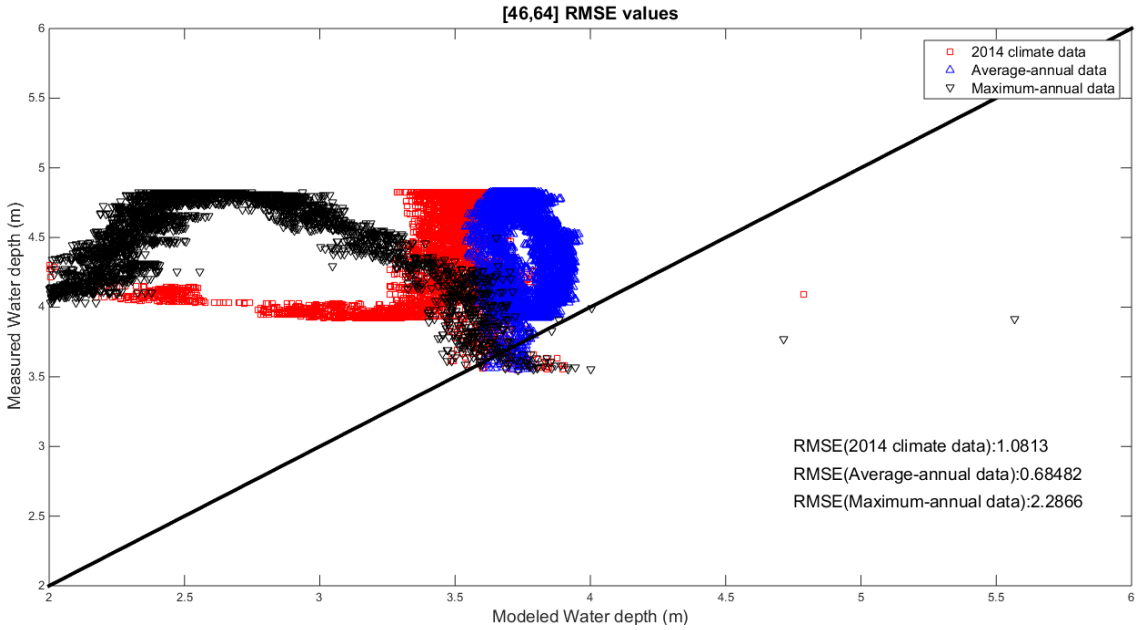

Figure 52. Comparison RMSE graph for [46, 64]

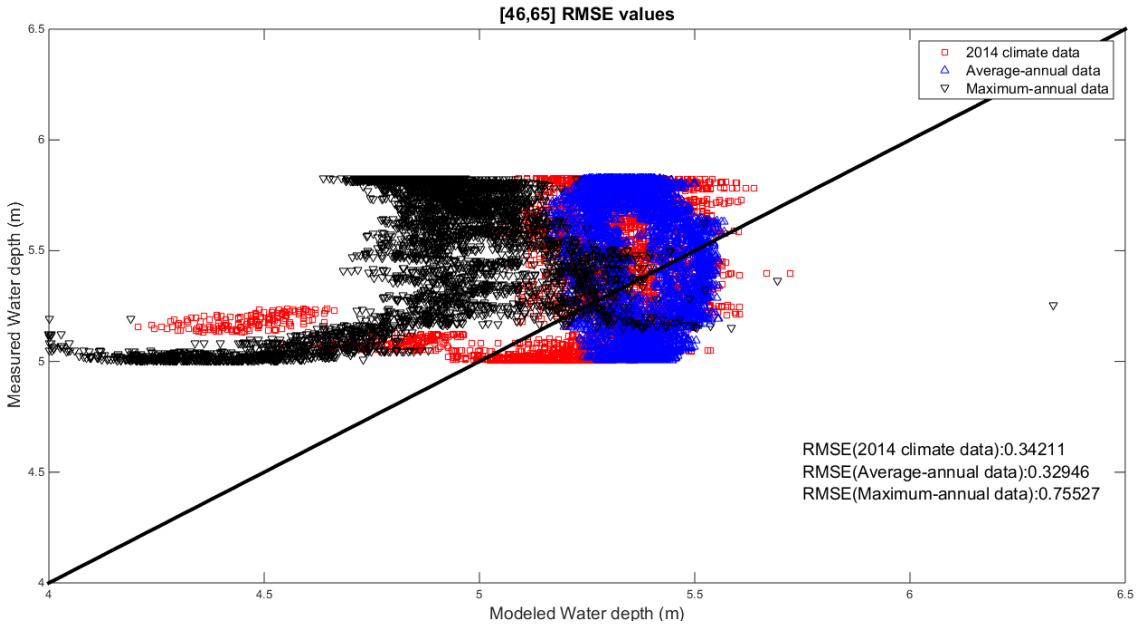

Figure 53. Comparison RMSE graph for [46, 65]

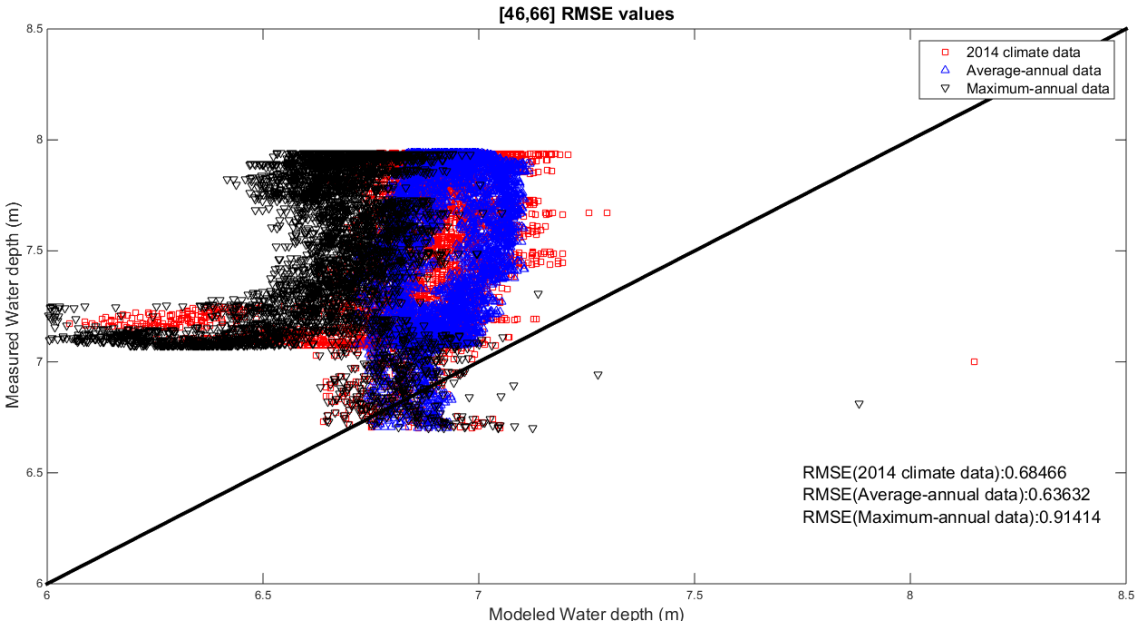

Figure 54. Comparison RMSE graph for [46, 66]

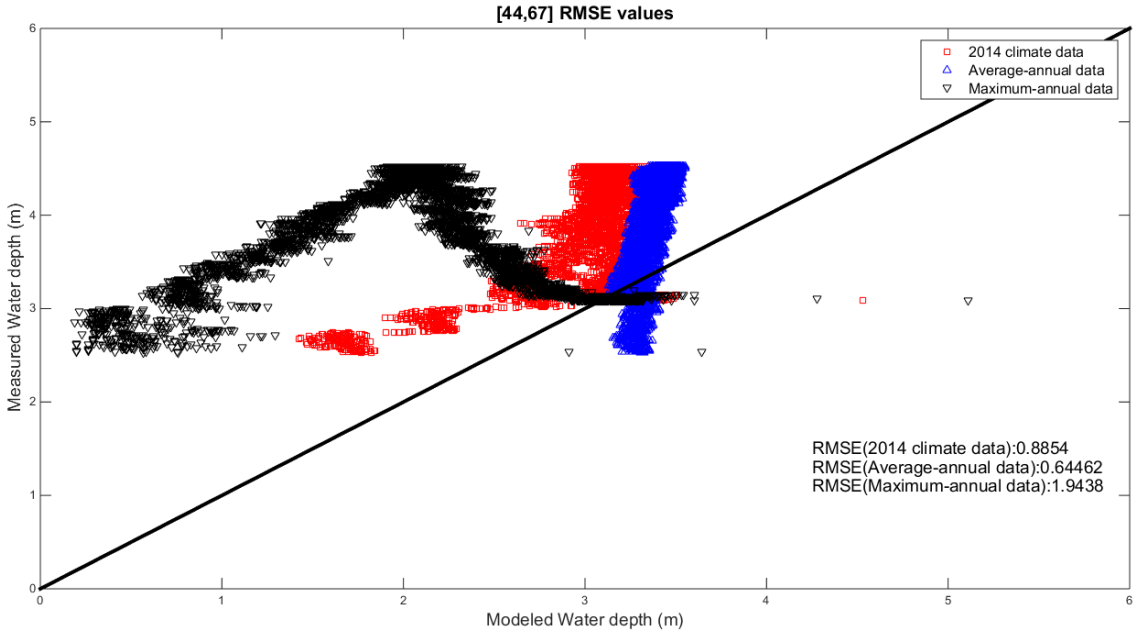

Figure 55. Comparison RMSE graph for [44, 67]

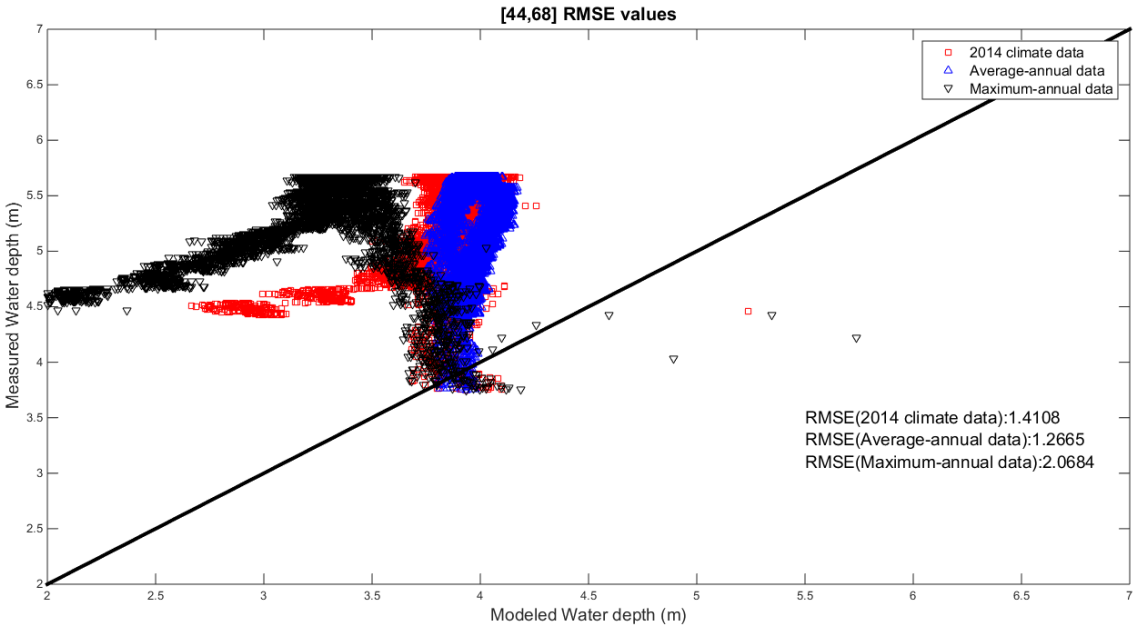

Figure 56. Comparison RMSE graph for [44, 68]

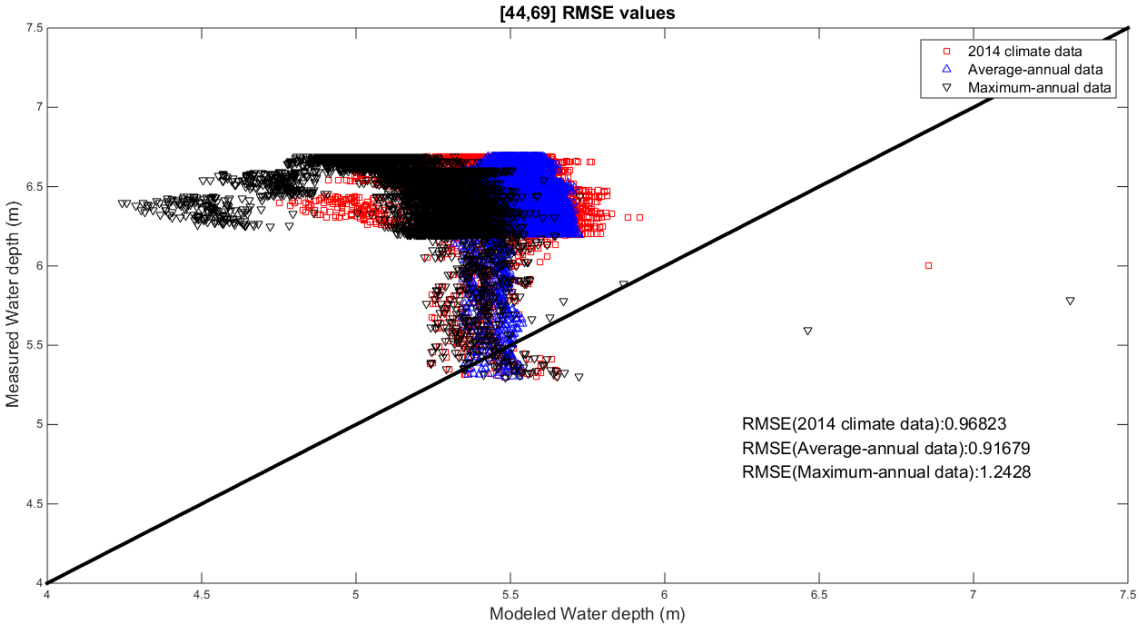

Figure 57. Comparison RMSE graph for [44, 69]

3.1.3 Conclusion

Through error analysis, it can be seen that average-annual data can reproduce the most reliable results. This fact can be reinforced by section 3.1.1, and the arranged RMSE results that are shown in Table 13 are also a good example. Therefore, the analysis of the nine proposed solutions will be based on the average-annual data model.

Table 13. RMSE results (water depths) for each grid point

Grid points	Incipient water depth (m)	RMSE (m)		
		Case 1 (2014)	Case 2 (Average-annual)	Case 3 (Maximum-annual)
48, 62	5.8	0.4474	0.5379	0.2589
47, 63	4.6	1.0871	0.7204	2.1421
46, 64	3.55	1.0813	0.6848	2.2866
46, 65	5.15	0.3421	0.3295	0.7553
46, 66	6.7	0.6847	0.6363	0.9141
44, 67	3.15	0.8854	0.6446	1.9438
44, 68	3.75	1.4108	1.2665	2.0684
44, 69	5.3	0.9682	0.9168	1.2428
Average Value	4.75	0.8634	0.7171	1.4515

3.2 Comparison of proposed countermeasures

Weathers and Voulgaris (2013) argued that most countermeasures for beach erosion can be divided into four solutions: “(1) hard stabilization (i.e. groins, jetties, sea walls, etc.), (2) soft stabilization (i.e. beach replenishment, inlet relocations, etc.,) (3) natural retreat of shoreline (i.e. no action), and (4) when needed, relocation of affected communities” (84). Historically, two countermeasures, hard stabilization and soft stabilization, have widely been used to manage beach erosion all over the world.

Therefore, there are two hard engineering and one soft engineering in this study. To be specific, hard engineering is comprised of submerged breakwaters and groins, and the method for soft engineering is beach nourishment. These countermeasures will perform in concert or respectively.

3.2.1 General explanation

KOGAS (2014) proposed a detail concept of each countermeasure in Table 14, and the nine countermeasures (Case A ~ Case I) are represented in Figure 58 ~ 66. The numbers in the red circles indicate grid points of the FLOW domain in Figure 41. All submerged breakwaters are comprised of 25Ton tetrapods two layers, and all groins are mainly made of riprap below 0.03m^3 with armor stones and 25Ton tetrapods. In the case of nourishment, a grab dredger with a bucket of 7.5m^3 is considered for both dredging and dumping. Additionally, from Figure 67 to Figure 74 represent a cross section view of the submerged breakwater and the groin. A location and size of groins for Case H and Case I are equal to the groins of Case F.

Table 14. Detail description of the nine countermeasures

	Countermeasure type	Description
Case A	Do Nothing	No countermeasure
Case B	2 Submerged breakwaters + nourishment	North submerged breakwater: width: 40m, length: 200m South submerged breakwater: width: 40m, length: 100m Nourishment: 248,000 m^3
Case C	2 Submerged breakwaters + nourishment + 1 north groin	North submerged breakwater: width: 40m, length: 200m South submerged breakwater: width: 40m, length: 100m Nourishment: 248,000 m^3 Groin: width: 10m, length: 124m
Case D	2 Submerged breakwaters + nourishment + 1 south groin	North submerged breakwater: width: 40m, length: 200m South submerged breakwater: width: 40m, length: 100m Nourishment: 248,000 m^3 Groin: width: 10m, length: 124m
Case E	2 Submerged breakwaters + nourishment + 2 groins	North submerged breakwater: width: 40m, length: 200m South submerged breakwater: width: 40m, length: 100m Nourishment: 248,000 m^3 2 groins: width: 10m, length: 62m (per each)
Case F	2 Submerged breakwaters + nourishment + 3 groins	North submerged breakwater: width: 40m, length: 200m South submerged breakwater: width: 40m, length: 100m Nourishment: 248,000 m^3 3 groins: width: 10m, length: 62m (per each)
Case G	Nourishment	Nourishment: 248,000 m^3
Case H	Nourishment + 3 groins (62m x 3 units)	Nourishment: 248,000 m^3 3 groins: width: 10m, length: 62m (per each)
Case I	3 groins (62m x 3 units)	3 groins: width: 10m, length: 62m (per each)

Figure 58. Description of Case A

Figure 59. Description of Case B

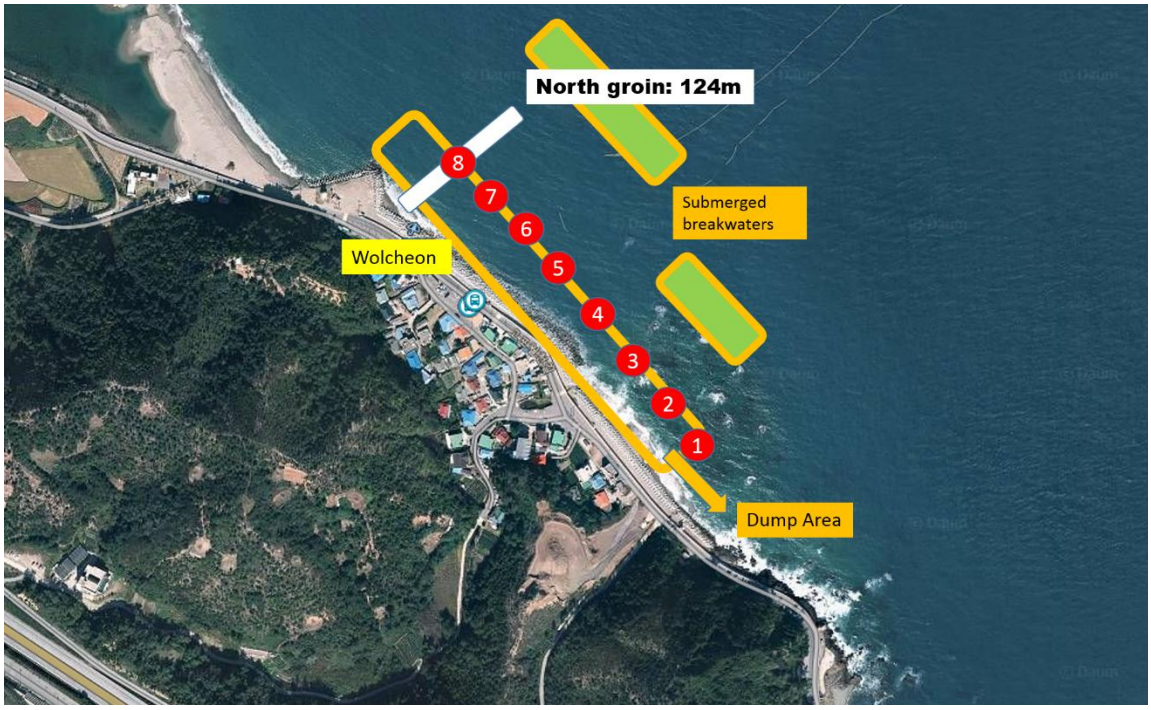

Figure 60. Description of Case C

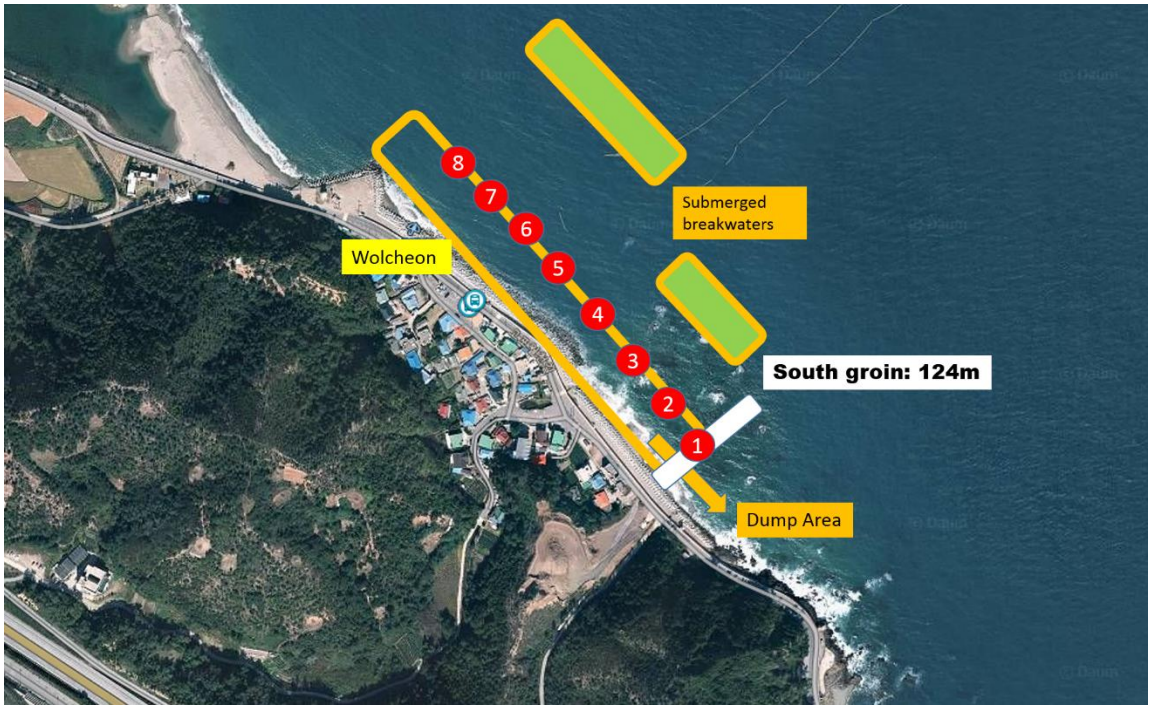

Figure 61. Description of Case D

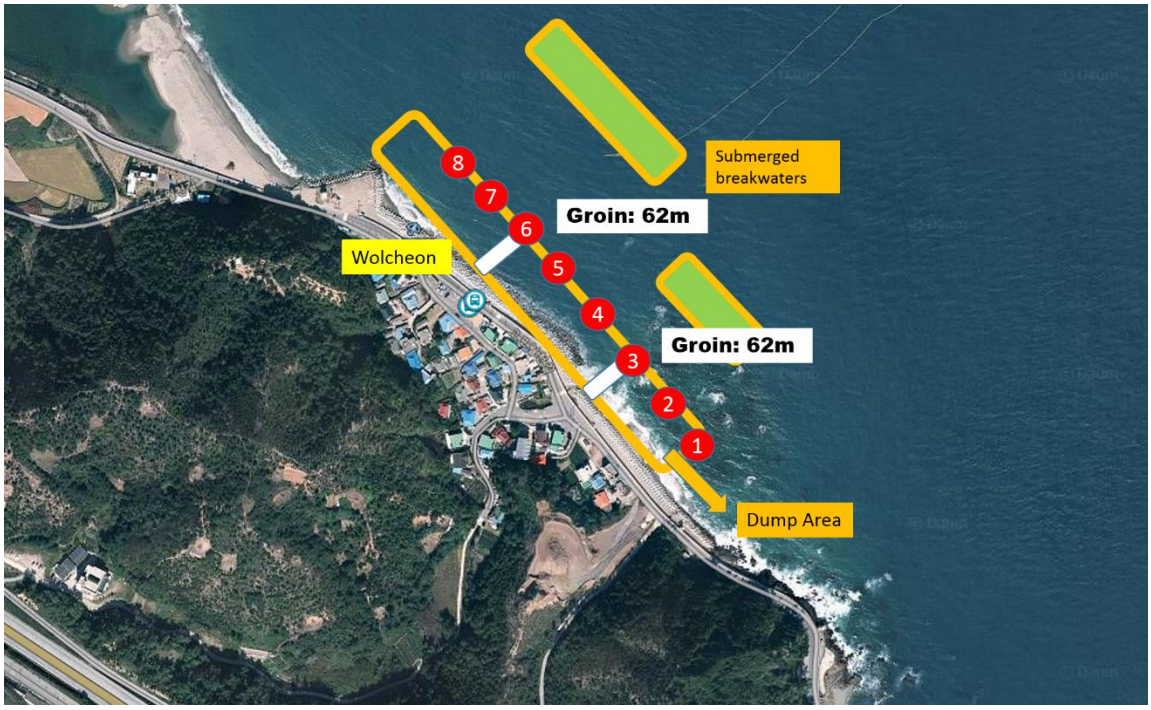

Figure 62. Description of Case E

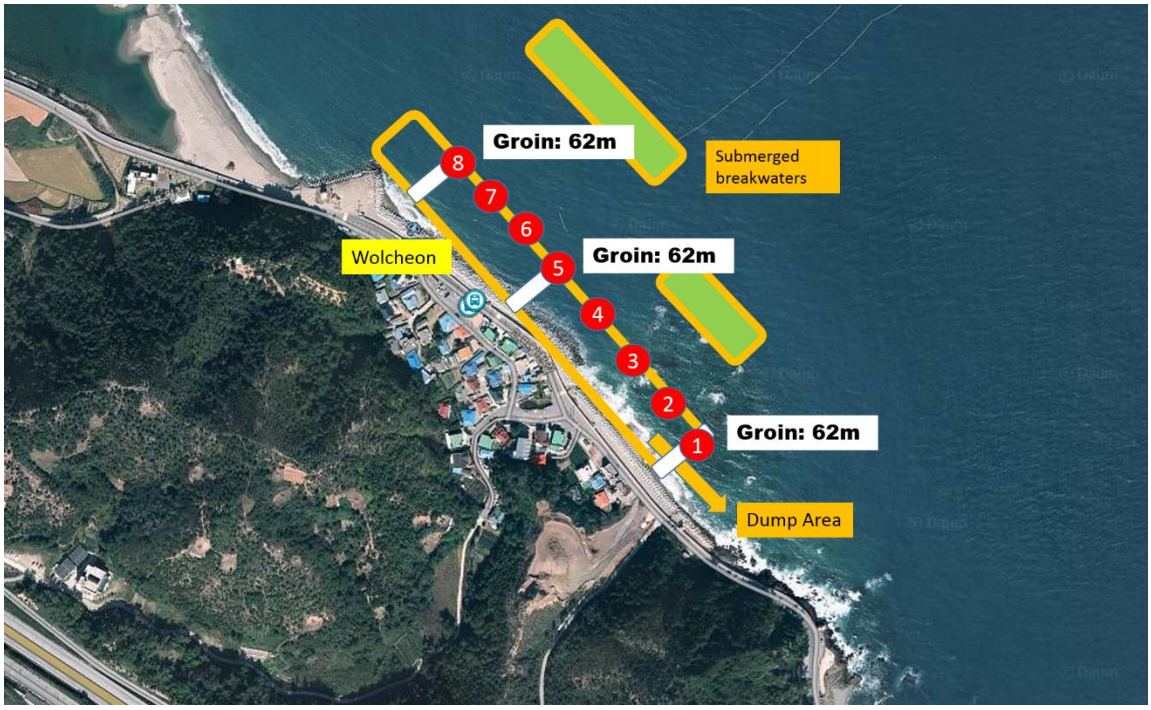

Figure 63. Description of Case F

Figure 64. Description of Case G

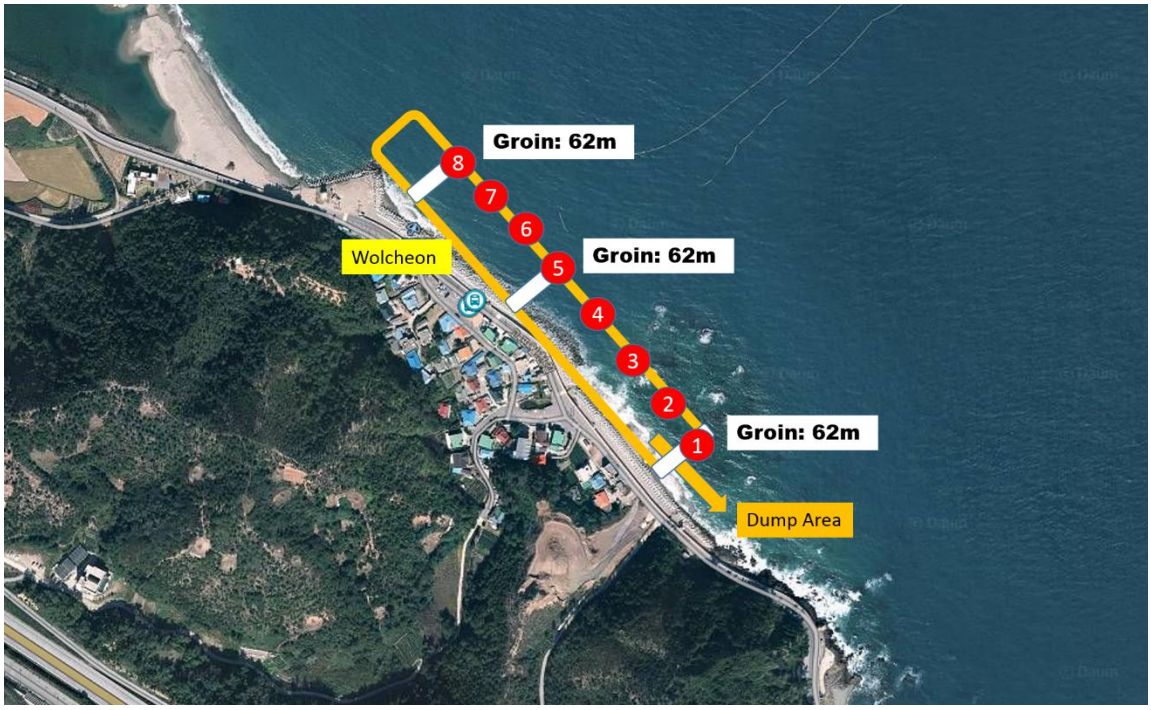

Figure 65. Description of Case H

Figure 66. Description of Case I

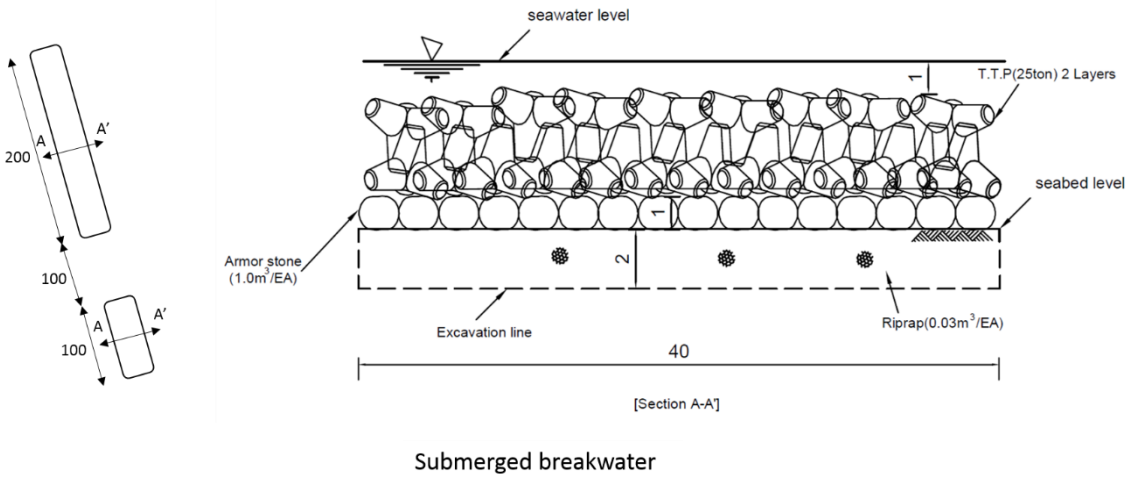

Figure 67. Cross section of submerged breakwaters

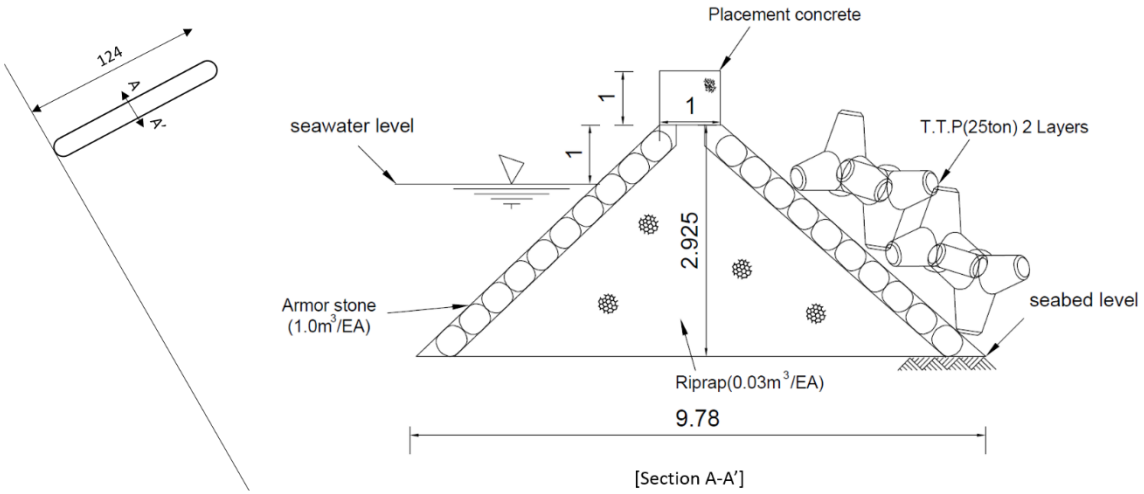

[Case C]

Figure 68. Cross section of north groin in Case C

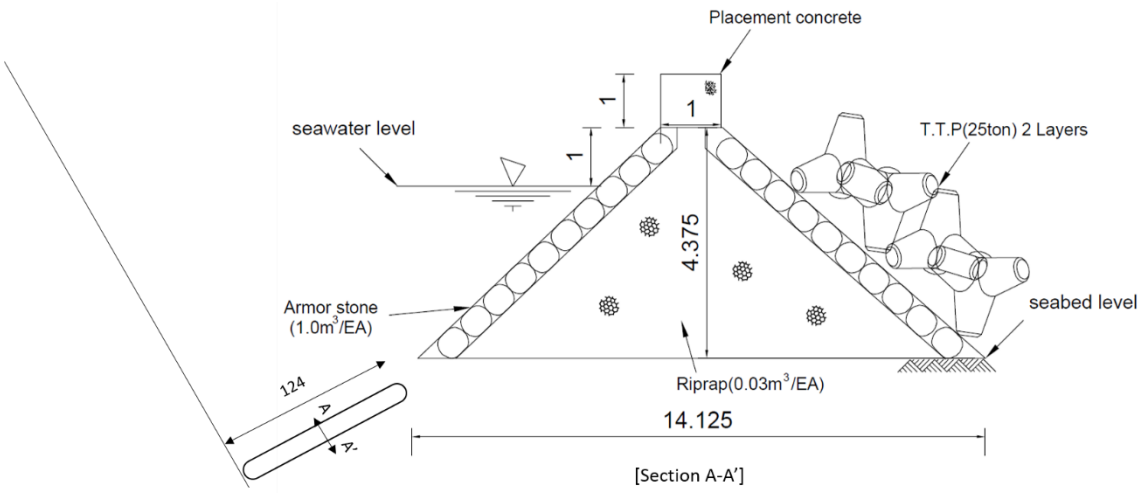

[Case D]

Figure 69. Cross section of south groin in Case D

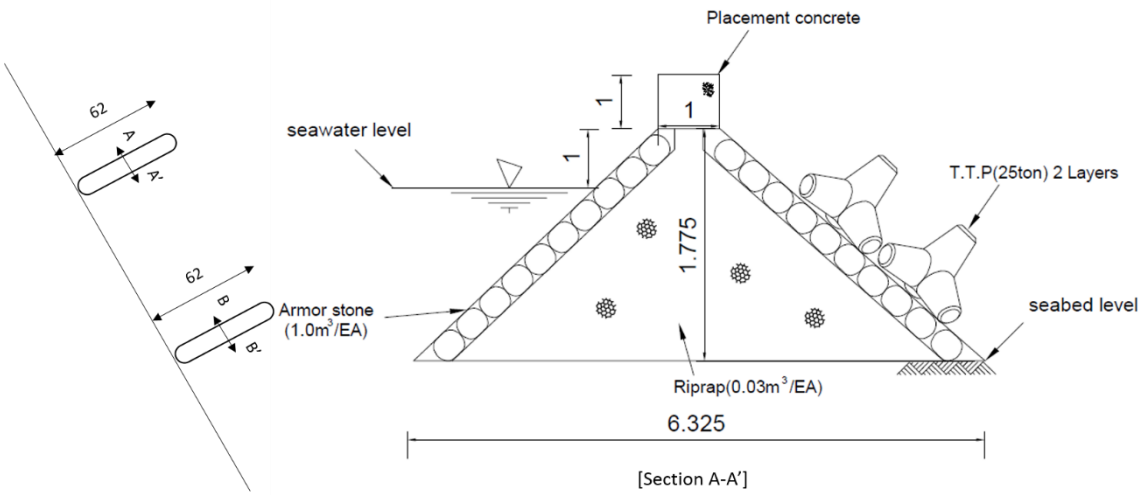

[Case E]

Figure 70. Cross section of north groin in Case E

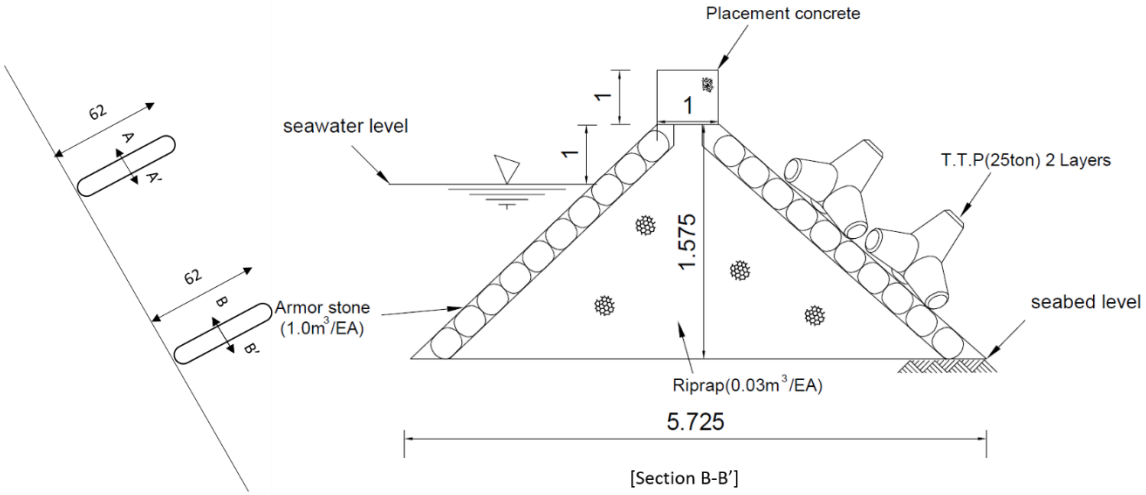

[Case E]

Figure 71. Cross section of south groin in Case E

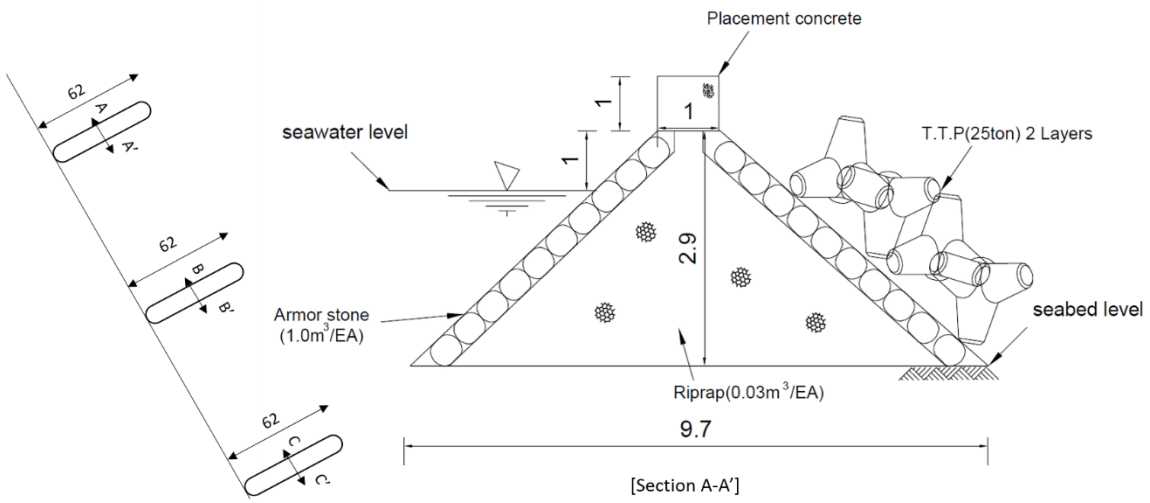

[Case F]

Figure 72. Cross section of north groin in Case F

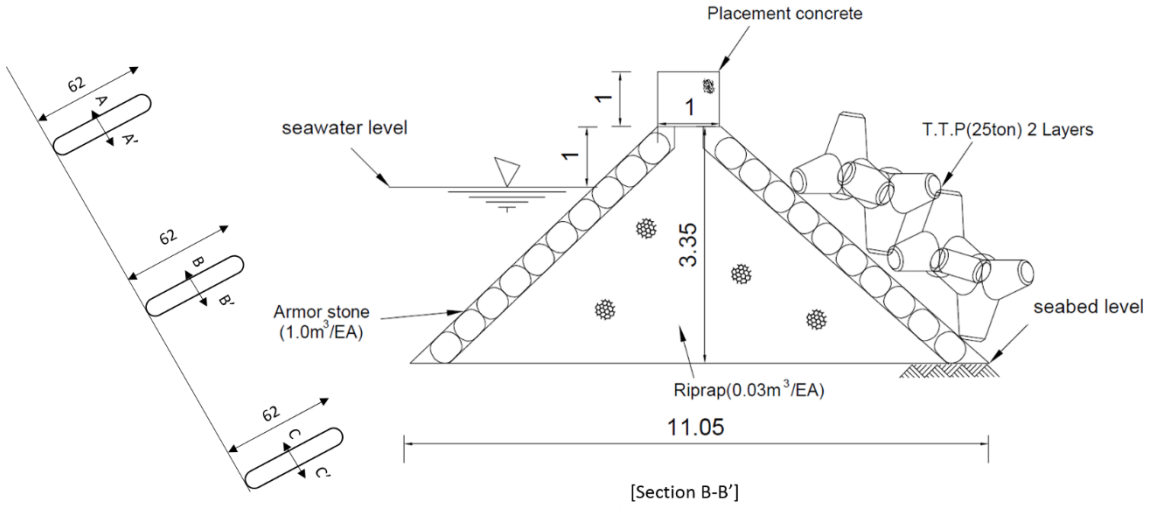

[Case F]

Figure 73. Cross section of middle groin in Case F

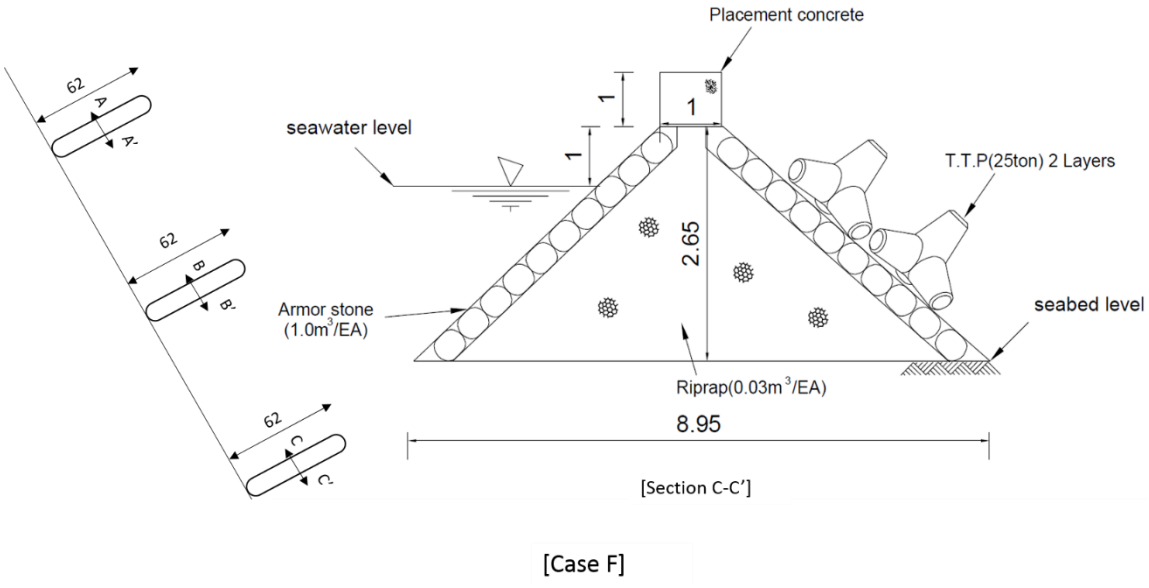

[Case F]

Figure 74. Cross section of south groin in Case F

3.2.1.1 Case A

Figure 75 shows seasonal (March, June, September, and December) water depths and total transport as a vector shape of arrows for Case A. Sequentially graphics, which are Figure 76 ~ 83, also represent the same parameters with Figure 75. From these figures, it is investigated that water depths are related to submerged breakwaters, and nearshore currents are also associated with the existence of the groins. The far offshore regions from shorelines seem not to be influenced by the artificial hard structures or nourishment in proposed countermeasures. With regards to the investigation of all models during the first half of the year, the total transport of sediments at Wolcheon Beach flow from the northern direction to the southern direction, and seem to be radiating from the Gagok River to the adjacent area. Similar movements of sediments

occur during the second half of the year, but a rip current of sediments is discovered at the southern region of Wolcheon Beach.

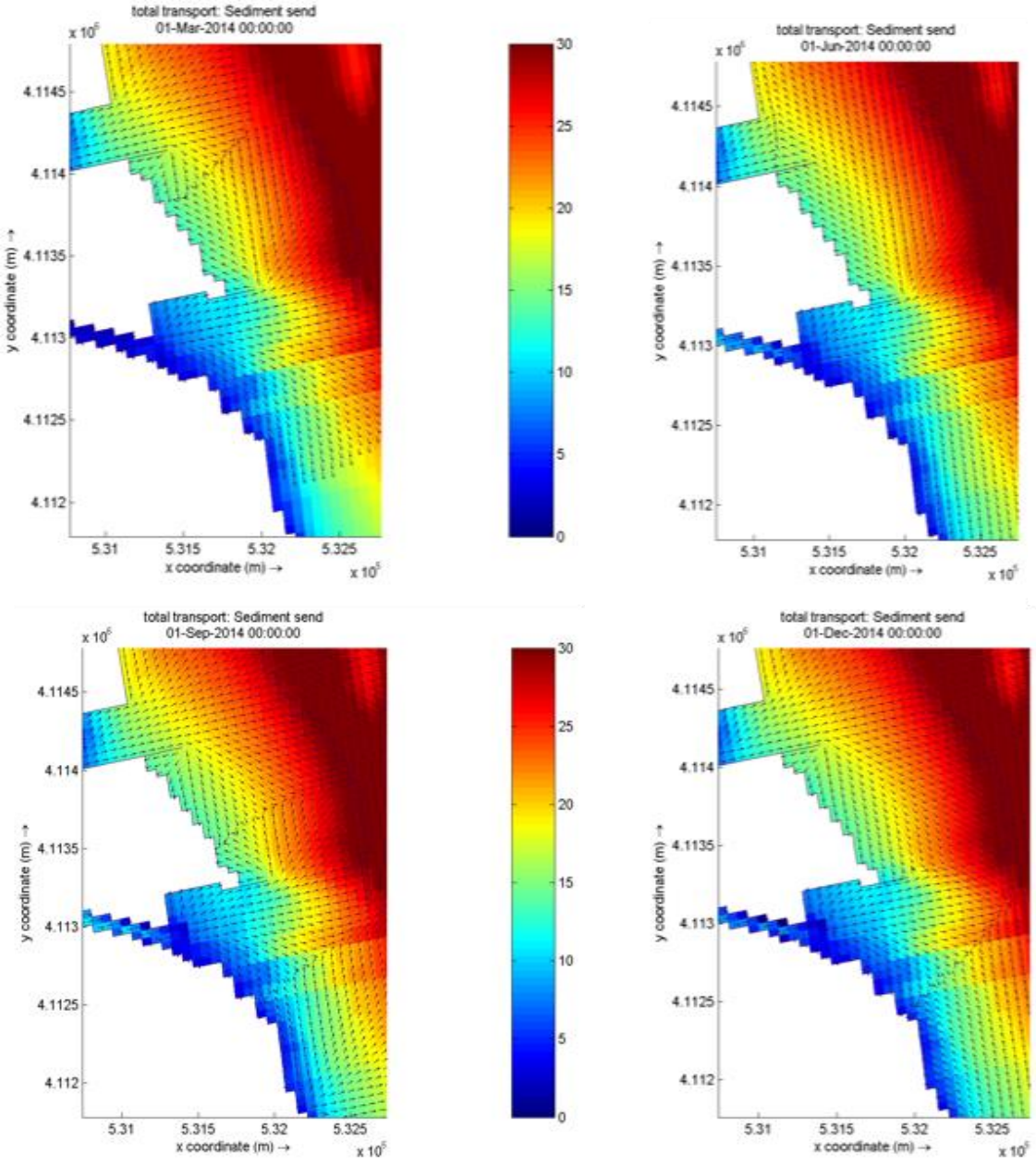

Figure 75. Seasonal water depths and total transport for Case A

3.2.1.2 Case B

Figure 76 shows for Case B.

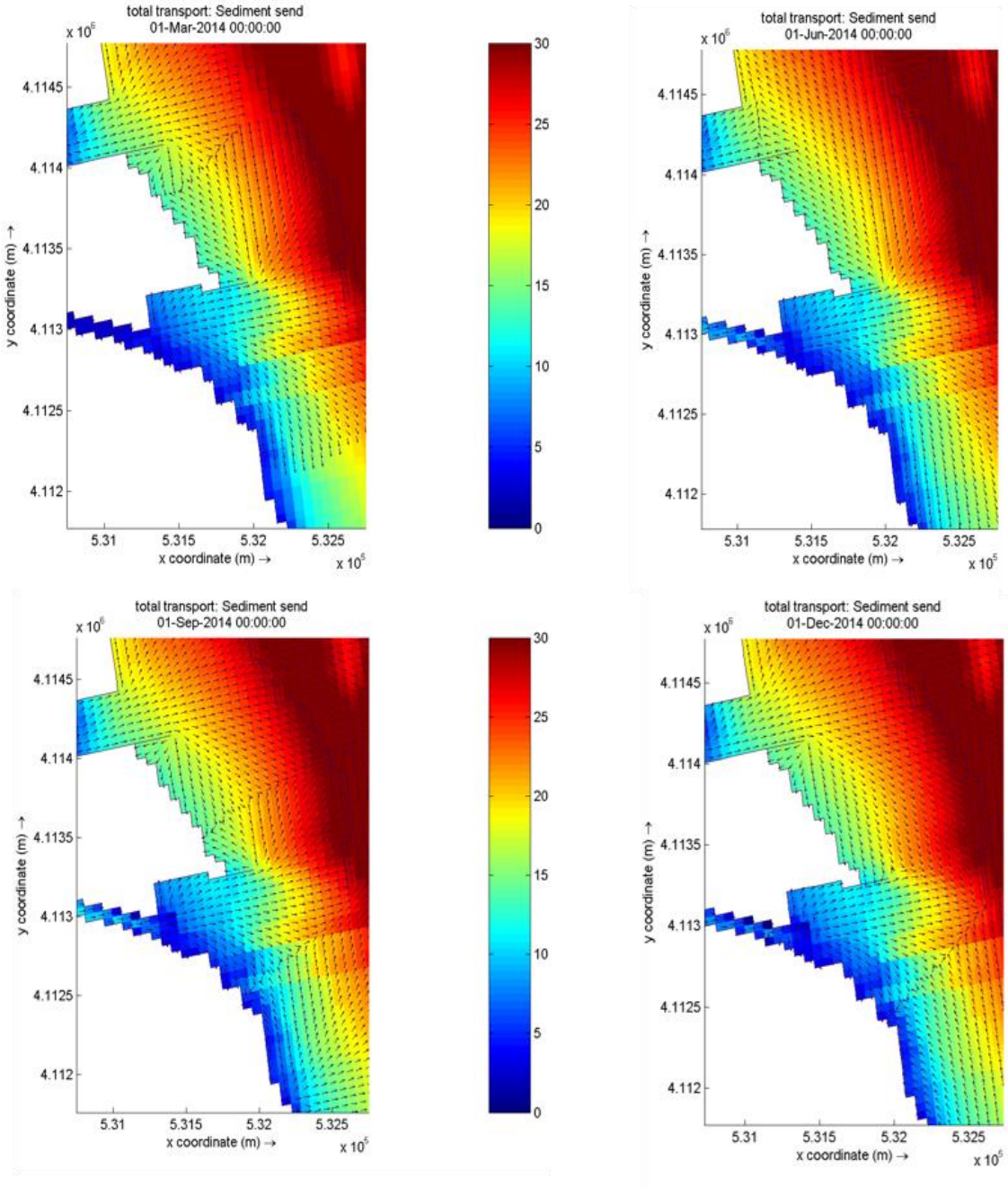

Figure 76. Seasonal water depths and total transport for Case B

3.2.1.3 Case C

Figure 77 shows for Case C.

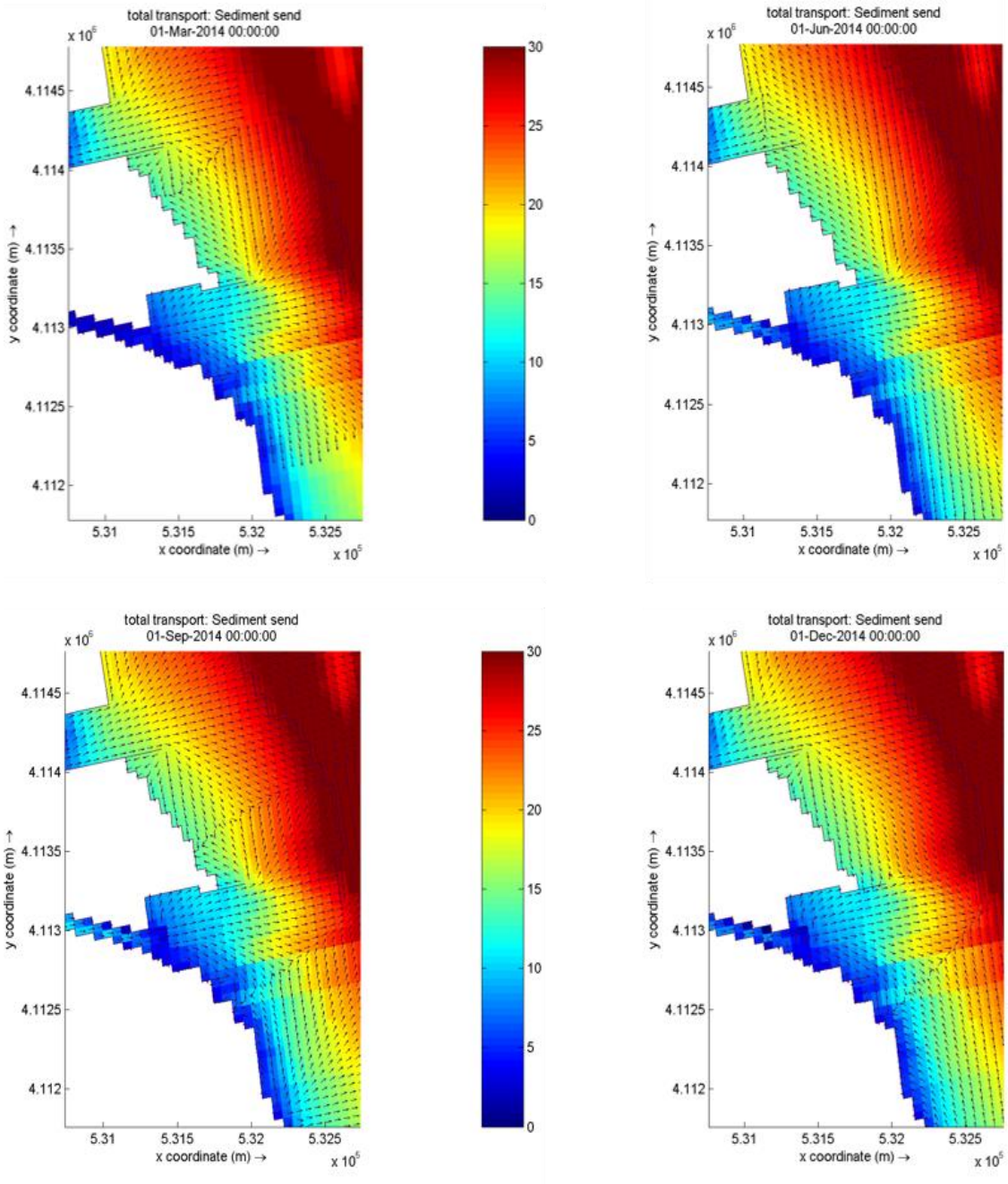

Figure 77. Seasonal water depths and total transport for Case C

3.2.1.4 Case D

Figure 78 shows for Case D.

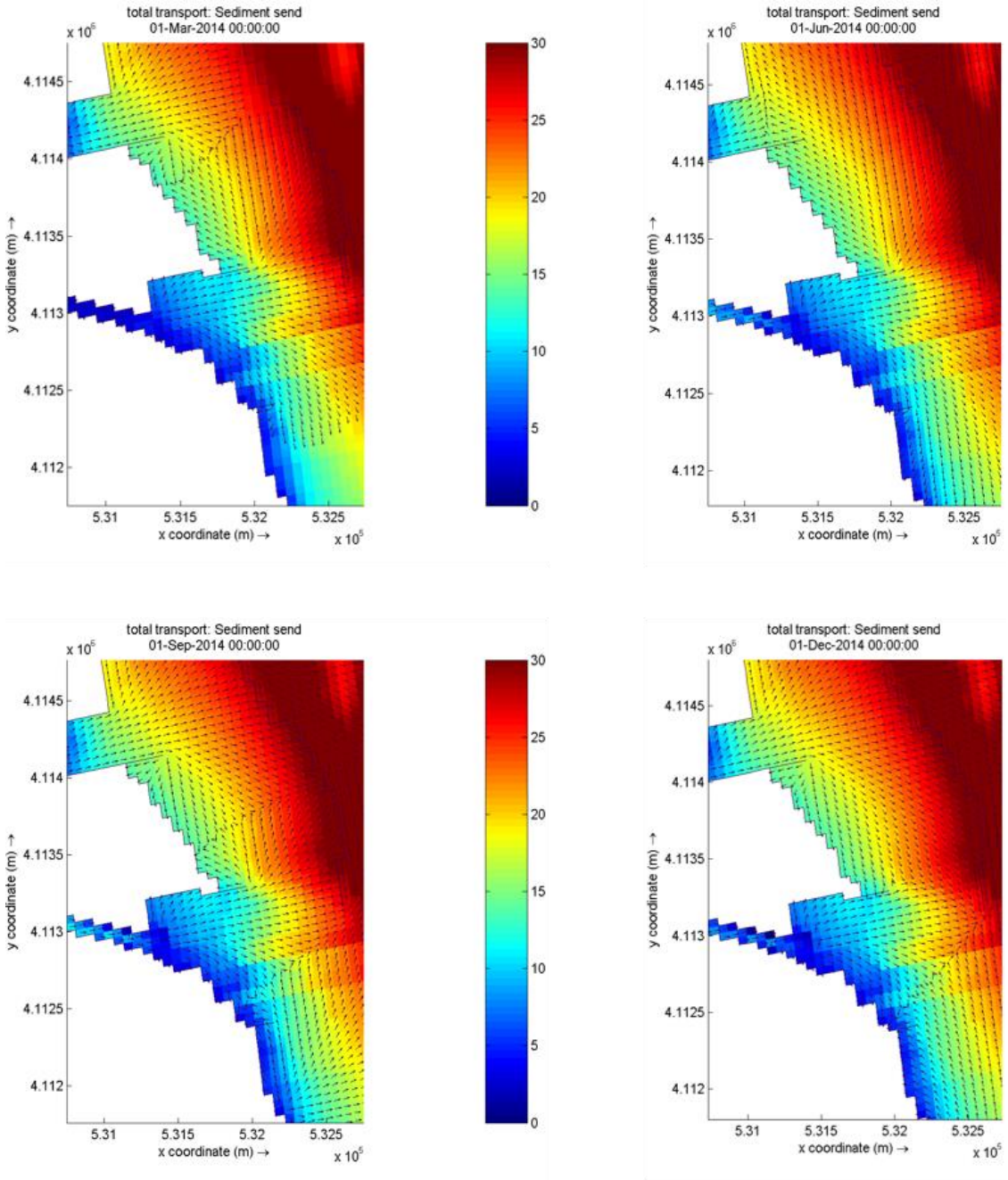

Figure 78. Seasonal water depths and total transport for Case D

3.2.1.5 Case E

Figure 79 shows for Case E.

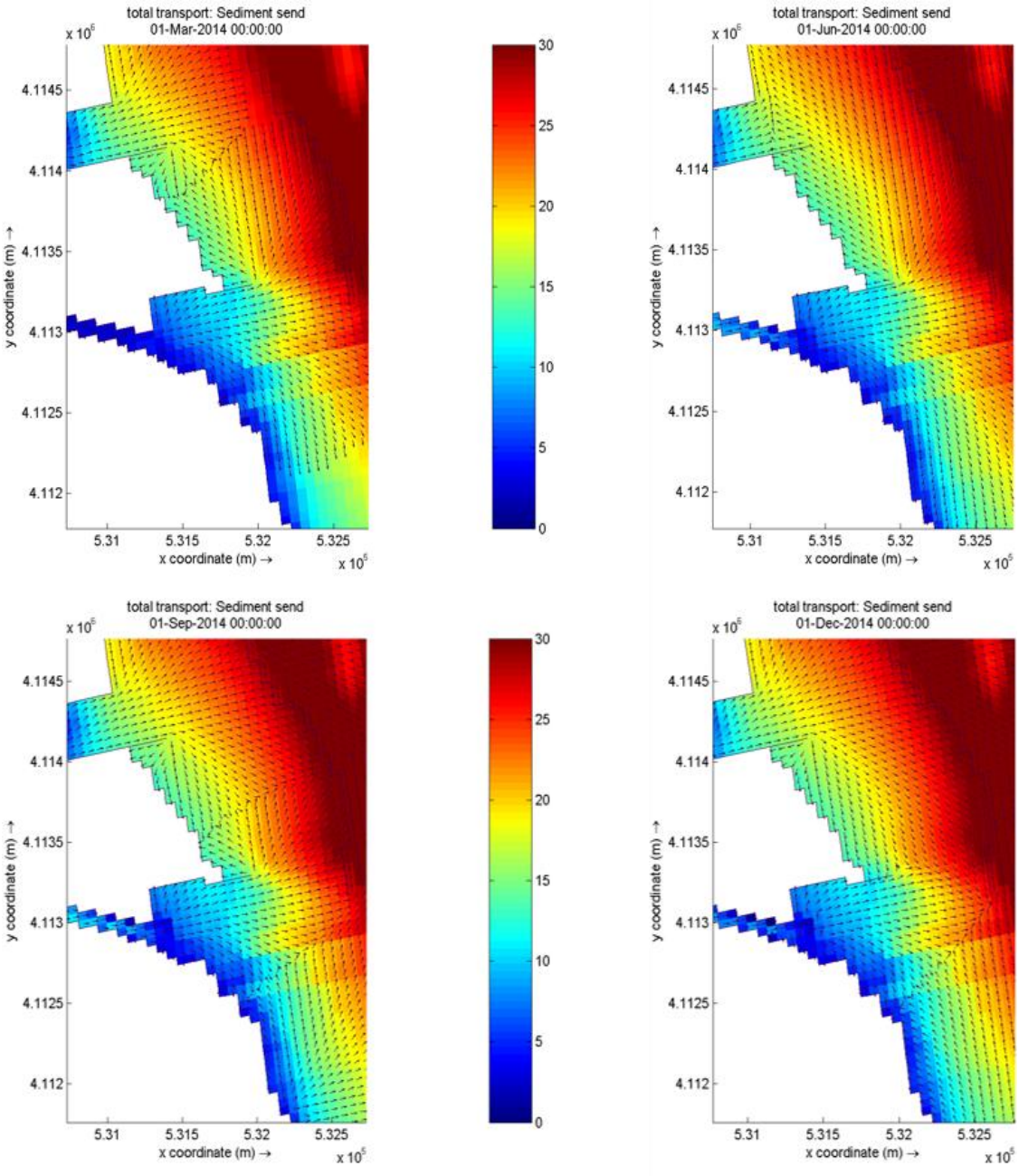

Figure 79. Seasonal water depths and total transport for Case E

3.2.1.6 Case F

Figure 80 shows for Case F.

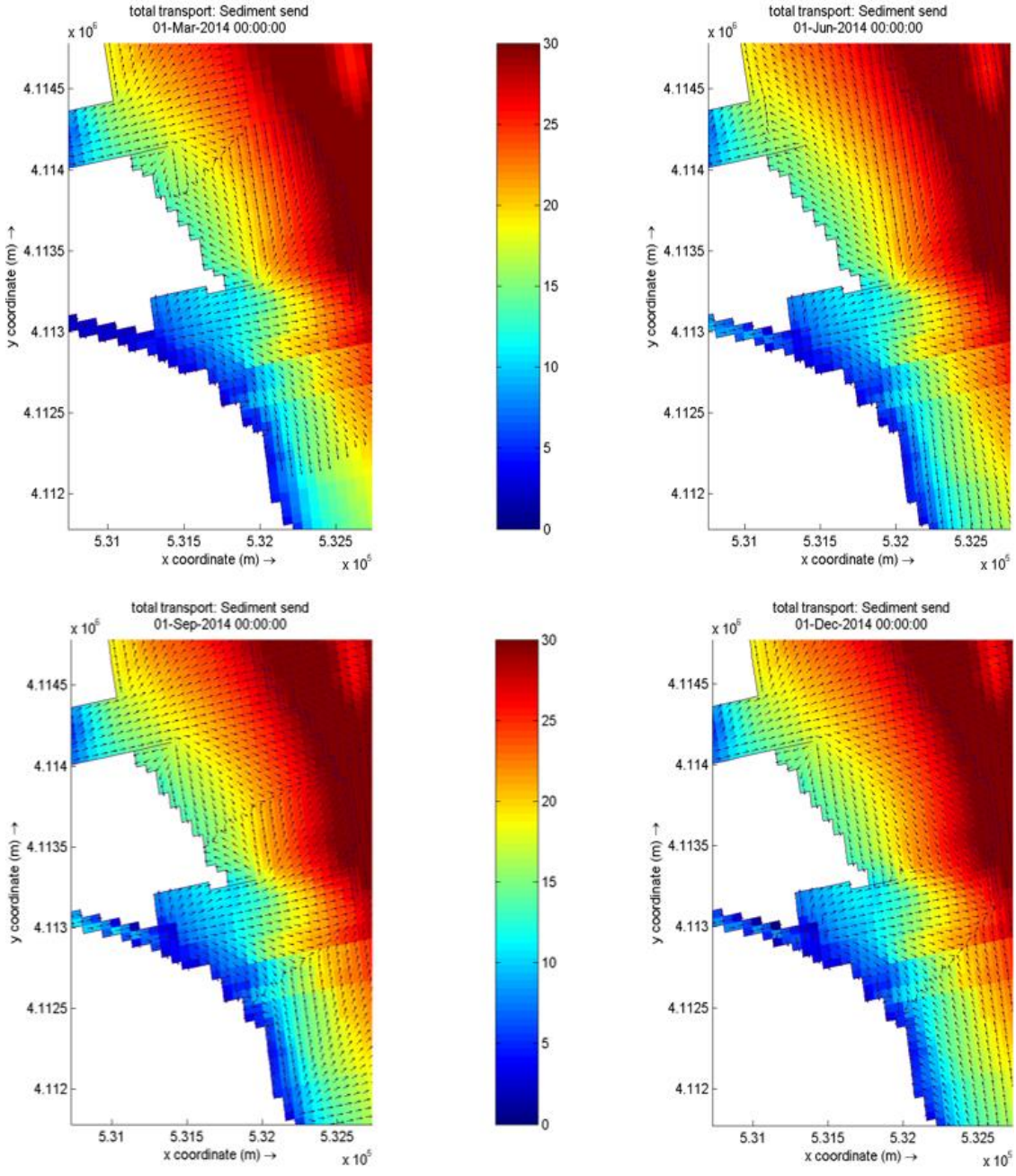

Figure 80. Seasonal water depths and total transport for Case F

3.2.1.7 Case G

Figure 81 shows for Case G.

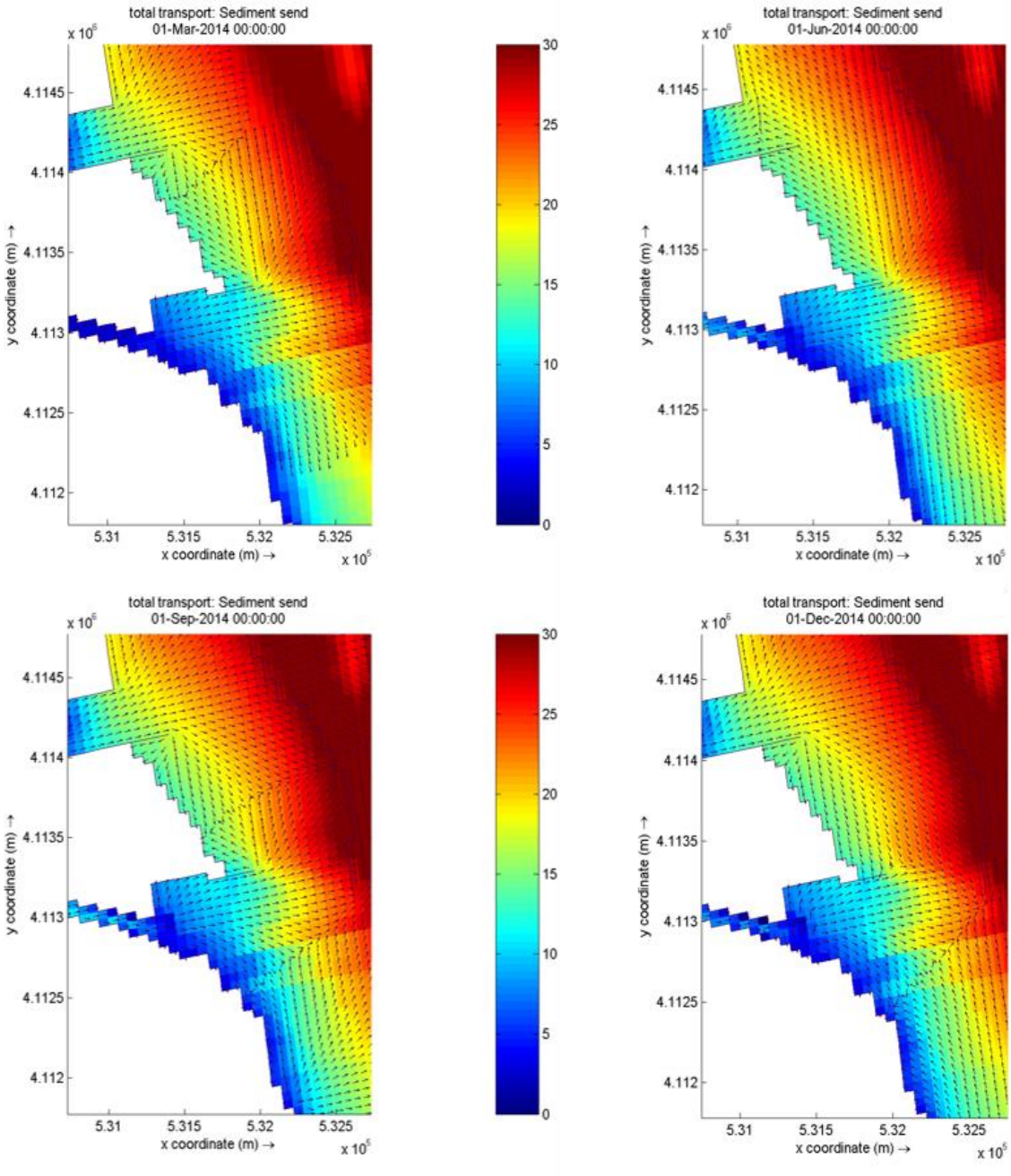

Figure 81. Seasonal water depths and total transport for Case G

3.2.1.8 Case H

Figure 82 shows for Case H.

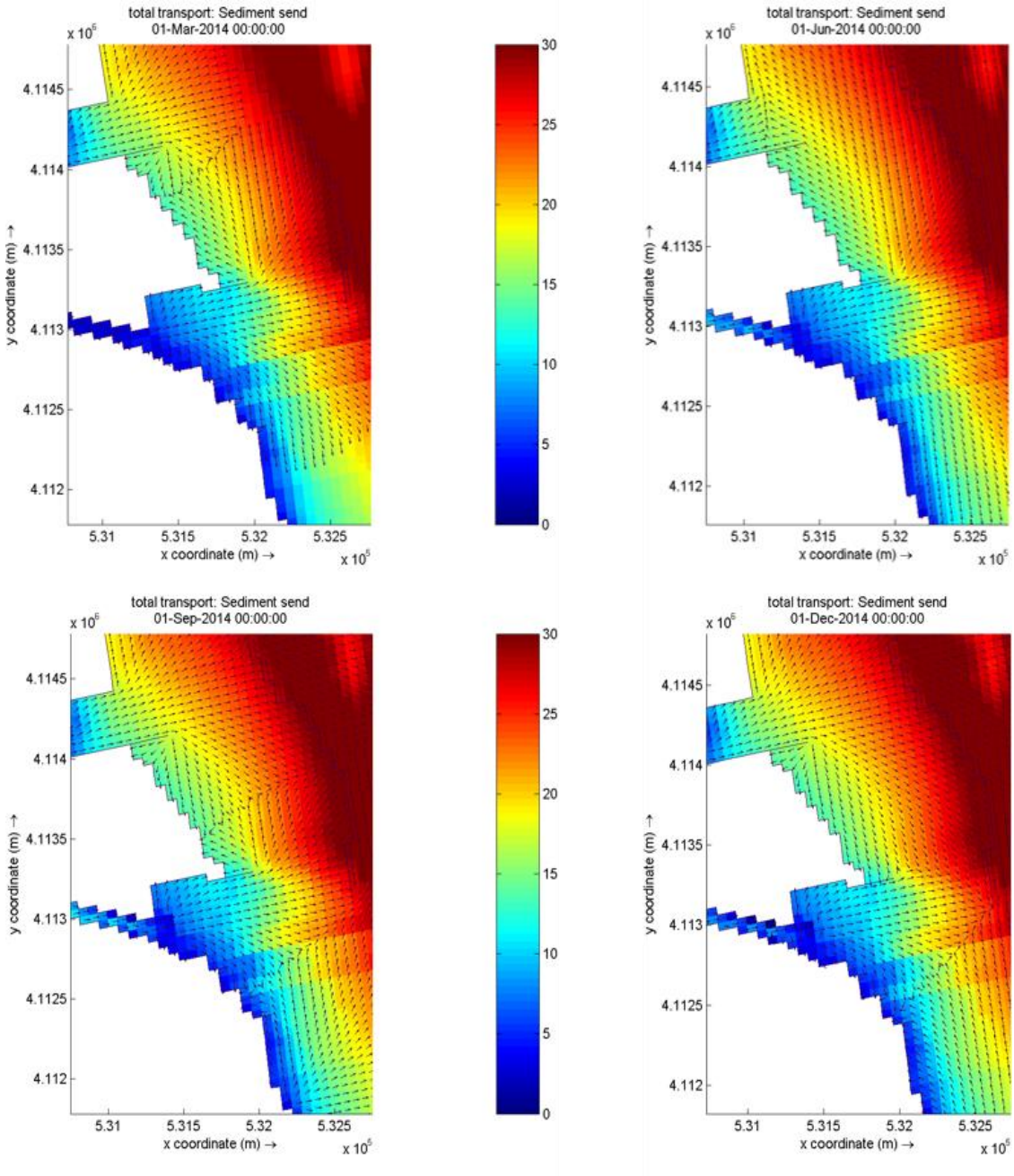

Figure 82. Seasonal water depths and total transport for Case H

3.2.1.9 Case I

Figure 83 shows for Case I.

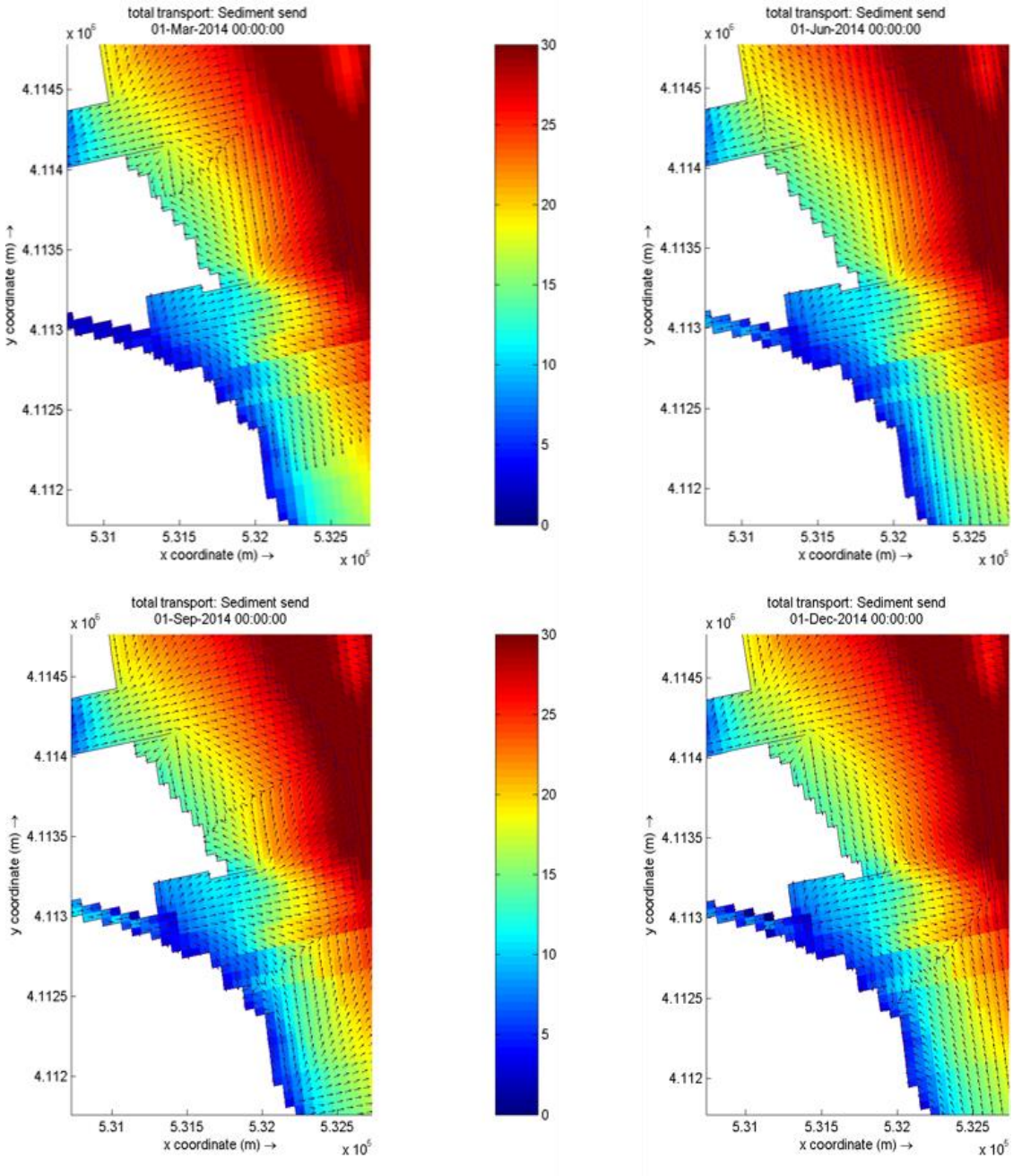

Figure 83. Seasonal water depths and total transport for Case I

3.2.2 Comparison of bathymetric results of the nine countermeasures

While the above represented graphics for the nine countermeasures well describe overall phenomena at the area of interest, it is not convenient to directly and quantitatively compare each model's effectiveness. Therefore, in similarity with the conclusion method for the selection of meteorological data, the degree of bathymetric change of each eight observational grid points will be a meaningful evaluative standard.

The rationale behind this is that a main purpose of this research is to determine the most effective model among the nine proposed solutions, not to establish a new design. For this aim, comparing bathymetric changes that reflect erosion and accretion of sediments can be a straightforward tool. Basically, the largest difference of water depths between Case A ("Do Nothing") and the other solutions can determine how proposed solutions affect the shoreline.

Additionally, due to the existence of channels at the eastern region of Wolcheon Beach, discontinuity seems to be emerged. In other words, a steep inclination of bathymetry in adjacent two grid cells causes this result.

Figure 84 ~ 91 show a fluctuation of water depths for each countermeasure at the specific observational grid points. Also, Table 15 explains a total summation of every two hours measured points (all 4320 time steps) during a year which is the above mentioned bathymetric gap of each solution with Case A for each grid point. These calculated values will be considered as a significant feature for the next section, particularly the economic analysis.

Although every graphic has a different incipient water depth for each grid point, their overall patterns are similar. From this fact, it is readily acknowledged that the water depth changes that can be assumed as harmonious between erosion and accretion are primarily governed by the meteorological parameters such as wind and waves. Also, a typical configuration, which shows erosion in summer and accumulation in winter, can be observed for all cases. This fact is the same consequence with the Investigation Reports regarding Environmental Impacts by KOGAS (2015).

We find that a nourishment countermeasure has no effect on bathymetric changes. A possible reason is that dredging and dumping as rejuvenation measure for Wolcheon Beach are fulfilled before the first time step of the FLOW module, so the model is just initialized with the nourished beach profile. Another possible reason is that a defined area of dumping should cover the observational grid points; however, a grid cell of the FLOW grid is 62m x 50m, which is greater than the dumping area. In other words, beach nourishment in the Delft 3D is treated as additional bathymetric information of the inner part of the polygon of dumping. If finer Flow grid is implemented for this region, effects of dumping might be discovered. It is obvious that beach nourishment is a worthy method to restore beach erosion, but its effectiveness is not clearly discovered in this study.

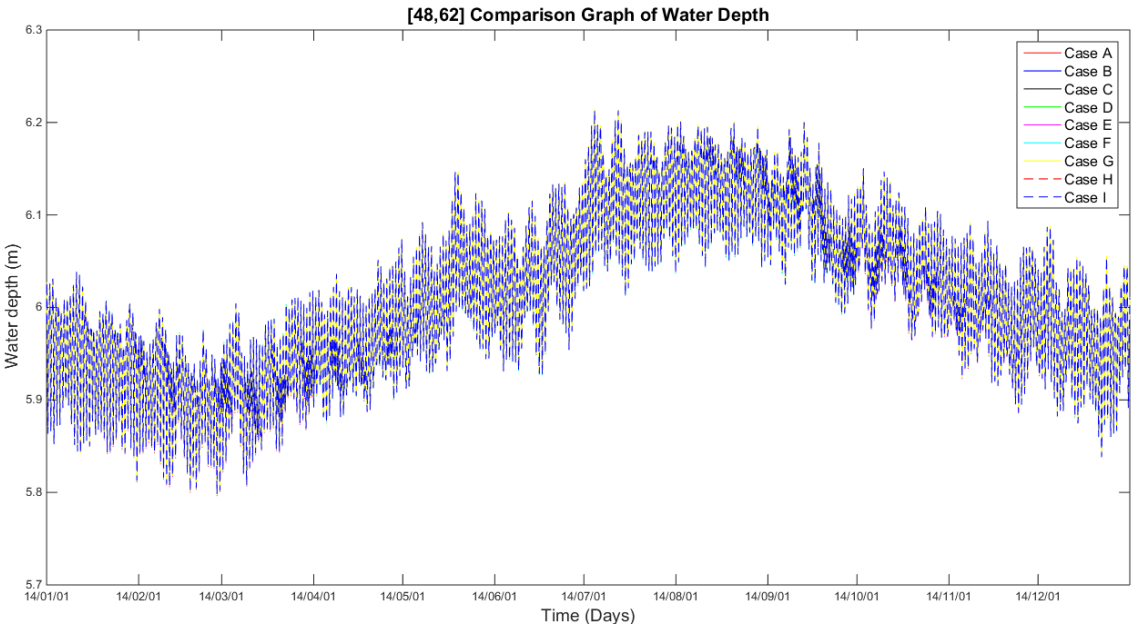

Figure 84. Comparison graph of fluctuation of water depths for [48, 62]

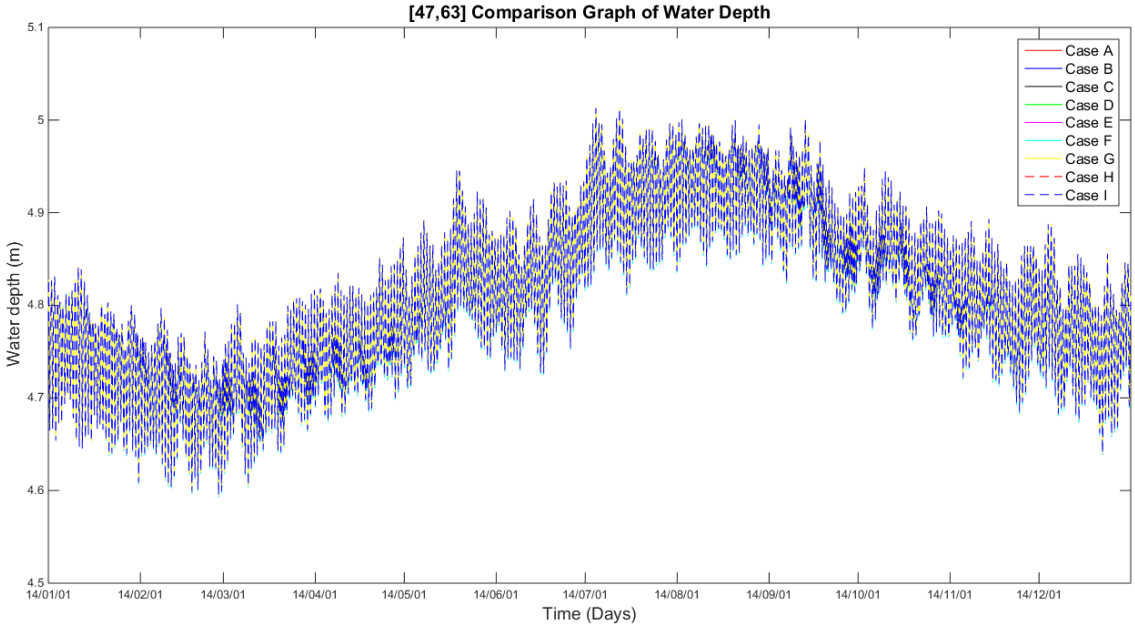

Figure 85. Comparison graph of fluctuation of water depths for [47, 63]

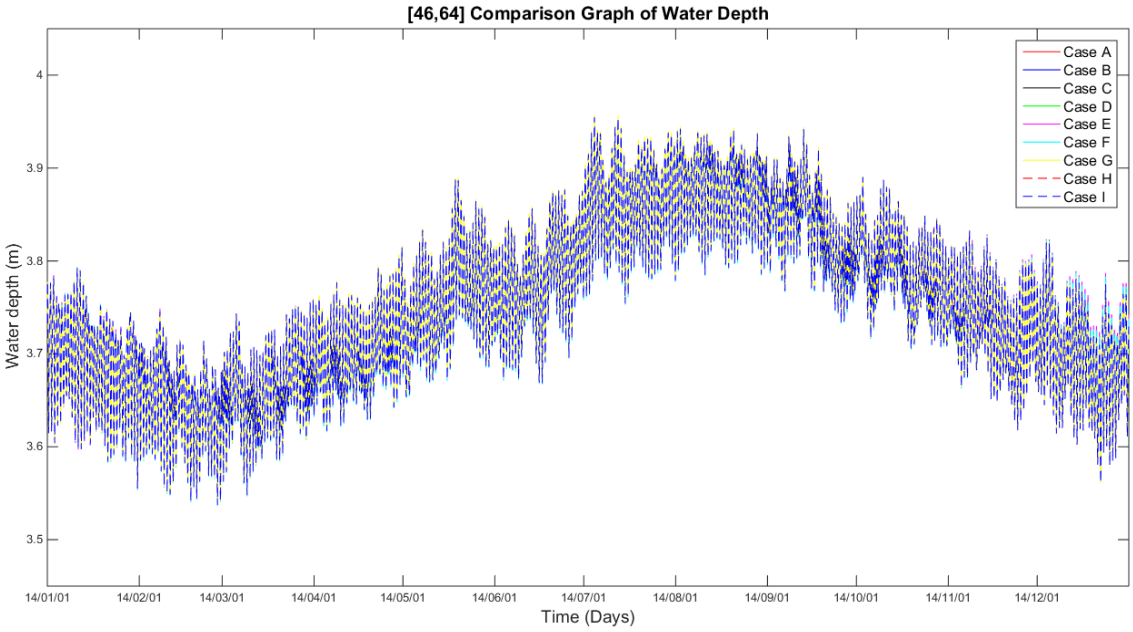

Figure 86. Comparison graph of fluctuation of water depths for [46, 64]

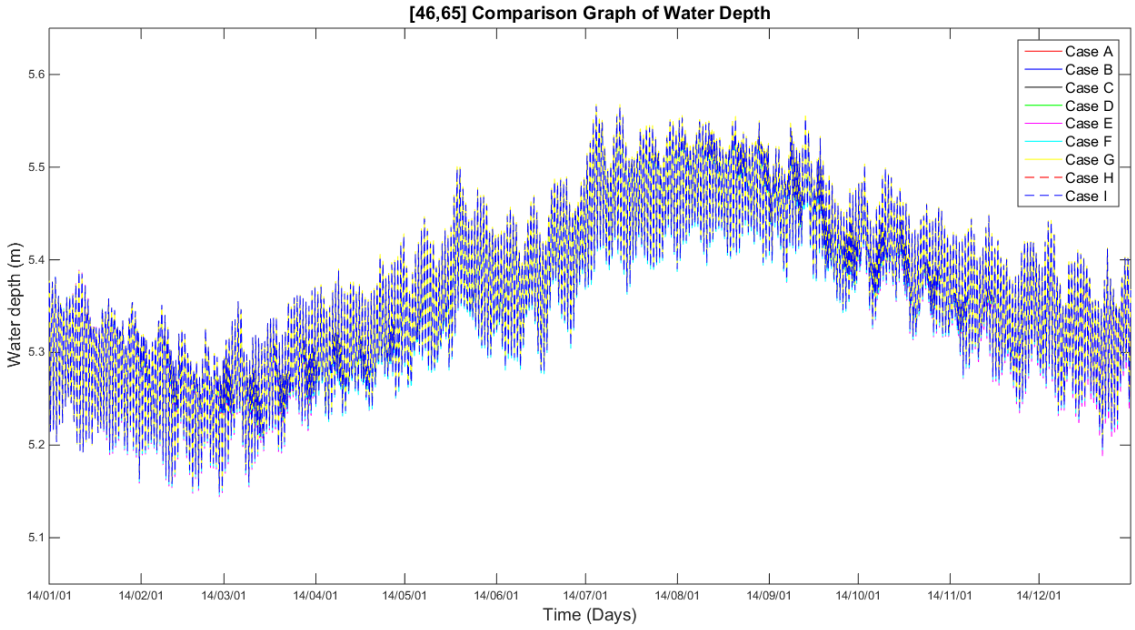

Figure 87. Comparison graph of fluctuation of water depths for [46, 65]

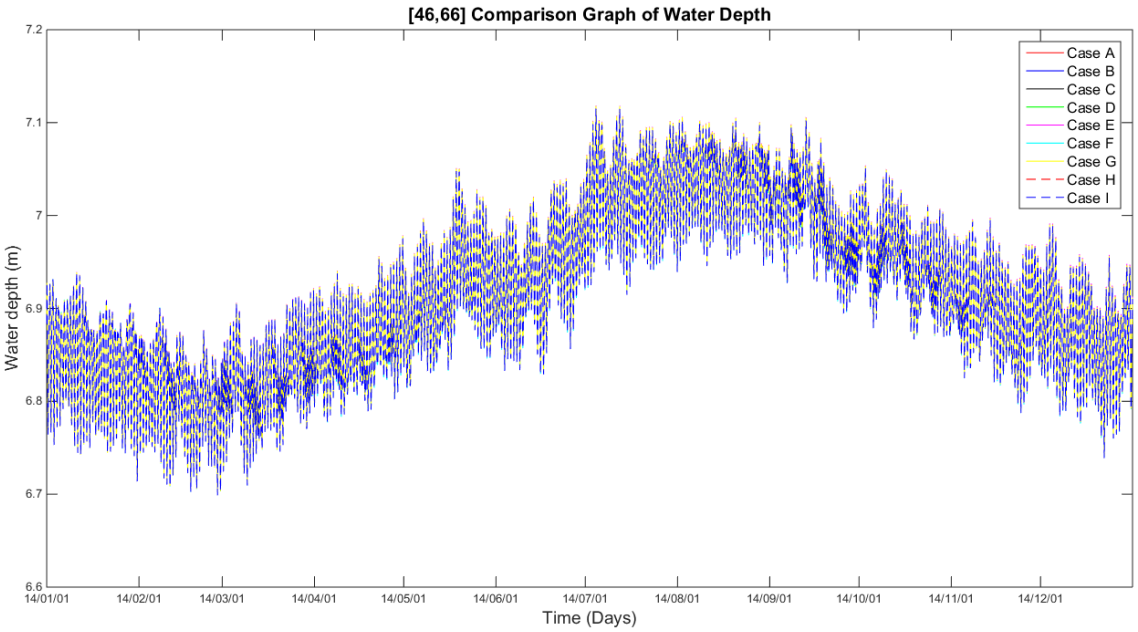

Figure 88. Comparison graph of fluctuation of water depths for [46, 66]

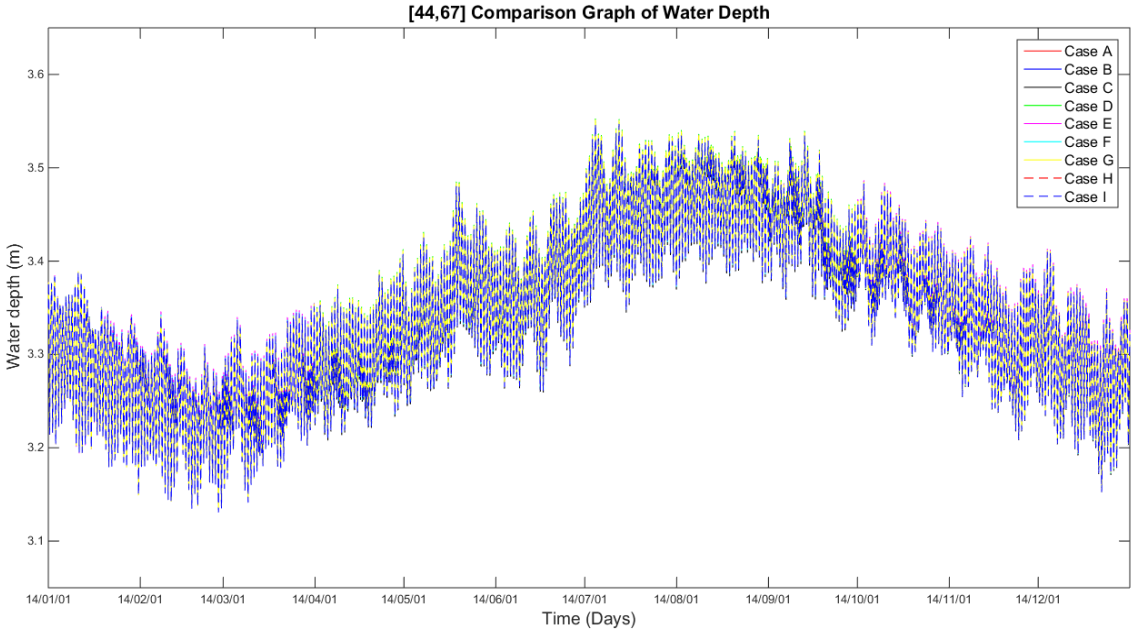

Figure 89. Comparison graph of fluctuation of water depths for [44, 67]

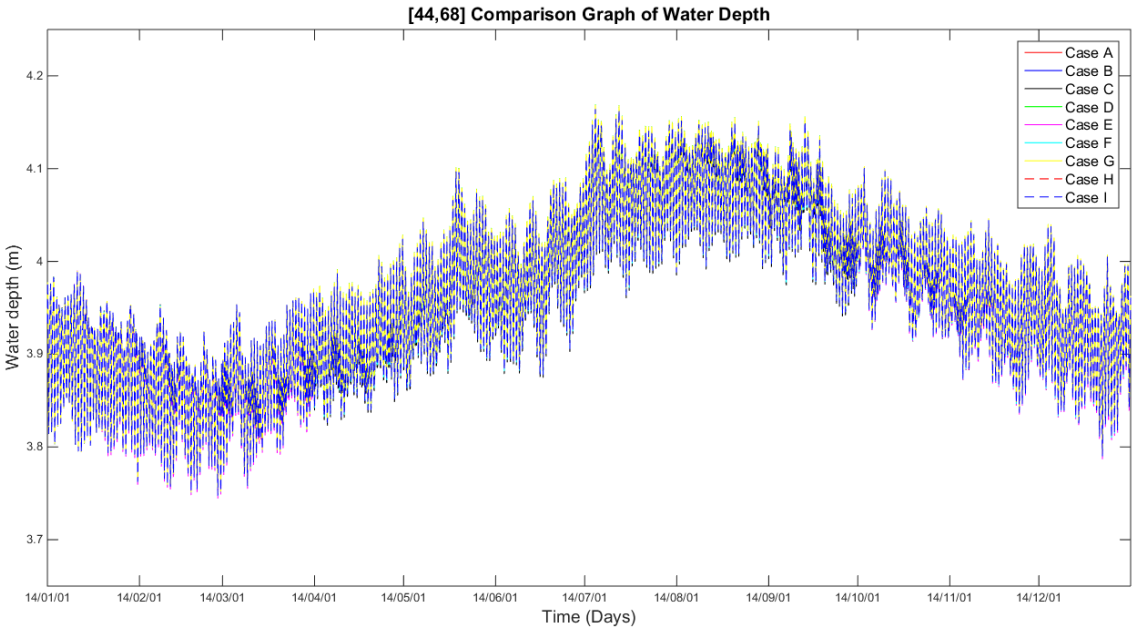

Figure 90. Comparison graph of fluctuation of water depths for [44, 68]

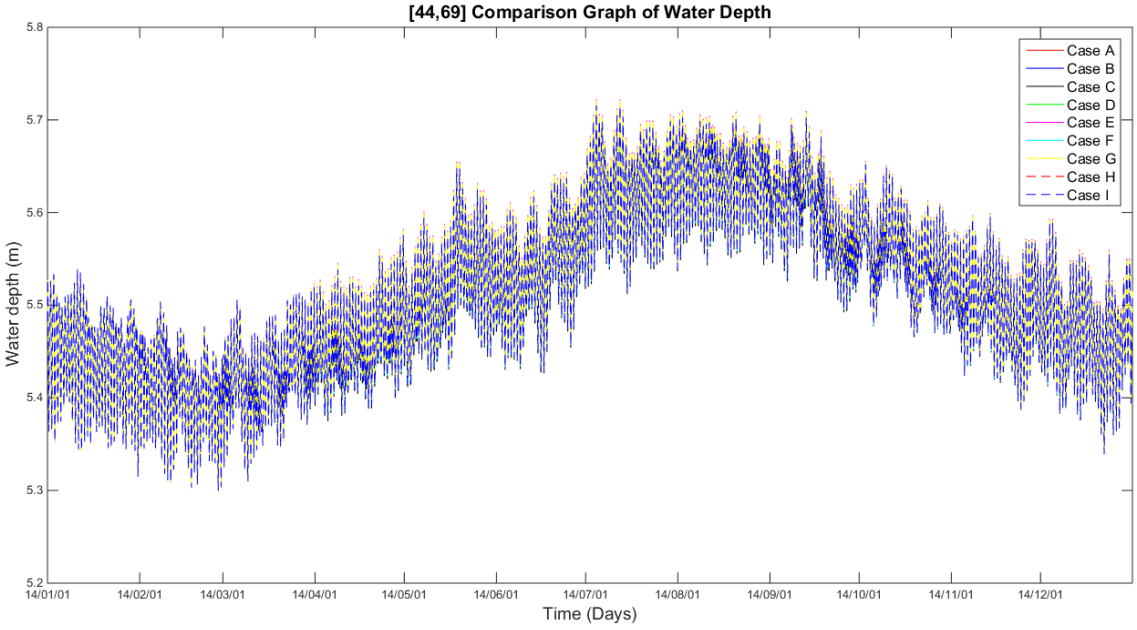

Figure 91. Comparison graph of fluctuation of water depths for [44, 69]

Table 15. Total differences (meter) of water depths between Case A and each case

	48,62	47,63	46,64	46,65	46,66	44,67	44,68	44,69	Total
Case B	3.761	8.587	1.4	12.062	0.569	-4.185	-0.002	-1.278	20.913
Case C	3.674	9.742	3.791	15.269	4.79	13.632	20.048	22.396	93.339
Case D	3.327	7.926	1.107	11.569	-0.481	-4.99	-0.823	-2.166	15.47
Case E	3.705	9.494	2.533	22.627	-2.915	-4.05	12.16	-4.752	38.8
Case F	1.909	10.225	6.701	18.614	7.703	5.878	12.048	14.371	77.449
Case G	0	0	0	0	0	0	0	0	0
Case H	1.659	1.894	5.498	6.732	7.719	9.65	11.625	15.21	59.984
Case I	1.659	1.894	5.498	6.732	7.719	9.65	11.625	15.21	59.984

Consequently, total differences of water depths between Case A (“Do Nothing”) and Case C including two submerged breakwater, nourishment, and one north groin is the largest as shown in Table 15. That means, Case C is revealed as the most effective countermeasure against beach erosion of Wolcheon Beach. Case F (two submerged breakwaters, nourishment, and three groins) could be the second appropriate result, and Case H (nourishment and three groins) could be the third solution.

4 ANALYSIS OF ECONOMIC, ENVIRONMENTAL, AND PUBLIC FACTORS

The previous section showed that Case C is the most effective countermeasure among the proposed resolutions. One interesting point is that the most expensive method with an abundance of barrier structures cannot always guarantee the best result. Therefore, it is strongly recommended that various aspects must be considered to determine what the best solution against beach erosion is, not only the functionality of the countermeasure, but also economic, environmental, and public factors.

4.1 Economic analysis

This section introduces the expenses for submerged breakwaters, nourishment, and groins, and compares them to their effectiveness. Reeve et al. (2012) well explained a relationship between economic pressure to constrain the cost of countermeasures and usefulness.

All expenses including material costs, labor costs, and overhead costs are estimated and occasionally assumed from an original design by KOGAS (2009) for the Samcheok LNG receiving terminal facilities. Unit prices of breakwater construction in 2010 and training dike construction in 2011 are a primary source for estimation, and annualized inflation rate is also considered respectively from 2010 or 2011 to 2016. The applied exchange rate between Korean currency (won) and U.S. dollar is 1189.5won/dollar, indirect cost (supposed rate: 25%) is also added, and successful bid cost rate is assumed 70 percent to produce the cost tables. Case A cost is estimated zero.

This study assumes that beach nourishment will be executed every two years during 20 years. Table 16 ~ 23 show the estimated expenses for each case (Case B ~ Case I).

Table 16. Cost table for Case B

Countermeasure	Work type	Unit price (USD)	Quantities	Unit	Total cost (USD)
2 Submerged breakwaters	Tetrapod fabrication	672	7,235	Each	4,862,703
	Tetrapod move & placement	657	7,235	Each	4,570,228
	Excavation for basement	2	24,000	m^3	52,421
	Riprap for basement	21	24,000	m^3	498,548
	Riprap leveling	22	12,000	m^2	263,959
	Armor stone	36	12,000	Each	428,523
	Armor stone leveling	26	12,000	m^2	312,923
Nourishment	Dredging	10	248,248	m^3	24,001,482
	Dumping	5	248,248	m^3	12,000,741
Subtotal					47,171,527
Indirect cost					11,792,882
Total					58,964,408
Successful bid cost					41,275,000

Table 17. Cost table for Case C

Countermeasure	Work type	Unit price (USD)	Quantities	Unit	Total cost (USD)
2 Submerged breakwaters	Tetrapod fabrication	672	7,235	Each	4,862,703
	Tetrapod move & placement	657	7,235	Each	4,570,228
	Excavation for basement	2	24,000	m^3	52,421
	Riprap for basement	21	24,000	m^3	498,548
	Riprap leveling	22	12,000	m^2	263,959
	Armor stone	36	12,000	Each	428,523
	Armor stone leveling	26	12,000	m^2	312,923
Nourishment	Dredging	10	248,248	m^3	24,001,482
	Dumping	5	248,248	m^3	12,000,741
North groin	Tetrapod fabrication	672	140	Each	94,095
	Tetrapod move & placement	657	140	Each	91,919
	Riprap for basement	21	1,955	m^3	40,610
	Riprap leveling	22	657	m^2	14,456
	Armor stone	36	657	Each	23,469
	Armor stone leveling	26	657	m^2	17,138
	Concrete	83	124	m^3	10,263
Subtotal					47,463,476
Indirect cost					11,865,869
Total					59,329,346
Successful bid cost					41,530,000

Table 18. Cost table for Case D

Countermeasure	Work type	Unit price (USD)	Quantities	Unit	Total cost (USD)
2 Submerged breakwaters	Tetrapod fabrication	672	7,235	Each	4,862,703
	Tetrapod move & placement	657	7,235	Each	4,570,228
	Excavation for basement	2	24,000	m^3	52,421
	Riprap for basement	21	24,000	m^3	498,548
	Riprap leveling	22	12,000	m^2	263,959
	Armor stone	36	12,000	Each	428,523
	Armor stone leveling	26	12,000	m^2	312,923
Nourishment	Dredging	10	248,248	m^3	24,001,482
	Dumping	5	248,248	m^3	12,000,741
South groin	Tetrapod fabrication	672	140	Each	94,095
	Tetrapod move & placement	657	140	Each	91,919
	Riprap for basement	21	4,103	m^3	85,224
	Riprap leveling	22	980	m^2	21,548
	Armor stone	36	980	Each	34,982
	Armor stone leveling	26	980	m^2	25,545
	Concrete	83	124	m^3	10,263
Subtotal					47,535,102
Indirect cost					11,883,776
Total					59,418,878
Successful bid cost					41,593,000

Table 19. Cost table for Case E

Countermeasure	Work type	Unit price (USD)	Quantities	Unit	Total cost (USD)
2 Submerged breakwaters	Tetrapod fabrication	672	7,235	Each	4,862,703
	Tetrapod move & placement	657	7,235	Each	4,570,228
	Excavation for basement	2	24,000	m^3	52,421
	Riprap for basement	21	24,000	m^3	498,548
	Riprap leveling	22	12,000	m^2	263,959
	Armor stone	36	12,000	Each	428,523
	Armor stone leveling	26	12,000	m^2	312,923
Nourishment	Dredging	10	248,248	m^3	24,001,482
	Dumping	5	248,248	m^3	12,000,741
2 groins	Tetrapod fabrication	672	72	Each	48,392
	Tetrapod move & placement	657	72	Each	47,272
	Riprap for basement	21	731	m^3	15,193
	Riprap leveling	22	374	m^2	8,237
	Armor stone	36	374	Each	13,373
	Armor stone leveling	26	374	m^2	9,765
	Concrete	83	124	m^3	10,263
Subtotal					47,324,023
Indirect cost					11,831,006
Total					59,155,029
Successful bid cost					41,408,000

Table 20. Cost table for Case F

Countermeasure	Work type	Unit price (USD)	Quantities	Unit	Total cost (USD)
2 Submerged breakwaters	Tetrapod fabrication	672	7,235	Each	4,862,703
	Tetrapod move & placement	657	7,235	Each	4,570,228
	Excavation for basement	2	24,000	m^3	52,421
	Riprap for basement	21	24,000	m^3	498,548
	Riprap leveling	22	12,000	m^2	263,959
	Armor stone	36	12,000	Each	428,523
	Armor stone leveling	26	12,000	m^2	312,923
Nourishment	Dredging	10	248,248	m^3	24,001,482
	Dumping	5	248,248	m^3	12,000,741
3 groins	Tetrapod fabrication	672	180	Each	120,979
	Tetrapod move & placement	657	180	Each	118,181
	Riprap for basement	21	3,031	m^3	62,957
	Riprap leveling	22	995	m^2	21,889
	Armor stone	36	995	Each	35,535
	Armor stone leveling	26	995	m^2	25,949
	Concrete	83	186	m^3	15,395
Subtotal					47,572,412
Indirect cost					11,893,103
Total					59,465,515
Successful bid cost					41,625,000

Table 21. Cost table for Case G

Countermeasure	Work type	Unit price (USD)	Quantities	Unit	Total cost (USD)
Nourishment	Dredging	10	248,248	m^3	24,001,482
	Dumping	5	248,248	m^3	12,000,741
Subtotal					36,002,223
Indirect cost					9,000,556
Total					45,002,778
Successful bid cost					31,501,000

Table 22. Cost table for Case H

Countermeasure	Work type	Unit price (USD)	Quantities	Unit	Total cost (USD)
Nourishment	Dredging	10	248,248	m^3	24,001,482
	Dumping	5	248,248	m^3	12,000,741
3 groins	Tetrapod fabrication	672	180	Each	120,979
	Tetrapod move & placement	657	180	Each	118,181
	Riprap for basement	21	3,031	m^3	62,957
	Riprap leveling	22	995	m^2	21,889
	Armor stone	36	995	Each	35,535
	Armor stone leveling	26	995	m^2	25,949
	Concrete	83	186	m^3	15,395
Subtotal					36,403,108
Indirect cost					9,100,777
Total					45,503,885
Successful bid cost					31,852,000

Table 23. Cost table for Case I

Countermeasure	Work type	Unit price (USD)	Quantities	Unit	Total cost (USD)
3 groins	Tetrapod fabrication	672	180	Each	120,979
	Tetrapod move & placement	657	180	Each	118,181
	Riprap for basement	21	3,031	m^3	62,957
	Riprap leveling	22	995	m^2	21,889
	Armor stone	36	995	Each	35,535
	Armor stone leveling	26	995	m^2	25,949
	Concrete	83	186	m^3	15,395
Subtotal					400,885
Indirect cost					100,221
Total					501,107
Successful bid cost					350,000

The bathymetric change results of the countermeasure should be compared to its total costs for every model. Also, this will be considered as a fundamental feasibility study of a Wolcheon Beach protection project for administrators or coastal engineers. Total differences of water depths (between Case A “Do Nothing” and each case) of all eight measured grid points and the successful bid cost of each case are employed to determine the financial effectiveness of each countermeasure.

Table 24. Financial effectiveness of each case

Countermeasure	Total bathymetric differences (cm) [A]	Successful bid cost (USD) [B]	Effectiveness ($\frac{B}{A}$) (USD/cm)
Case B	2,091	41,275,000	19,736
Case C	9,334	41,530,000	4,449
Case D	1,547	41,593,000	26,886
Case E	3,880	41,408,000	10,672
Case F	7,744	41,625,000	5,375
Case G	0	31,501,000	0
Case H	5,998	31,852,000	5,310
Case I	5,998	350,000	58

In a purely economic view, Case I is the most effective method for Wolcheon Beach. However, beach nourishment in this study cannot be applied due to limitation of the established the grid domain. If higher-resolution grids are employed, effects of rejuvenation of beach should be apparent. Taking this into account, Case H will be a substantial and reasonable solution instead of Case I. Also, Case C is the possible countermeasure as a traditional hard stabilization, and it is the most economic method except for Case I. Consequently, Case C and Case H could both be fundamental solutions in the economic analysis.

4.2 Environmental analysis

Inevitably, major construction projects can cause environmental changes. Therefore, most environmental acts are concentrated on how they can reduce transformation caused by human activities. In this section, SWOT analysis is applied in order to evaluate the diverse environmental aspects of the countermeasures including

submerged breakwaters, beach nourishment, and groins. This matrix type method has been utilized to arrange an object's strengths, weaknesses, opportunities, and threats. From Table 25 to Table 27 the organized contents according to SWOT analysis are explained.

Table 25. SWOT method for submerged breakwaters

Internal factors	Strengths	Weaknesses
	Most powerful countermeasure against beach erosion	Cause numerous environmental changes due to its grand scale
External factors	Opportunities	Threats
	Preferred as the traditional solution among the persons interested	• Local residents might be opposed due to decreasing of the amount of harvested fish • Compensation for established fish farms

Table 26. SWOT method for beach nourishment

Internal factors	Strengths	Weaknesses
	• Eco-friendly • Accumulated sands that might generate congestion at the Gagok estuary will be recycled	Repetitive work (annually or every two years) might continuously damage flora and fauna
External factors	Opportunities	Threats
	Increase in tourists	-

Table 27. SWOT method for groins

	Strengths	Weaknesses
Internal factors	• Most economic and environmentally friendly countermeasure • Historically and widely used across the world	Placement of ripraps should generate suspended soil, which might damage flora and fauna in large region
	Opportunities	Threats
External factors	Increase in anglers who can fish on the groins and tourists	• Local residents might be opposed due to decreasing of the amount of harvested fish • Compensation for established fish farms

Through SWOT analysis, beach replenishment can be considered the most eco-friendly method among the three proposed countermeasures. This is because a suitable borrow area at the Gagok estuary can be easily identified, and the existence of the adjacent borrow area can provide the similar grain size of the original sands at Wolcheon Beach. Correspondingly, anticipated flooding of the Gagok River caused by congestion of the Gagok estuary can be solved simultaneously through beach recharge.

4.3 Public analysis

In public analysis, mainly, three perspectives will be introduced as follows:

(1) Comparison the degree of difficulty for acquiring working permits between two acts in Korea (“Environmental Impact Assessment Act” and “Marine Environment Management Act”) for construction;

(2) Local residents’ resentment for the project or their requirements for approval;

(3) Political factors associated with the administration, politicians, and elections.

The above two analyses can be determined and predicted by engineers or environmentalists, but public factors can be considered the most difficult part, because of its contingency or unquantifiable characteristics to a project manager.

4.3.1 Construction permits

There are two primary acts to regulate construction of a coastal region in Korea. Firstly, the more comprehensive and more severe law is the "Environmental Impact Assessment Act" for generating extensive environmental changes. This act mainly deals with overall environmental changes which affect the natural ecological environment, social and economic fields, etc. from a major construction project. The Samcheok LNG receiving terminal construction project has been affected by this act, therefore the construction of the proposed countermeasures in this study also must comply with the regulations.

The similar but more compact, "Marine Environment Management Act" is to make clear the obligations of the people and the responsibilities of the State for the preservation and management of the marine environment. This act restricts construction works through two articles: "Consultation on utilization of sea areas" and "Simplified consultation on utilization of sea areas." A regulatory decision which articles shall be applied is concluded by the size of construction works. Basically, the small size's proposed countermeasure is readily accepted as a solution, and it can guarantee a more harmonious process with acts or the administration. Therefore, it is obvious that

acquiring the permits of “Simplified consultation on utilization of sea areas” is easier than “Consultation on utilization of sea areas.”

The “Enforcement Degree of the Prevention of Marine Pollution Act” reveals the size limits of construction works for acquiring permits of “Simplified consultation on utilization of sea areas”, which is as a peripheral facility should have an overall length shorter than 150m, and its utilized area should be smaller than 3,000m^2. In order to fulfill this restriction, submerged breakwaters should not be approved; in contrast, all groin types’ countermeasures can be applied to obtain simplified construction permits.

4.3.2 Local residents

Local residents are important stakeholders across the entire life cycle of a construction project, but from the position of a project manager, their influence should be properly controlled through negotiation with a sincere attitude and sufficient compensation. This is because they tend to raise objections to proposed solutions and require more financial reward. This fact will be a significant obstacle to progress of the construction project.

Approximately 100 people live near Wolcheon Beach, and the majority of them are fisherman. They also have stores or restaurants for tourists during summer season. Thus, they are susceptible to environmental changes because they have continuously suffered the effects of the erosion of Wolcheon Beach. This fact has ultimately caused the decrease of revenue. Therefore, they have a concern that another construction work might aggravate the recession of the shoreline of Wolcheon Beach.

For these reasons, it appears that people who live in Wolcheon town wish for small scale construction work: a groin that also can act as an attraction for anglers and tourists, or an eco-friendly beach replenishment that can restore Wolcheon Beach and incomes of local residents.

4.3.3 Politics

The above mentioned anxieties of inhabitants will directly be changed to a social pressure to a political territory. Especially, this compression is reinforced and deepened by elections. There are three important elections in Korea which are: local elections for a mayor or the governor of a province, general election for the National Assembly, and a presidential election. Although politicians generally tend to approve of a civil appeal, during the election they strongly concentrate on how they can satisfy complaints from citizens to win the election. This point generates substantial problems to a project management. Naturally, appeals from local residents should cause the rise of business expenses, and postpone procedures of a project. Also, before elections, politicians who are in the ruling party that have substantive authority, should intensely recommend or even press that companies must promote business expansion to release more currency for voters as an economy invigorating policy. Therefore, an important decision or a commencement of the construction project had better avoid the specific season for elections to proceed with a harmonious project. Table 28 shows a plan for the next three primarily elections.

Table 28. Schedule for elections related to Samcheok LNG terminal project

	Before	After
Local election	June 4, 2014	June 13, 2018
General election	April 13, 2016	April, 2020
Presidential election	December 19, 2012	December 20, 2017

4.4 Comprehensive conclusion

Writing about countermeasures for coastal erosion, Basco (2003) said that amalgamation between traditional hard engineering and soft engineering has been applied across the world. Structural alternatives and nonstructural alternatives must be combined for coastal hazard mitigation and reduce the total cost of the project. Therefore, considering economic, environmental, and political characteristics, Case H could be a reasonable solution including nourishment and 3 groins as consolidation between hard stabilization and soft stabilization.

5 CONCLUSIONS AND FUTURE WORKS

Wolcheon Beach has suffered from erosion during several years, so this thesis concentrates on that countermeasures proposed by KOGAS which is the ultimate solution to alleviate beach erosion. The optimal countermeasure Case H, which includes beach replenishment and three groins, is determined through a numerical modeling by the Delft 3D, analysis of economic, environmental, and public characteristics.

In order to establish the computational numerical model, the FLOW and the WAVE module are implemented for this study. Their combination called online coupling is used primarily to both drive and predict the bathymetric changes at the eight observational points. In addition, the morphology module describes the result of bed transport and suspended transport of sediments. Prior to consideration of countermeasures, model results from three different sets of meteorological information, which are data for the year 2014, average-annual data during 2001 ~ 2014, maximum-annual data during 2001 ~ 2014, are compared with measured bathymetric survey results by KOGAS. Through results comparison and error analysis, average-annual meteorological data are applied to establish the baseline model.

Three essential components for coastal erosion mitigation are considered, either separately or as a common system. These are submerged breakwaters, beach nourishment, and groins because they are currently widely used across the globe. In order to investigate the nine proposed solutions, in similarity with the selection of meteorological data, water depths at the eight grid points in each model are compared to

Case A “Do Nothing”. The total differences between Case A and each evaluated case are considered an important tool to judge the effectiveness of the models. Through this process, Case C including two submerged breakwaters, nourishment, and one north groin determines the most effective method.

Further investigation into three aspects of a construction project is performed. This is because physical process are not the only considerations. Monetary concerns, natural circumstances, and public factors also must be deliberated for the success of the project. Case C has an advantage for an economic viewpoint. However, Case H with beach recharge and three groins is the most favorable method through environmental analysis, because it can be seen an eco-friendly solution. Also, in public analysis, Case H is considered the most appropriate countermeasure, because construction permits for groins are more readily acquired than those for submerged breakwaters, and furthermore, it can attract tourists who provide more currency to local residents. Therefore, this method should easily derive approval from citizens who live in Wolcheon town, and this fact also helps to reduce the social pressure coming from politicians to KOGAS. Consequently, Case H, this ultimate countermeasure, can bring about the redemption for Wolcheon Beach.

There is an intrinsic characteristic with regards to coastal construction works. That is, it is irrevocable, once it is originated. Thus, several future works will be needed for this study to reinforce the conclusion. Firstly, although it will require more computational endeavor, a more fined FLOW grid and using domain decomposition might be implemented to build a more reliable numerical model. That means,

simulations would benefit from higher grid resolution. Secondly, a hydraulic model experiment should be performed to confirm the consequences of the established numerical model. Lastly, continuous environmental monitoring must be executed during construction and after complement of the project.

REFERENCES

Basco, D.R. *Coastal engineering manual: Part V chapter 3*. US Army Corps of Engineers, 2003.

Booij, N., R.C. Ris, and L.H. Holthuijsen. "A third-generation wave model for coastal regions: 1. Model description and validation." *Journal of Geophysical Research: Oceans* 104. C4 (1999): 7649-7666.

Hasselmann, K., T.P. Barnett, E. Bouws, H. Carlson, D.E. Cartwright, K. Enke, J.A. Ewing, H. Gienapp, D.E. Hasselmann, P. Kruseman, A. Meerburg, P. Műller, D.J. Olbers, K. Rithcher, W. Sell, and H. Walden. *Measurements of wind-wave growth and swell decay during the Joint North Sea Wave Project (JOHNSWAP)*. Deutsches Hydrographisches Institut, 1973.

Jiang, B. *Multi-dimensional error analysis of nearshore wave modeling tools, with application toward data-driven boundary correction*. MS Thesis. Texas A&M University, 2010.

Korea Gas Corporation. *Design report of revetment and reclamation construction*. Seongnam, South Korea: Korea Gas Corporation, 2009.

Korea Gas Corporation. *Analysis of countermeasures for erosion of Wolcheon Beach*. Seongnam, South Korea: Korea Gas Corporation, 2014.

Korea Gas Corporation. *Investigation reports regarding environmental impacts (the first quarter of 2015)*. Seongnam, South Korea: Korea Gas Corporation, 2015.

Korea Ocean Observing and Forecasting System. *Tidal height history*. Retrieved from <http://www.khoa.go.kr/koofs/kor/oldobservation/obs_past_search.do>, 1 Nov. 2015.

Lesser, G.R., J.A. Roelvink, J.V. Kester, and G.S. Stelling. "Development and validation of a three-dimensional morphological model." *Coastal Engineering* 51.8 (2004): 883-915.

National Climate Data Service System of Korea. *Buoy history*. Retrieved from <htttp://sts.kma.go.kr/jsp/home/contents/statistics3/newStatisticsSearch.do?menu=SEA_BUOY>, 1 Nov. 2015.

Reeve, D., A. Chadwick, and C. Fleming. *Coastal engineering: processes, theory and design practice*. CRC Press, 2012.

Roelvink, J.A. “Coastal morphodynamic evolution techniques.” *Coastal Engineering* 53.2 (2006): 277-287.

Roelvink, J.A., and D.J. Walstra. “Keeping it simple by using complex models.” *Advances in hydro-science and engineering* 6 (2004): 1-11.

South Korea. The Ministry of Land, Transport and Maritime Affairs of Korea. *Second coast improve plan*. Gwacheon, South Korea: The Ministry of Land, Transport and Maritime Affairs of Korea, 2012.

Weathers, H.D., and G. Voulgaris. “Evaluation of beach nourishment evolution models Using Data from Two South Carolina, USA Beaches: Folly Beach and Hunting Island.” *Journal of Coastal Research* 69. sp1 (2013): 84-98.

Yoshida, J., K. Udo, Y. Takeda, and A. Mano. “Framework for proper beach nourishment as an adaptation to beach erosion due to sea level rise.” *Journal of Coastal Research* 70. sp1 (2014): 467-472.

APPENDIX A

FLOW INPUT FILE

```
Ident = #Delft3D-FLOW  .03.02 3.41.02#
Commnt=
Runtxt= #No countermeasure           #
      #Averaged data               #
Filcco= #coa1.grd#
Fmtcco= #FR#
Anglat=  3.7169000e+001
Grdang=  0.0000000e+000
Filgrd= #coa1.enc#
Fmtgrd= #FR#
MNKmax= 107 182 1
Thick =  1.0000000e+002
Commnt=
Fildep= #coa1.dep#
Fmtdep= #FR#
Commnt=
Commnt=                      no. dry points: 0
Commnt=                      no. thin dams: 69
Filtd = #coa1.thd#
Fmttd = #FR#
Commnt=
Itdate= #2014-01-01#
Tunit = #M#
Tstart=  0.0000000e+000
Tstop =  5.2554000e+005
Dt    = 0.4
Tzone = 0
Commnt=
```

Sub1 = # W #

Sub2 = #PCW#

Namc1 = #Sediment send   #

Commnt=

Wnsvwp= #N#

Filwnd= #Averaged wind.wnd#

Fmtwnd= #FR#

Wndint= #Y#

Commnt=

Zeta0 = 1.8400000e-001

U0   = [.]

V0   = [.]

S0   = [.]

C01   = 0.0000000e+000

Commnt=

Commnt=   no. open boundaries: 3

Filbnd= #coa1.bnd#

Fmtbnd= #FR#

FilbcT= #coa1.bct#

FmtbcT= #FR#

FilbcC= #coa1.bcc#

FmtbcC= #FR#

Rettis= 0.0000000e+000

       0.0000000e+000

       0.0000000e+000

Rettib= 0.0000000e+000

       0.0000000e+000

       0.0000000e+000

Commnt=

Ag   = 9.8100000e+000

Rhow = 1.0250000e+003

Alph0 = [.]

Tempw = 1.5000000e+001

Salw = 3.1000000e+001

Rouwav= #FR84#

Wstres= 6.3000000e-004 0.0000000e+000 7.2300000e-003 1.0000000e+002

Rhoa = 1.2750000e+000

Betac = 5.0000000e-001

Equili= #N#

Tkemod= # #

Ktemp = 0

Fclou = 0.0000000e+000

Sarea = 0.0000000e+000

Temint= #Y#

Commnt=

Roumet= #C#

Ccofu = 5.0000000e+000

Ccofv = 5.0000000e+000

Xlo = 0.0000000e+000

Vicouv= 3.0000000e+002

Dicouv= 3.0000000e+001

Htur2d= #N#

Irov = 0

Filsed= #coa1.sed#

Fmtsed= #FR#

Filmor= #coa1.mor#

Fmtmor= #FR#

Commnt=

Iter = 2

Dryflp= #YES#

Dpsopt= #MAX#

Dpuopt= #MOR#

Dryflc= 1.0000000e-001

Dco = -9.9900000e+002

Tlfsmo= 1.4400000e+003

ThetQH= 0.0000000e+000

Forfuv= #Y#

Forfww= #N#

Sigcor= #N#

Trasol= #Cyclic-method#

Momsol= #Cyclic#

Commnt=

Commnt= no. discharges: 9

Filsrc= #coa1.src#

Fmtsrc= #FR#

Fildis= #coa1.dis#

Fmtdis= #FR#

Commnt= no. observation points: 11

Filsta= #coa1.obs#

Fmtsta= #FR#

Commnt= no. drogues: 11

Filpar= #coa1.par#

Fmtpar= #FR#

Commnt=

Commnt=

Commnt= no. cross sections: 3

Filcrs= #coa1.crs#

Fmtcrs= #FR#

Commnt=

SMhydr= #YYYYY#

SMderv= #YYYYYY#

SMproc= #YYYYYYYYYY#

PMhydr= #YYYYYY#

PMderv= #YYY#

PMproc= #YYYYYYYYYY#

SHhydr= #YYYY#

SHderv= #YYYYY#

SHproc= #YYYYYYYYYY#

SHflux= #YYYY#

PHhydr= #YYYYYY#

PHderv= #YYY#

PHproc= #YYYYYYYYYY#

PHflux= #YYYY#

Online= #N#

Waqmod= #N#

WaveOL= #Y#

Prhis = 0.0000000e+000 120 5.2554000e+005

Flmap = 0.0000000e+000 120 5.2554000e+005

Flhis = 0.0000000e+000 120 5.2554000e+005

Flpp = 0.0000000e+000 120 5.2554000e+005

Flrst = 1440

Commnt=

Cstbnd= #yes#

Gammax= 0.2

SgtThr= 99

UgrThr= 99

Commnt=

APPENDIX B

WAVE INPUT FILE

```
Delft3D WAVE GUI version 4.92.01
*
********** Datagroup Description ***************************************
*
* Project name
'samcheok'
* Project number
'001'
* Description
'No countermeasure'
'Averaged climate ata'
''
*
********** Datagroup Hydrodynamics *************************************
*
* Y/N Use bathmetry, use waterlevel, use current, use wind
1 1 1 1
*
********** Datagroup Grids *********************************************
*
* Number of computational grids
1
* Filename computational grid
'coa.grd'
* Y/N bathymetry is based on computational grid, filename bathymetry grid
1 ''
* Filename bathymetry data
'coanew.dep'
```

```
* Directional space: type, number of directions,
*                    start-direction, end-direction
*   - type: 1 = circle, 2 = sector
2 36  3.4000000e+002  1.6000000e+002
* Frequency space: lowest frequency, highest frequency, number of frequency bins,
*                 grid to nest in, Y/N write output for this grid
 5.0000001e-002  1.0000000e+000 24 0 1
*
********** Datagroup Time frame ****************************************
*
* Number of tidal time points, Reference date
1 2014-01-01
* Time, h, u, v
 0.00000000000000000e+000  1.8400000e-001  0.0000000e+000  0.0000000e+000
* Water level correction, extend flow data on the last # grid(s),
* extend bathymetry, water level, current, wind
 0.0000000e+000 0 1 1 1 1
*
********** Datagroup Boundaries ****************************************
*
* Number of boundaries
3
* Boundary name, specifications, defined-by, conditions-along-boundary
*   - specifications: 1 = from-file, 2 = parametric
*   - defined-by: 1 = orientation,
*                 2 = grid-coordinates,
*                 3 = xy-coordinates
*   - conditions-along-boundary: 1 = uniform, 2 = space-varying
'Boundary 1' 2 1 1
* Orientation
*   1 = N, 2 = NW, 3 = W, 4 = SW, 5 = S, 6 = SE, 7 = E, 8 = NE
7
```

```
* Shape, period, width-energy, peak enhancement factor, spreading
*   - shape: 1 = Jonswap, 2 = Pierson-Moskowitz, 3 = Gauss
*   - period: 1 = Peak, 2 = Mean
*   - width-energy: 1 = Power, 2 = Degrees
1 1 1  3.3000000e+000  9.9999998e-003
* Significant wave height, peak period, direction, energy distribution
 9.9100000e-001  4.9390001e+000  9.0000000e+001  4.0000000e+000
* Boundary name, specifications, defined-by, conditions-along-boundary
*   - specifications: 1 = from-file, 2 = parametric
*   - defined-by: 1 = orientation,
*                 2 = grid-coordinates,
*                 3 = xy-coordinates
*   - conditions-along-boundary: 1 = uniform, 2 = space-varying
'Boundary 2' 2 1 1
* Orientation
*   1 = N, 2 = NW, 3 = W, 4 = SW, 5 = S, 6 = SE, 7 = E, 8 = NE
5
* Shape, period, width-energy, peak enhancement factor, spreading
*   - shape: 1 = Jonswap, 2 = Pierson-Moskowitz, 3 = Gauss
*   - period: 1 = Peak, 2 = Mean
*   - width-energy: 1 = Power, 2 = Degrees
1 1 1  3.3000000e+000  9.9999998e-003
* Significant wave height, peak period, direction, energy distribution
 0.0000000e+000  0.0000000e+000  0.0000000e+000  4.0000000e+000
* Boundary name, specifications, defined-by, conditions-along-boundary
*   - specifications: 1 = from-file, 2 = parametric
*   - defined-by: 1 = orientation,
*                 2 = grid-coordinates,
*                 3 = xy-coordinates
*   - conditions-along-boundary: 1 = uniform, 2 = space-varying
'Boundary 3' 2 1 1
* Orientation
```

```
*   1 = N, 2 = NW, 3 = W, 4 = SW, 5 = S, 6 = SE, 7 = E, 8 = NE
1
* Shape, period, width-energy, peak enhancement factor, spreading
*   - shape: 1 = Jonswap, 2 = Pierson-Moskowitz, 3 = Gauss
*   - period: 1 = Peak, 2 = Mean
*   - width-energy: 1 = Power, 2 = Degrees
1 1 1  3.3000000e+000  9.9999998e-003
* Significant wave height, peak period, direction, energy distribution
 0.0000000e+000  0.0000000e+000  0.0000000e+000  4.0000000e+000
*
********** Datagroup Obstacles ****************************************
*
* Number of obstacles
4
* Obstacle type (1 = dam, 2 = sheet)
2
* Transmission coefficient
 0.0000000e+000
* Reflection (0/1), specular or diffuse (1/2), reflection coefficient [0-1]
0 1  0.0000000e+000
* Number of corner points
2
* X-Y segment coordinates
 5.3171700e+005  4.1155870e+006
 5.3179400e+005  4.1147760e+006
* Obstacle type (1 = dam, 2 = sheet)
2
* Transmission coefficient
 0.0000000e+000
* Reflection (0/1), specular or diffuse (1/2), reflection coefficient [0-1]
0 1  0.0000000e+000
* Number of corner points
```

```
2
* X-Y segment coordinates
 5.3192100e+005  4.1147730e+006
 5.3260500e+005  4.1131670e+006
* Obstacle type (1 = dam, 2 = sheet)
2
* Transmission coefficient
 0.0000000e+000
* Reflection (0/1), specular or diffuse (1/2), reflection coefficient [0-1]
0 1  0.0000000e+000
* Number of corner points
2
* X-Y segment coordinates
 5.3114900e+005  4.1140930e+006
 5.3139200e+005  4.1141430e+006
* Obstacle type (1 = dam, 2 = sheet)
2
* Transmission coefficient
 0.0000000e+000
* Reflection (0/1), specular or diffuse (1/2), reflection coefficient [0-1]
0 1  0.0000000e+000
* Number of corner points
2
* X-Y segment coordinates
 5.3177500e+005  4.1132560e+006
 5.3195800e+005  4.1132930e+006
*
********** Datagroup Physical parameters ********************************
*
* Gravity, water density, north, minimum depth
 9.8100004e+000  1.0250000e+003  9.0000000e+001  5.0000001e-002
* Convention, set-up, forces
```

```
*   - convention: 1 = nautical, 2 = cartesian
*   - set-up: 0 = no set-up, 1 = activated
*   - forces: 1 = radiation stress, 2 = wave energy dissipation rate
1 0 2
* Type of formulations
*   0 = none, 1 = 1st, 2 = 2nd, 3 = 3rd generation
3
* Depth induced breaking, alpha, gamma
*   - breaking: 0 = de-activated, 1 = B&J model
1  1.0000000e+000  7.3000002e-001
* Bottom friction, friction coefficient
*   - friction: 0 = de-activated, 1 = Jonswap,
*             2 = Collins, 3 = Madsen et al.
1  6.7000002e-002
* Non-linear triad interactions, alpha, beta
*   - interactions: 0 = de-activated, 1 = LTA
0  1.0000000e-001  2.2000000e+000
* Diffraction, smoothing coefficient, smoothing steps, adaptation of propagation
*   - interactions: 0 = de-activated, 1 = activated
0  2.0000000e-001 5 1
* Y/N windgrowth, white-capping, quadruplets, refraction, frequency shift
1 1 1 1 1
*
********** Datagroup Numerical parameters ******************************
*
* Directional space, frequency space
 5.0000000e-001  5.0000000e-001
* Hs-Tm01, Hs, Tm01, percentage of wet grid points, maximum number of iterations
 3.9999999e-002  3.9999999e-002  3.9999999e-002  9.0000000e+001 8
*
********** Datagroup Output curves *************************************
*
```

```
* Number of output curves
0
*
********** Datagroup Output parameters **********************************
*
* Level of test output, debug level, Y/N compute waves, Y/N activate hotstart file
* Output time interval, Computational mode: 0 = stationary, 1 = non-stationary
0 0 1 0  1.2000000e+002 0
* Y/N output to Flow grid; filename of Flow grid
1 'coa1.grd'
* Y/N output to locations
0
```

APPENDIX C

MORPHOLOGY INPUT FILE

```
[MorphologyFileInformation]
  FileCreatedBy    = Delft3D-FLOW-GUI, Version: 3.41.02
  FileCreationDate = Thu Dec 17 2015, 16:20:23
  FileVersion      = 02.00
[Morphology]
  EpsPar         = false                 Vertical mixing distribution according to van Rijn
(overrules k-epsilon model)
  IopKCW         = 1                     Flag for determining Rc and Rw
  RDC            = 0.01            [m]   Current related roughness height (only used if IopKCW
<> 1)
  RDW            = 0.02            [m]   Wave related roughness height (only used if IopKCW
<> 1)
  MorFac         =  1.0000000e+000   [-]   Morphological scale factor
  MorStt         =  7.2000000e+002   [min] Spin-up interval from TStart till start of
morphological changes
  Thresh         =  5.0000000e-002   [m]   Threshold sediment thickness for transport and
erosion reduction
  MorUpd         = true                  Update bathymetry during FLOW simulation
  EqmBc          = true                  Equilibrium sand concentration profile at inflow
boundaries
  DensIn         = false                 Include effect of sediment concentration on fluid density
  AksFac         =  1.0000000e+000   [-]   van Rijn's reference height = AKSFAC * KS
  RWave          =  2.0000000e+000   [-]   Wave related roughness = RWAVE * estimated
ripple height. Van Rijn Recommends range 1-3
  AlfaBs         =  1.0000000e+000   [-]   Streamwise bed gradient factor for bed load
transport
  AlfaBn         =  1.5000000e+000   [-]   Transverse bed gradient factor for bed load
transport
```

Sus = 1.0000000e+000 [-] Multiplication factor for suspended sediment reference concentration

Bed = 1.0000000e+000 [-] Multiplication factor for bed-load transport vector magnitude

SusW = 1.0000000e+000 [-] Wave-related suspended sed. transport factor

BedW = 1.0000000e+000 [-] Wave-related bed-load sed. transport factor

SedThr = 1.0000000e-001 [m] Minimum water depth for sediment computations

ThetSD = 4.0000000e-001 [-] Factor for erosion of adjacent dry cells

HMaxTH = 1.5000000e+000 [m] Max depth for variable THETSD. Set < SEDTHR to use global value only

FWFac = 1.0000000e+000 [-] Vertical mixing distribution according to van Rijn (overrules k-epsilon model)